TAMPEREEN TEKNILLINEN YLIOPISTO
TAMPERE UNIVERSITY OF TECHNOLOGY
Julkaisu 844 • Publication 844

Yaning Zou

Analysis and Mitigation of I/Q Imbalances in Multi-Antenna Transmission Systems

Tampere 2009

Tampereen teknillinen yliopisto. Julkaisu 844
Tampere University of Technology. Publication 844

Yaning Zou

Analysis and Mitigation of I/Q Imbalances in Multi-Antenna Transmission Systems

Thesis for the degree of Doctor of Technology to be presented with due permission for public examination and criticism in Tietotalo Building, Auditorium TB109, at Tampere University of Technology, on the 13th of November 2009, at 12 noon.

Tampereen teknillinen yliopisto - Tampere University of Technology
Tampere 2009

Thesis Supervisor:

Mikko Valkama, Professor
Department of Communications Engineering
Tampere University of Technology
Tampere, Finland

Pre-examiners:

Markku Juntti, Professor
Department of Electrical and Information Engineering
University of Oulu
Oulu, Finland

Aarne Mämmelä, Research Professor
VTT Technical Research Centre of Finland
Oulu, Finland

Opponents:

Markku Juntti, Professor
Department of Electrical and Information Engineering
University of Oulu
Oulu, Finland

Tim Schenk, Senior Scientist
Distributed Sensor Systems Department
Philips Research Europe
Eindhoven, The Netherlands

ISBN 978-952-15-2251-2 (printed)
ISBN 978-952-15-2287-1 (PDF)
ISSN 1459-2045

Abstract

The implementation challenges in building compact and low-cost radios for future wireless systems are continuously growing. This is partially due to the introduction of multi-antenna transmission techniques as well as the use of wideband communication waveforms and high-order symbol alphabets. In general, implementations of several parallel radios with wide bandwidth and high performance are required in single devices. Then, to keep the overall implementation costs and size feasible, simplified radio architectures and lower-cost electronics are typically used. This in turn implies that various nonidealities in the used analog radio frequency (RF) modules, stemming from the unavoidable physical limitations of the used electronics, are expected to play a critical role in future multi-antenna radio systems.

In this thesis, one example of such nonidealities, called in-phase/quadrature (I/Q) imbalance related to the amplitude and phase matching of transceiver I/Q branches, is studied in a multi-antenna communication system context. Assuming the individual analog front-ends are based on the direct-conversion radio architecture, the essence of the thesis concentrates on the analysis and digital compensation of the I/Q imbalance effects in multi-antenna transmission systems. Both transmitter and receiver sides are taken into account. In most of studies carried out in this thesis, the I/Q imbalances are assumed to be frequency-dependent and both single-carrier and multi-carrier waveforms are considered. More specifically, analytical signal models for depicting the imbalanced analog front-end processing are derived for three types of multi-antenna transmission systems, namely the space-time coded (STC) single-carrier (SC) transmission system, the space-time coded (STC)-orthogonal frequency division multiplexing (OFDM) transmission system and the spatial multiplexing (SM)-multiple-input multiple-output (MIMO)-OFDM transmission system. The resulting waveform distortion and link performance degradation are then analyzed in terms of the achievable signal-to-interference ratio (SIR) at detector input in the receiver. This analysis offers a valuable analytical tool for assessing the I/Q imbalance effects in typical multi-antenna systems, without lengthy system simulations. The analysis results also indicate that in general the I/Q imbalance effects are fundamentally different and more challenging in the multi-antenna context compared to traditional single-antenna systems. Two types of digital compensation methods are then also proposed for combating the I/Q imbalance effects on the receiver side. The first approach is based on algebraic properties of the derived signal models combined with proper pilot data and is applicable in both single-carrier and multi-carrier multi-antenna transmission systems. The second one is based on blind signal separation principles and is mainly targeted for the single-carrier transmission case. The compensation performance of both

methods is verified using extensive computer simulations. The results indicate that the proposed techniques can efficiently mitigate the signal distortion and performance degradation due to I/Q imbalance. Some practical problems such as the effects of channel estimation errors, residual carrier offsets and pilot interpolation are also considered in the thesis. Finally, pilot-based compensation techniques for combating the I/Q imbalance effects in individual OFDM transmitters and receivers are also developed in the thesis. Generally, this approach offers an alternative way to cope with the I/Q imbalance effects in the multi-antenna scenario by calibrating the individual radios in an efficient manner on both sides of a wireless link.

Preface

The research work presented in this thesis was carried out during the years 2005 to 2009 at the Department of Communications Engineering (DCE) at Tampere University of Technology (TUT), Tampere, Finland. Without the guidance and help of many people, this thesis would not have reached its current form. Therefore, I would like to thank all the current and earlier personnel of DCE for providing the most inspiring and pleasant work environment.

I would like to express my deepest gratitude to my supervisor Prof. Mikko Valkama for providing such a great opportunity to join and work in his group and also for his invaluable guidance, fruitful discussions, continuous encouragement and support as well as friendship during the research work leading to this thesis. Also I want to devote my special thanks to Prof. Markku Renfors, the head of DCE, for his wise and insightful consultation and continuous support as well as creating such a great atmosphere at the department. I would like to meanwhile thank Dr. Gernot Hueber, from the RF innovation group at Danube Integrated Circuit Engineering GmbH & Co KG (DICE), Austria, and Prof. Andreas Springer, from the Institute for Communications & Information Engineering at Johannes Kepler University (JKU), Austria, for their hospitality, considerate arrangements and interesting discussions during my research visit and stay in Austria.

I am also grateful to the thesis reviewers, Prof. Markku Juntti, University of Oulu, Finland, and Res. Prof. Aarne Mämmelä, VTT Technical Research Centre of Finland, for their careful reviews and constructive comments and feedback.

Also, I would like to thank my colleagues in the RF-DSP group at DCE/TUT, as well as other colleagues in the department for good cooperation, pleasant atmosphere and fruitful discussions. I especially would like to mention, without the intention to forget anyone: M.Sc. Lauri Anttila, M.Sc. Ali Shahed, M.Sc. Ville Syrjälä, M.Sc. Nikolay Tchamov (Jr), Lic. Tech. Jukka Rinne, M.Sc. Tero Ihalainen, Dr. Tech. Toni Huovinen, Dr. Tech. Simona Lohan, M.Sc. Vesa Lehtinen, M.Sc. Danai Skournetou, M.Sc. Toni Levanen, M.Sc. Tobias Hidalgo, M.Sc. Ari Asp, and M.Sc. Jussi Turkka. In addition, I want to thank Dr. Georg Strasser, from DICE, Austria, for his friendly company in the office and fruitful discussions during my research visit.

The research work was financially supported by the Tampere Graduate School in Information Science and Engineering (TISE), the Academy of Finland (under the project "Understanding and mitigation of analog RF impairments in multi-antenna transmission systems"), the Finnish Funding Agency for Technology and Innovation (Tekes; under the project "Advanced techniques for RF impairment mitigation in future wireless radio

systems"), the Technology Industries of Finland Centennial Foundation, the Nokia Foundation and the HPY Foundation, all of which are gratefully acknowledged. I would also like to thank Dr. Pertti Koivisto, coordinator of TISE, Tarja Erälaukko, Kirsi Viitanen, Sari Kinnari, Saara Kallio, Marianna Jokila and Nitta Laitinen, the earlier and current secretaries of DCE, Elina Orava, international coordinator, and Ulla Siltaloppi, personnel assistant of the Faculty of Computing and Electrical Engineering, for their help with practical and everyday matters.

Finally, I wish to express my warmest and most heartful thanks to my parents Chunshu Yan and Shuiyin Zou for their constant help, parenting, guidance and love throughout my life as well as for their unselfish support while I am studying and living thousands of miles away. Meanwhile, I want to say thanks to all my relatives and dear friends who have shown me their true hearts and unconditional love. At last, I would like to deeply thank my husband Ville-Petteri Lampo for understanding, caring and support during this work and for his sweet and tender love during the everyday life.

Tampere, September, 2009.

Yaning Zou

Contents

List of Publications

This thesis consists of the following publications:

[P1] Y. Zou, M. Valkama, and M. Renfors, "Digital compensation of I/Q imbalance effects in space-time coded transmit diversity systems," *IEEE Transactions on Signal Processing*, vol. 56, issue 6, pp. 2496–2508, June 2008.

[P2] Y. Zou, M. Valkama, and M. Renfors, "Analysis and compensation of transmitter and receiver I/Q imbalances in space-time coded multi-antenna OFDM systems," *EURASIP Journal on Wireless Communications and Networking* (Special Issue on Multicarrier Systems), vol. 2008, 16 pages, Article ID 391025.

[P3] G. Hueber, Y. Zou, K. Dufrene, R. Stuhlberger, and M. Valkama, "Smart front-end signal processing for advanced wireless receivers", *IEEE Journal of Selected Topics in Signal Processing* (Special Issue on DSP Techniques for RF/Analog Circuit Impairments), vol. 3, issue 3, pp. 472–487, June 2009.

[P4] M. Valkama, Y. Zou, and M. Renfors, "On I/Q imbalance effects in MIMO space-time coded transmission systems," in *Proc. IEEE Radio and Wireless Symposium (RWS'06)*, San Diego, CA, Jan. 2006, pp. 223–226.

[P5] Y. Zou, M. Valkama and M. Renfors, "Performance analysis of space-time coded MIMO-OFDM systems under I/Q imbalance," in *Proc. IEEE International Conference on Acoustics, Speech, and Signal Processing (ICASSP'07)*, Honolulu, HI, Apr. 2007, pp. 341–344.

[P6] Y. Zou, M. Valkama, and M. Renfors, "Compensation of frequency-selective I/Q imbalances in space-time coded multi-antenna OFDM systems," in *Proc. IEEE International Symposium on Communications, Control and Signal Processing (ISCCSP'08),* St. Julians, Malta, Mar. 2008, pp. 123–128.

[P7] Y. Zou, M. Valkama, and M. Renfors, "Pilot-based compensation of frequency-selective I/Q imbalances in direct-conversion OFDM transmitters", in *Proc. IEEE Vehicular Technology Conference (VTC'08)* Fall*,* Calgary, Canada, Sep. 2008.

[P8] Y. Zou, M. Valkama, and M. Renfors, "Performance analysis of spatial multiplexing MIMO-OFDM systems under frequency-selective I/Q imbalances", in *Proc. International Wireless Communications and Mobile Computing Conference (IWCMC' 09)*, Leipzig, Germany, June 2009, pp. 1381–1386.

List of Supplementary Publications

[S1] Y. Zou, M. Valkama, and M. Renfors, "Carrier frequency offset estimation in multiantenna transmission systems based on single-carrier modulation," in *Proc. IEEE International Conference on Circuits and Systems for Communications (ICCSC'08),* Shanghai, China, May 2008, pp. 402–406.

List of Abbreviations

3G	third generation
3GPP	Third Generation Partnership Project
4G	fourth generation
ADC	analog-to-digital converter
AGC	automatic gain control
BB	baseband
BER	bit error rate
BSS	blind signal separation
CFO	carrier frequency offset
CINR	channel-to-interference-plus-noise ratio
CP	cyclic prefix
D/A	digital-to-analog
DC	direct current
EASI	equivariant adaptive separation via independence
FFT	fast Fourier transform
FT	Fourier transform
GI	guard interval
I/Q	in-phase/quadrature
IC	integrated circuit
ICI	intercarrier interference
IF	intermediate frequency
IMT-A	International Mobile Telecommunications-Advanced
LNA	low-noise amplifier
IRR	image rejection ratio
LO	local oscillator
LPF	low-pass filter

LTE	Long Term Evolution
MIMO	multiple-input multiple-output
ML	maximum likelihood
MMSE	minimum mean-square error
MRC	maximal ratio combining
MSI	multi-stream interference
OFDM	orthogonal frequency division multiplexing
OSUC	ordered successive cancellation
PSK	phase shift keying
QAM	quadrature amplitude modulation
RF	radio frequency
RX	receiver
SC	single-carrier
SER	symbol error rate
SINR	signal-to-interference-plus-noise ratio
SIR	signal-to-interference ratio
SISO	single-input single-output
SM	spatial multiplexing
SNR	signal-to-noise ratio
STBC	space-time block code
STC	space-time code
TDMA	time division multiple access
TX	transmitter
UMTS	Universal Mobile Telecommunications System
WSS	wide-sense stationary
WSSUS	wide-sense stationary-uncorrelated scattering
ZF	zero-forcing

List of Principal Symbols

a, b, c, d	signal combination coefficients in STC single-carrier systems
$a(k)$,$b(k)$,$c(k)$,$d(k)$	signal combination coefficients in STC-OFDM systems
$A(\alpha_1, \alpha_2, k)$	term for calculation of analytical SIR in terms of α_1, α_2 and k
$a_i(k), b_i(k)$	signal combination coefficients in SM-MIMO-OFDM systems
$A_i(k), B_i(k)$,$C_i(k)$	terms for evaluation of SINR at i-th receiver
$a_{RX,c}(k)$,$b_{RX,c}(k)$	coefficients for receiver imbalance compensation
$a_{TX,c}(k)$,$b_{TX,c}(k)$	coefficients for transmitter imbalance calibration
B_c	coherence bandwidth
$\mathbf{B}_{IQ}(n)$	compensation matrix at step n
$b_{RX}(t), B_{RX}(f)$	receiver branch filter impulse response or frequency-response
$b_{TX}(t), B_{TX}(f)$	transmitter branch filter impulse response or frequency-response
C_{erg}	ergodic capacity
$c_i(k)$, $d_i(k)$	signal combination coefficients in SM-MIMO-OFDM systems
$c_{RX}(t)$	common responses of the receiver I and Q branch filtering
$c_{TX}(t), C_{TX}(k)$	common responses of the transmitter I and Q branch filtering
$E_{j,i}(k)$	channel estimation error at i-th receiver
f	frequency
f_{LO}	frequency of local oscillator
$\mathrm{g}(\cdot)$	memoryless nonlinear function
$\mathbf{g}(k), \overline{\mathbf{g}}(k)$	vector of receiver I/Q imbalance properties
$g_{m,RX}(t)$,$G_{m,RX}(f)$	effective receiver I/Q imbalance impulse or frequency-response
$g_{m,TX}(t)$,$G_{m,TX}(f)$	effective transmitter I/Q imbalance impulse or frequency-response
$G_{m,RX(i)}(k)$	effective I/Q imbalance frequency-response at i-th receiver
$G_{m,TX(j)}(k)$	effective I/Q imbalance frequency-response at j-th transmitter
g_{TX}, g_{RX}	gain imbalance in transmitter or receiver I/Q mixer
$\mathbf{H}, \mathbf{H}(k)$	matrix of channel frequency-responses

$H_{FB}(k)$	total effective feedback frequency-response
h_i	complex channel coefficient from one transmitter to the receiver i
$\mathbf{H}_{IQ}$,$\mathbf{H}_{TOT,m}(k)$	coefficient matrix
$h_{j,i}$,$H_{j,i}(k)$,$H_{j,i}^{(ii)}(k)$	complex channel coefficient from the transmitter j to the receiver i
h_{tot},$H_T(k)$,$H_T^{(ii)}(k)$	the total sum of channel powers
i	receiver index
$\mathbf{I}$	identity matrix
i_1, i_2, l	integers
j	transmitter index or imaginary unit (clear from context)
J_t, J_f	interpolation factor
k, k_1, k_2	subcarrier index
$K_{m,RX}$,$K_{m,RX(i)}$	frequency-independent I/Q imbalance coefficients in receivers
$K_{m,TX}$,$K_{m,TX(j)}$	frequency-independent I/Q imbalance coefficients in transmitters
L	total number of multipath channel taps
$L_{RX}, L_{RX}(f)$	image rejection ratio in individual receivers
$L_{TX}, L_{TX}(f)$	image rejection ratio in individual transmitters
m	effective I/Q imbalance coefficient index or signal reception index
n	discrete-time index
$\mathbf{n}, \mathbf{n}(k)$	additive channel noise vector at receiver input
$n_{m,i}, n_{m,i}(k)$,$n_i, n_i(k)$	additive channel noise at i-th receiver input
N_R, N_T	the number of receive antennas or transmit antennas
N_s	multiplexing gain
N_{FFT}	size of FFT
p	example real and imaginary part of complex pilot symbol
$\mathbf{P}$	channel power-delay profile
$P(l)$	average power of the l-th tap of channel power-delay profile
P_H	average channel power
$\mathbf{r}_\Sigma(k), \mathbf{r}_{RX}(k)$	received signal vector for receiver imbalance estimation
$\mathbf{R}_m(k), \mathbf{T}_m(k)$	matrix of transmitter imbalance or receiver imbalance parameters
$s, s_m, s_m(k)$	transmitted data symbol

$\mathbf{s}, \mathbf{s}(k)$	transmitted signal vector
$\mathbf{s}_c, \mathbf{s}_{IQ}, \mathbf{s}_c(k), \overline{\mathbf{s}}(k)$	transmitted data vector in compensation context
$\hat{\mathbf{s}}_{IQ}(n)$	estimated signal vector in the receiver
$s_m^{(n)}, s_m^{(n)}(k)$	transmitted symbol in n -th pilot block
$s_{m,I}, s_{m,Q}$	real and imaginary parts of transmitted data symbol
$\hat{\mathbf{s}}_{ML}, \hat{\mathbf{s}}_{ML}(k)$	signal at ML receiver output
$\hat{\overline{\mathbf{s}}}_{ML}(k)$	signal at ML receiver output after imbalance compensation
s_p	pilot symbol
$\mathbf{S}_p$	allocated pilot structure in compensation context
$S_p^{(m)}(k)$	pilot symbol for receiver imbalance estimation
$\hat{\mathbf{s}}_{ZF}, \hat{\mathbf{s}}_{ZF}(k)$	signal at ZF receiver output
$\hat{\overline{\mathbf{s}}}_{ZF}(k)$	signal at ZF receiver output after imbalance compensation
t	time
t_c	coherence time
x	complex-variable
$\mathbf{x}, \mathbf{x}(k), \overline{\mathbf{x}}(k)$	signal vector at receiver input in SM multi-antenna systems
$\mathbf{x}^{ideal}(k)$	ideal signal vector at receiver input in SM-MIMO-OFDM systems
$x_i, x_i(k)$	signal at i -th receiver input
x_I, x_Q	real part and imaginary part of complex-valued signal
$x_{LO}^{TX}(t), x_{LO}^{RX}(t)$	complex local oscillator signal in transmitters or receivers
$X_{m,fb}(k)$	signal at feedback loop output in transmitter imbalance estimation
$x_{m,i}, x_{m,i}(k)$	signal at i -th receiver input in STC multi-antenna systems
$x_{m,i,p}^{(n)}, x_{m,i,p}{}^{(n)}(k)$	received pilot at i -th receiver input in STC multi-antenna systems
$x_{m,p,i}(k)$	received pilot at i -th receiver input in SM-MIMO-OFDM systems
$\mathbf{x}_{P,i}(k)$	received pilot vector at receiver input in SM-MIMO-OFDM systems
y	signal at diversity combiner output
$\mathbf{y}, \mathbf{y}(k)$	signal vector at combiner output in pilot-based compensation context
$Y_{fb}(k)$	signal for transmitter imbalance estimation
$\mathbf{y}_{IQ}, \mathbf{y}_{IQ}(n)$	received signal vector in BSS compensation context
$y_m, y_m(k)$	signal at diversity combiner output in STC multi-antenna systems

$y_m^{ideal}, y_m^{ideal}(k)$	ideal signal at diversity combiner output without imbalances
$y_{m,I}, y_{m,Q}$	real and imaginary part of reception in STC single-carrier systems
$y_{m,p}, y_{m,p}(k)$	observation in STC multi-antenna systems during pilot period
$\mathbf{y}_p, \mathbf{y}_p(k)$	received pilot vector at combiner output in STC multi-antenna systems
$z(t)$,$Z(f)$,$Z(k)$	the ideal complex baseband equivalent under perfect matching
$Z_c(k)$	predistorted signal in transmitter imbalance calibration
$Z_p^{(m)}(k)$	pilot symbol for transmitter imbalance estimation
$Z_{RX}^{(m)}(k)$	received pilot signal for receiver imbalance estimation
$z_{RX}(t), Z_{RX}(f)$	the baseband equivalent under I/Q mismatch in receivers
$Z_{RX,c}(k)$,$Z_{TX,c}(k)$	signal at receiver imbalance compensator output
$z_{TX}(t), Z_{TX}(f)$	the baseband equivalent under I/Q mismatch in transmitters
$\alpha, \alpha_1, \alpha_2, \beta_{N_R}$	parameters for SIR calculations
γ_{RX}	average receiver input SNR
$\delta(t)$	Dirac delta function
Δf	frequency offset
$\Delta\omega$	angular frequency offset
$\boldsymbol{\theta}, \boldsymbol{\theta}(k), \boldsymbol{\theta}_i(k)$	parameter vector
μ	adaption step-size
$\xi_{j,i}(k)$	channel-to-interference-plus-noise ratio at i-th receiver
$\xi_{j,i}^{\max}(k)$	upper-bound of channel-to-interference-plus-noise ratio at i-th receiver
$\overline{\rho}_{all}^{\max}(k)$	equivalent overall SIR on receiver side
$\rho_i(k)$	signal-to-interference-plus-noise ratio at i-th receiver input
$\rho_i^{\max}(k)$	maximum signal-to-interference-plus-noise ratio at i-th receiver input
$\overline{\rho}_i^{\max}(k)$	equivalent SIR at i-th receiver
σ_n^2	average noise power
σ_p	average power ratio of the used pilot data and the data constellation
σ_s^2	average signal power
$\tau_{\max}$	maximum delay spread
ϕ_{TX}, ϕ_{RX}	phase difference in transmitter or receiver I/Q mixer

$\phi_{TX(j)}, \phi_{RX(i)}$	phase difference in *j*-th transmitter or *i*-th receiver
$\mathbf{\Phi}, \mathbf{\Phi}(k)$	coefficient matrix in I/Q imbalance compensation context
$\chi, \chi(k)$	average signal-to-interference ratio
$\chi_{(i)}(k), \chi_{(ii)}(k)$	analytical SIR for channel profile *(i)* or channel profile *(ii)*
$\chi_{def}(\alpha_1, \alpha_2, k)$	analytical SIR in terms of α_1, α_2 and k
$\psi(N_R)$	nonlinear function of N_R
ω_{LO}	angular frequency of local oscillator
$\Omega_{\mathbf{s}}$	the set of all the possible signal vectors

$(\cdot)^{-1}$	inverse
$(\cdot)^{T}$	transposition
$(\cdot)^{-T}$	inverse of transposition
$(\cdot)^{*}$	complex conjugation
$(\cdot)^{H}$	Hermitian transposition
$\lvert\cdot\rvert$	absolute value
$\lVert\cdot\rVert$	norm or length of a vector
$\hat{\cdot}$	estimated value
$[\cdot]_j$	j-th row of the vector
$[\cdot]_{j,i}$	i-th column and j-th row of the matrix
$\det[\cdot]$	determinant of matrix
$\mathrm{diag}\{\cdot\}$	diagonal matrix
$E[\cdot]$	statistical expectation
$\mathrm{Im}[\cdot]$	imaginary part of complex variable
$\mathrm{Re}[\cdot]$	real part of complex variable

Chapter 1

Introduction

1.1 Motivation and Background

The growing demands for various multimedia and personal wireless communications services call for the development of sophisticated transmission technologies to support high data rate and high system capacity over limited spectral resources in future wireless systems. The so-called fourth generation (4G) or International Mobile Telecommunications-Advanced (IMT-Advanced or IMT-A) mobile phone developments form good examples within the emerging cellular networks, where link spectral efficiencies in the order of 10 (bits/s)/Hz are commonly stated as a driving working assumption, see, e.g., [23], [66], [90] and the references therein. To achieve such a target, in addition to time and frequency, also the spatial dimension is deployed by implementing multiple transmit antennas and multiple receive antennas in single devices. Such multi-antenna transmission link is depicted at general level in Figure 1-1. Thus a multidimensional transmission system "matrix" composed of space, frequency and time elements is essentially constructed. Combined with the multipath propagation phenomenon of the physical radio channels, a number of different ways to efficiently improve system capacity and link quality can then be devised by deploying proper multiple-input multiple-output (MIMO) transmission techniques. Some of these techniques have already been used and stated as part of e.g. the current 3G Universal Mobile Telecommunications System (UMTS) standard [3], [4] as well as the emerging 3G Partnership Project (3GPP) Long Term Evolution (LTE) standard [1], [2].

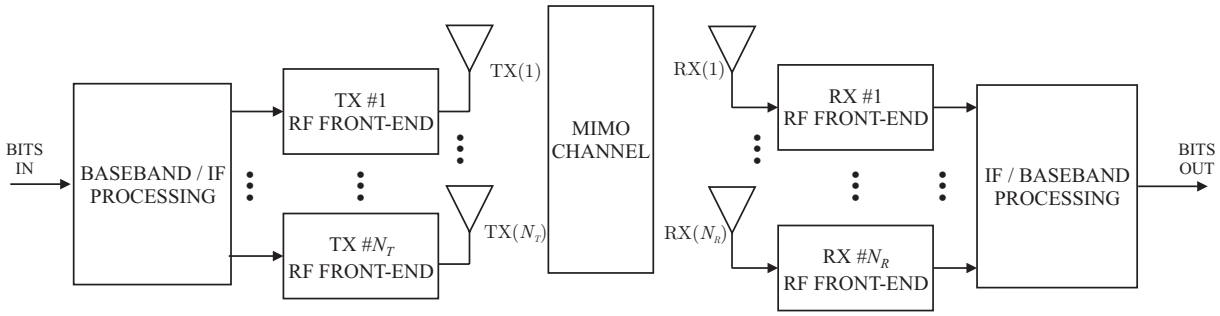

Figure 1-1: *Conceptual block-diagram of a multi-antenna transmission link with N_T transmit antennas and N_R receive antennas.*

Besides the system capacity and link quality issues, one crucial aspect in the evolution of wireless systems is in general the design and implementation of the needed terminal equipment, and especially the radio transceivers in them. With multiple transmit and/or receive antennas, also multiple radio implementations are needed, and the limited overall implementation resources cause big restrictions on the size and cost of individual radios, especially on the handheld terminal side. Thus rather simple radio frequency (RF) front-ends, such as the direct-conversion and low-intermediate frequency (low-IF) radios [5]–[8], [37], [57], [74], [75], are likely to be deployed. The so-called "dirty-RF" paradigm, referring to the effects of various unavoidable nonidealities of the used radio transceiver analog RF electronics and modules, becomes then one essential ingredient in this context [8], [29], [108]. Good examples of such nonidealities are, e.g., oscillator phase noise, power amplifier nonlinearities, and I/Q branch amplitude and phase mismatches. As a result, the resulting signal distortion and performance degradation have to be carefully taken into account in future wireless system design. In general, the nature and role of these RF impairments depend strongly on the applied radio architecture as well as on the used communications waveforms. Thereon, in the context of multi-antenna transmission systems using high-order modulation and spatial signal processing, the role of the RF impairments is likely to be more critical than in more traditional existing single-antenna wireless systems. Comprehensive understanding and proper mitigation of the impacts of RF impairments become thus crucial from both system design and RF circuit development points of view.

1.2 Scope of the Thesis: I/Q Modulation, Multi-Antenna Communications and Implementation Nonidealities

Embedded with the simplest frequency translation idea, the direct-conversion topology has been considered as one of the most promising radio architectures for developing future wireless transceivers. Different from more traditional superheterodyne radio, the direct-conversion architecture directly down-converts RF signals to baseband (BB) or up-converts BB signals to RF without any intermediate frequency stages, and is also referred to as homodyne or zero-IF architecture in the literature [5], [37], [57], [74], [75]. Then fewer analog components and blocks are needed compared to superheterodyne architecture. This inherent simplicity offers the direct-conversion radio important advantages, e.g., used silicon area, implementation cost and power consumption, over the heterodyne counterpart [5], [37], [57], [74], [75]. In addition, the location of channel selection filters at baseband enables the possibility of implementing multiple or adjustable filter bandwidths more easily, without consuming extra silicon area [37]. This is considered as one of the key elements towards building ever more flexible multi-mode receivers in the future.

Though simple in theory, the implementation of direct-conversion radios faces a number of problems and technical challenges. As shown in Figure 1-2, in-phase/quadrature (I/Q) mixing is applied in the down-conversion and up-conversion stages [37], [75]. Ideally, this mixing approach builds on two local oscillator (LO) signals with exactly 90º phase difference and equal amplitudes, and also contains two independent but identical signal paths in the circuits. However in practice, even with state-of-the-art advanced RF integrated circuit (IC) technology, the nominal 90º phase shift and the equal amplitudes of the I and Q signal paths can only be realized up to finite accuracy. Furthermore, the differences in the frequency-responses of the I and Q branch low-pass filters (LPFs), data converters and amplifiers also contribute to effective overall amplitude and phase mismatches. In general, total effective amplitude and phase imbalances in the order of 1%–5% and 1º–5º are typically stated feasible. The resulting corruption on the down-converted or up-converted signal waveform can easily degrade the system performance and raise, e.g., the symbol error rate (SER) or bit error rate (BER) [5], [37], [57], [74], [75] in the detection. This is the I/Q imbalance problem which is also the central theme in this thesis.

In yet more general context of multi-band or low-IF radio transceiver, the above-mentioned I/Q imbalances cause interference between mirror-frequency bands. This is potentially even a bigger problem, compared to plain single-channel zero-IF case, due to possibly different dynamics in the signals at different bands. For reference, see, e.g., [10],

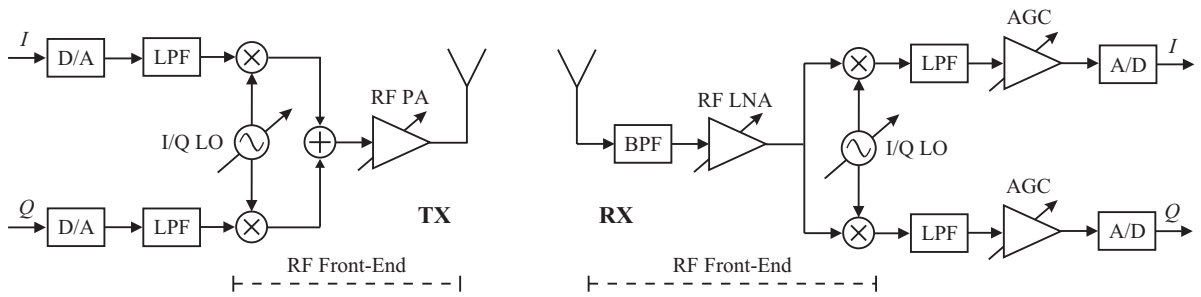

Figure 1-2: *Conceptual radio transmitter (left) and radio receiver (right) block-diagrams using quadrature or I/Q mixing.*

[11], [106]. In this thesis, however, we focus on the single-channel direct-conversion or zero-IF transceiver case.

For fully evaluating and appreciating the above I/Q imbalance problem in wireless systems, the used system transmission scheme, together with the used modulation scheme, must be carefully taken into account as well [5], [37], [75]. In this thesis, the I/Q imbalance problem is analyzed and discussed in a multi-antenna communication system context using high-order symbol alphabets. Both single-carrier modulated waveforms and multi-carrier modulated waveforms are considered in the implementation. In general, multi-antenna transmission methods have drawn intensive and wide research interest in both communication theoretic and signal processing research societies as well as in wireless telecommunication industry. A large number of theories and approaches have been developed for analyzing and obtaining the benefits of newly involved transmission dimension - space, see, e.g., [9], [13], [27], [31], [34], [51], [68], [69], [79], [90], [98]–[102], [114] and the references therein. Without consuming additional bandwidth and transmit power, the developed techniques can potentially achieve much higher link spectral efficiency or better link quality than their single antenna counterparts. However, most existing performance and capacity studies do not take the possible radio implementation deficiencies into account in any way. In this thesis, the I/Q imbalance problem is addressed in the context of two typical multi-antenna transmission schemes, namely the Alamouti transmit diversity scheme [9], [68], [102] and the spatial multiplexing (SM) scheme [31], [68], [102], [114], respectively. In both schemes, explicit channel knowledge is not required on the transmitter side, so for example link performance analysis under imperfect RF components is mathematically tractable. In both Alamouti transmit diversity as well as spatial multiplexing multi-antenna schemes, several parallel radios need to be implemented in one single device. If the direct-conversion topology is then applied in all the used transceivers, each of which having their own imbalance problem, it is

expected that the I/Q imbalance problem will play a big role and become much more complicated compared to single-antenna systems. Yet the current studies reported in the literature on the I/Q imbalance related problems mostly focus on individual radios. Thus building proper understanding on the role of I/Q imbalances and the corresponding solutions in the multi-antenna transmission context from link-level performance point of view is seen very important and crucial.

In general, the focus in this thesis is mainly on the I/Q imbalance related topics. There are other important practical aspects in the direct-conversion radio architecture as well, e.g., the so-called direct current (DC)-offset problem as well as nonlinear signal distortion problems [5]–[7], [26], [37], [45], [53], [57], [74], [75], [103], [108]. However, these issues are out of the scope of this thesis, and are thus not considered in the continuation. Notice also that in [28], a so-called RF-MIMO architecture is proposed which has rather different implementation characteristics compared to the parallel transceiver architecture assumed in this thesis. More specifically, in the RF-MIMO system concept, only single I/Q up-conversion branch (on the transmitter side) and single I/Q down-conversion branch (on the receiver side) are deployed, and all the essential spatial signal processing is then carried out already at RF. Such alternative RF architectures are also outside the main scope of this thesis.

1.3 Earlier and Related Work on I/Q Imbalance Problem

While there has been extensive research on the I/Q imbalance related problems in the single-input single-output (SISO) system context, see, e.g., [10]–[12], [15], [36], [49], [52], [54], [55], [60], [62], [76]–[78], [85], [89], [95], [97], [104]–[110], [112], [113] and the references therein, the topic of analysis and compensation of I/Q imbalances in multi-antenna transmission systems has only recently started to receive some interest in the research community. Intuitively, the transceiver chains in the multi-antenna communications can be seen as the composition of several individual transmitters and receivers or several SISO transmission chains. This implies that many of the previous research results for both analysis and compensation of I/Q imbalances obtained for the SISO case could be reused in the multi-antenna transmission case. Yet those results, especially from the overall link-level performance point of view, are still not necessarily adequate for the purpose of fully appreciating the I/Q imbalance effects in the multi-antenna transmission systems which is also one of the outputs of this thesis. Indeed, one of the main outcomes of this thesis is that the overall multi-antenna link performance under I/Q imbalances can easily be much lower than what might have been expected based on the performance of individual radios. Thus it is

generally important to understand and cope with the I/Q imbalance problem also at link-level where all the transmission chains and components are taken into account and considered as a whole. Some publications exist in the literature taking this viewpoint [19], [20], [35], [44], [56], [59], [65], [72], [73], [80]–[83], [91]–[94], [96].

On the compensation side in multi-antenna transmission links, the main focus in the existing literature is on the mitigation of frequency-independent I/Q imbalances in SM-orthogonal frequency division multiplexing (OFDM) systems [44], [56], [72], [73], [80]–[83], [91], [92], [96]. Though the space-time coding (STC) element is also briefly touched in [94] and [96], the main consideration there is anyway on frequency-independent receiver I/Q imbalances. In practice, OFDM modulation is usually applied in cases where the bandwidths of transmitted signal waveforms are in the order of several or tens of MHz. Thus the assumption of having frequency-independent I/Q imbalances in multi-antenna OFDM modulated system is not so realistic from hardware implementation point view. In a fairly recent publication [81], a combination of pilot-based estimation and decision-directed processing techniques is proposed for processing also frequency-dependent I/Q imbalance. But again the space-time coding element is not addressed in [81] and only direct spatial multiplexing scheme is assumed. In [92] and [93], compensation procedures for mitigation of frequency-dependent I/Q imbalance in both spatial multiplexing and space-time coding transmission links are proposed but the actual compensation parameter estimation task is totally neglected. Recently in [19] and [48], I/Q imbalance mitigation and analysis aspects in STC-OFDM systems are also studied but all the algorithm developments and performance analyses are still conducted based on the frequency-independent I/Q imbalance assumptions. Very recently in [33] and [61], statistics based blind methods as well as pilot-based estimation-compensation schemes have been proposed for mitigation of frequency-selective I/Q imbalances in multi-antenna transmission links. In [83], in turn, some link performance analysis is carried out in SM-MIMO-OFDM transmission context but the impact of transmitter I/Q imbalances and receiver I/Q imbalances on the link performance are considered only in a separate manner.

1.4 Outline and Main Results of the Thesis

In this thesis, the topic of analysis and mitigation of I/Q imbalance effects in the multi-antenna transmission systems is thoroughly studied. Both transmitter and receiver sides of the link are taken into account, and in most of the studies, frequency-selective I/Q imbalances are assumed, as will be shortly reviewed below and in more details in the forthcoming chapters.

Altogether compared to the time frame of this thesis work and the thesis publications [P1]–[P8], no prior art in comprehensive multi-antenna link-level performance analysis with proper frequency-dependent I/Q imbalance models is available in the literature. Similarly on the compensation side, only the work reported in [81], carried out independently of this thesis work, is addressing the estimation-compensation task of frequency-selective I/Q imbalances in multi-antenna transmission links. Thus this thesis work can be seen as pioneering work in this research field.

As a starting point, the basic ideas of multi-antenna transmission are briefly discussed in Chapter 2. Two typical transmission schemes, the STC scheme as well as the SM scheme, are introduced. For both single-carrier modulated waveforms and multi-carrier modulated waveforms, the overall link signal models are then given assuming perfectly matched I and Q branches in all radios. Then the signal models for depicting both frequency-independent and frequency-dependent I/Q imbalance effects in individual transmitters and receivers are briefly formulated in Chapter 3. This generally forms the very basic foundation of all the research output and analysis later on.

Next, in Chapter 4 to Chapter 6, the impact of I/Q imbalances on the above transmission schemes is analyzed in closed-form and novel imbalance mitigation algorithms are proposed as well. More specifically, in Chapter 4, the frequency-independent I/Q imbalance case is examined within the Alamouti transmit diversity scheme. Single-carrier modulated waveforms and frequency-flat channels are assumed as the basic system setup. The overall link signal model under I/Q imbalances is derived and the resulting signal degradation is addressed analytically in terms of the resulting signal-to-interference ratio (SIR). This analysis basically forms a solid foundation for fully appreciating the imbalance effects without lengthy system simulations in single-carrier STC context. In addition, two compensation algorithms based on either training/pilot signals or blind signal processing are proposed. The practical aspects of the proposed algorithms such as robustness against channel estimation errors and carrier frequency offset (CFO) are also briefly discussed. Similar performance analysis on the overall link performance is continued in Chapters 5 and 6, targeting for both STC-OFDM and SM-MIMO-OFDM transmission systems, respectively. Different from the assumption in Chapter 4, the bandwidths of the used signal waveforms in both chapters are assumed to be in the order of 1–20 MHz. Thus the properties of I/Q imbalances in transceivers as well as the properties of the radio channels are expected to vary as a function of frequency in practice. Therefore, the link signal models and the corresponding link performance analysis, in terms of SIR, are derived and carried out in frequency domain in a subcarrier-wise manner. Stemming from the developed signal models, effective pilot-based

algorithms are then also proposed to mitigate or compensate the dominant frequency-selective I/Q imbalance effects in STC-OFDM and SM-MIMO-OFDM systems. Again, several practical aspects in the compensation context such as channel estimation and pilot-subcarrier interpolation are also addressed, which demonstrates the feasibility of proposed algorithms in practical wireless system setups. Here a so-called channel-to-interference-plus-noise ratio (CINR) is also defined and applied for analyzing and quantifying the impacts of I/Q imbalances and additive channel noise on pilot-based channel estimation quality. In general, comprehensive reference simulations are used in Chapter 4 to Chapter 6 to illustrate the validity and accuracy of the SIR and CINR analysis and the good compensation performance of the proposed mitigation techniques in practical multi-antenna transmission systems.

In addition to link-oriented imbalance studies, some studies on mitigation and calibration of frequency-selective I/Q imbalances in individual OFDM transceivers are also reported in this thesis in Chapter 7. By deploying a feedback loop from RF to baseband, together with a properly-designed pilot signal structure, the subcarrier-wise transmitter and receiver I/Q imbalance values for all the radios in one single terminal can be estimated. Based on the obtained imbalance knowledge, the I/Q imbalance effects on the actual transmit waveform and receive waveform are then efficiently mitigated by applying baseband predistortion and postdistortion on the mirror-subcarrier signals in each radio, respectively. Notice that, compared to the statistics based approach, one major benefit of the proposed pilot-based approach is that the estimation period is much shorter, indicating much shorter calibration time. Meanwhile as the coordination between the transmitting side and the receiving side of the actual communication link is not compulsory here, the proposed algorithm can be basically applied to any OFDM modulated multi-antenna system. It is independent of the used equalization techniques and multi-access schemes (multi-user or single-user) and thus forms an alternative way to efficiently compensate the I/Q imbalance effects in OFDM radios.

The general conclusions of the thesis are drawn in Chapter 8. A short summary of the thesis publications [P1]–[P8] is given in Chapter 9 where the author's contributions to the publications are clarified as well.

In general, the main idea in composing this thesis was to state the new analysis, ideas and results originally reported in [P1]–[P8] as a complete yet fluent summary. The link-level performance analysis as well as the frequency-selective I/Q imbalance models, and compensation methods for all the transmitters and receivers in the link, presented in Chapter 4 to Chapter 7 clearly form the main contributions as well as novelties of this thesis. In principle, in most of the forthcoming material, the signal modeling and performance analysis aspects are

emphasized for presentation purposes. Much more detailed view concerning the performance of the proposed compensation techniques are given in the original papers [P1]–[P8].

1.5 Basic Notations and Assumptions

Throughout this thesis, the so-called I/Q notation of the form $x = x_I + jx_Q$ is deployed for any complex-valued quantity x, where x_I and x_Q denote the corresponding real and imaginary parts, i.e., $\mathrm{Re}[x] = x_I$ and $\mathrm{Im}[x] = x_Q$. Superscript $(\cdot)^*$ denotes complex conjugation. Bold-face lower-case letters, like $\mathbf{a}$, are used for column-vectors, while bold-face upper-case letters, such as $\mathbf{A}$, for matrices. Superscripts $(\cdot)^T$, $(\cdot)^H$ and $(\cdot)^{-1}$ denote transposition, conjugate (Hermitian) transposition and matrix inverse, respectively. Unless otherwise mentioned explicitly, all the signals throughout this thesis are assumed to be complex-valued, wide-sense stationary (WSS) circular random signals with zero mean (for explicit definitions, see, e.g, [67] and [84]).

Chapter 2

Basic Concepts in Multi-Antenna Communications

One of the important challenges in wireless system design is to meet the fast-rising demands on link throughput and network capacity over limited spectral resources. The importance of improving link spectral efficiency and quality is thus considerably highlighted [23], [66], [90]. Thereon, multi-antenna transmission methods have been proposed [30], [31], [34], [68], [102] and are currently widely recognized as one mandatory physical layer element in the development of future wireless systems [1]–[4], [23], [66], [90]. In general, the use of multiple transmit and receive antennas brings an additional dimension, space, to the wireless system design [38], [86], [111]. It enables a wide range of alternative approaches for improving the system performance, in terms of capacity, range and link reliability. Yet the design and implementation complexity are, in turn, substantially increased. Thus understanding the trade-offs between the achievable system performance and needed implementation resources are generally seen important.

2.1 General Ideas and Multiple-Input Multiple-Output Systems

In a general multi-antenna transmission scenario, by definition, multiple transmit (TX) and receive (RX) antennas are deployed. Thus multiple radio channels linking the transmitter and receiver are essentially created. Now if the individual antenna elements are spaced sufficiently far apart, the fading characteristics of these radio channels are independent of each other. Combined with proper transmitter and receiver signal processing, multiple parallel “data pipes” can then be created, to improve the overall link data rate and spectral efficiency. Another alternative, stemming from different transmitter and receiver signal processing, is to use the different fading characteristics to improve the link reliability in terms of diversity.

In the following sections, principal link-level models for two typical and fairly basic multi-antenna transmission schemes, the Alamouti transmit diversity scheme [9], [68], [102], and the spatial multiplexing transmission scheme [31], [68], [102], [114], are briefly discussed with single-carrier as well as multi-carrier waveforms. In general, both schemes have their own strengths and weaknesses and may not necessarily form any ultimate solution for future multi-antenna wireless transmission systems. Yet they do anyway form the very basic core of many currently emerging multi-antenna transmission approaches [30], [31], [34], [51], [71], [79], [90], [98], [99], [114], and are also the basis for more advanced waveform developments. In addition, the main concern of this research is not in proposing or devising new multi-antenna waveform solutions but obtaining clear and thorough insight into the radio implementation aspects in multi-antenna transmission context. Thus, even though fairly simple in theory, the Alamouti transmit diversity and spatial multiplexing transmission schemes are used as the main multi-antenna waveform solutions in this thesis.

2.2 Ordinary Receive Diversity

One important benefit of deploying multiple transmit and/or receive antennas is the possibility for increased link reliability and the improved received signal quality against fading. The philosophy here is that if one antenna is experiencing deep fading, it is unlikely that the other ones are experiencing the same fading situation. Thus, a robust link can be obtained by properly combining the signals received through different fading realizations.

Conceptually simplest example is ordinary receive diversity where the transmit signal is received through multiple parallel receivers. This is illustrated in Figure 2-1. Assuming the bandwidth of transmitted signals is much narrower than the channel coherence bandwidth B_c [102], defined as $B_c \simeq 1/\tau_{\max}$ where $\tau_{\max}$ denotes the maximum delay spread of the channel, the transmission channels can be generally characterized as frequency-flat or one tap channels [70], [102]. Denoting now the baseband equivalent complex channel coefficient from the transmitter to the receiver i by h_i, $i \in \{1,2,...,N_R\}$, the signal sample in the i-th receiver is given by

$$x_i = h_i s + n_i \tag{2.1}$$

where n_i denotes noise and s is the transmit symbol. Then diversity gain over an individual transmitter-receiver link can be obtained by combining the samples as

$$y = \sum_{i=1}^{N_R} h_i^* x_i = \sum_{i=1}^{N_R} \left|h_{1,i}\right|^2 s + \sum_{i=1}^{N_R} h_i^* n_i \ . \tag{2.2}$$

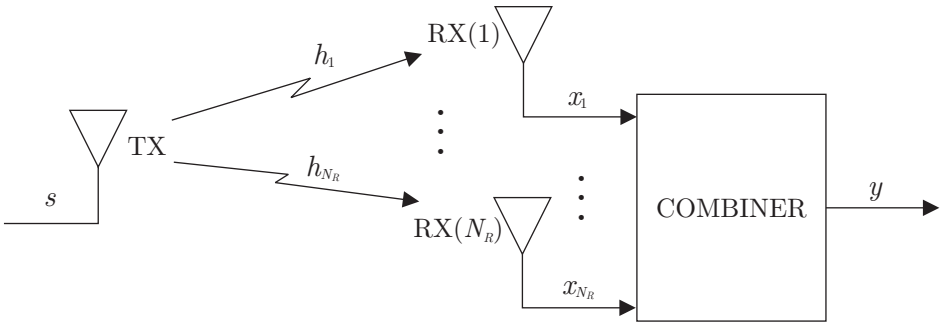

Figure 2-1: *Ordinary receive diversity principle.*

This combining scheme is known as the maximum ratio combining (MRC) [14], [18], [42]. Compared to individual link fading characteristics, this essentially improves the link quality in terms of the detection error probability, by improving the statistics of the instantaneous signal-to-noise ratio (SNR). This is called diversity gain [14], [18], [42], [68], [102], and the exact diversity order can be quantified in terms of the slope of the detection error rate vs. average SNR curve at high SNR regime. The use of coherent combining on the receiver side improves also the overall effecitve received SNR (compared to no diversity case), which is typically called array gain or power gain [14], [18], [42], [68], [102]. For the above MRC scheme, both the diversity order and array gain equal the number of receivers [14], [18], [42], [68], [102].

2.3 Transmit Diversity Using Space-Time Coding

Compared to above receive diversity, obtaining transmit diversity by simply transmitting the same data from multiple parallel transmit antennas is not feasible. This is because the overall transmit power or energy is divided equally between the transmitters (assuming no channel knowledge is available on the transmitter side), and the resulting distribution of the received instantaneous SNR is identical to the corresponding SISO case.

One interesting extension to above-mentioned plain spatial "processing" is then to take the time-axis also into play. One good example of such techniques is the so-called Alamouti transmit diversity scheme or Alamouti space-time block code (STBC) [9], [68], [102]. As shown in Figure 2-2, this scheme requires the implementation of two transmit antennas and can also be combined with additional receive diversity using N_R receive antennas. Now, given two consecutive data symbols s_1 and s_2 entering the transmitter, the idea in short is to transmit these symbols in parallel during the first signaling interval over the two transmit antennas. Then during the second signaling interval, symbols $-s_2^*$ and s_1^* are transmitted

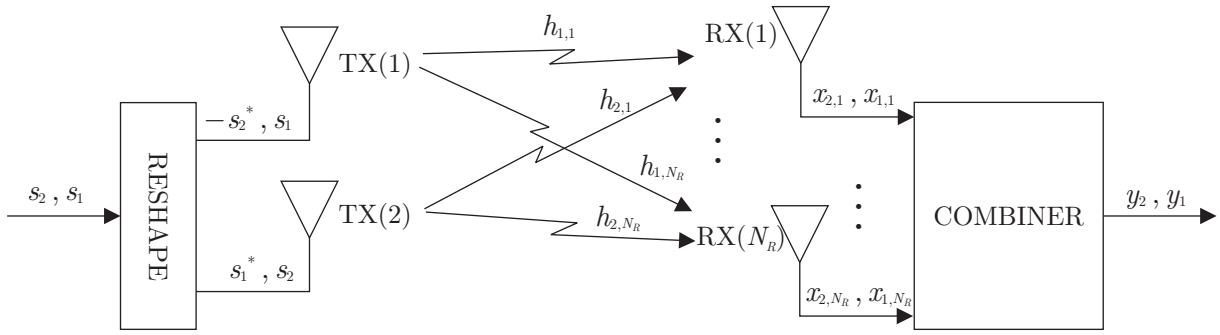

Figure 2-2: *The basic* $2 \times N_R$ *Alamouti transmit diversity transmission scheme.*

correspondingly. Denoting the baseband equivalent complex channel coefficient from the transmitter j to the receiver i by $h_{j,i}$, $j \in \{1,2\}$, $i \in \{1,2,...,N_R\}$ (frequency-flat channels assumed again, as in [9]), the corresponding signal samples in the i-th receiver are given by

$$\begin{aligned} x_{1,i} &= h_{1,i}s_1 + h_{2,i}s_2 + n_{1,i} \\ x_{2,i} &= -h_{1,i}s_2^* + h_{2,i}s_1^* + n_{2,i}. \end{aligned} \tag{2.3}$$

Then diversity gain over the individual transmitter-receiver links can be obtained by combining the samples as

$$\begin{aligned} y_1 &= \sum_{i=1}^{N_R}(h_{1,i}^*x_{1,i} + h_{2,i}x_{2,i}^*) = \sum_{i=1}^{N_R}(|h_{1,i}|^2 + |h_{2,i}|^2)s_1 + \sum_{i=1}^{N_R}(h_{1,i}^*n_{1,i} + h_{2,i}n_{2,i}^*) \\ y_2 &= \sum_{i=1}^{N_R}(h_{2,i}^*x_{1,i} - h_{1,i}x_{2,i}^*) = \sum_{i=1}^{N_R}(|h_{1,i}|^2 + |h_{2,i}|^2)s_2 + \sum_{i=1}^{N_R}(h_{2,i}^*n_{1,i} - h_{1,i}n_{2,i}^*). \end{aligned} \tag{2.4}$$

Assuming independent channels $h_{j,i}$, it is highly unlikely that all the channels are in a bad state simultaneously and the quality of the overall link is thus improved. Similarly as in case of receive diversity, the increase in the link reliability stems from the improved statistics of the instantaneous SNR at the combiner output. The resulting overall diversity order of $2N_R$ is equivalent to the earlier plain receive diversity with $2N_R$ parallel receivers. Yet only N_R receiver implementations are required here [9]. Thus the STBC scheme is a more efficient solution from the receiver implementation point of view (in terms of receiver complexity) which is essential, e.g., in mobile terminals.

2.4 Spatial Multiplexing

In addition to improving the link quality of wireless transmission through diversity, the deployment of multiple antenna elements can also be used to increase the data transmission

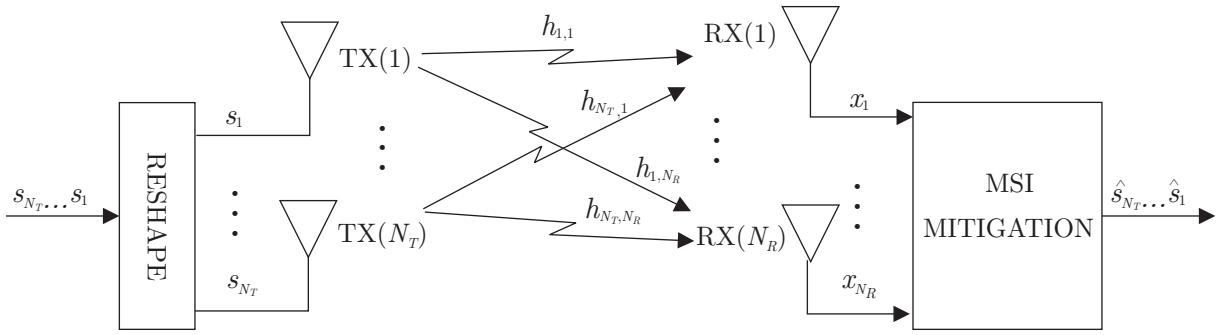

Figure 2-3: *The basic $N_T \times N_R$ spatial multiplexing transmission scheme.*

rate by simultaneously transmitting parallel data streams through parallel TX antennas. Thus, instead of adding redundant information along space and time as in STBC scheme, multiple data samples $\mathbf{s} = [s_1,\ s_2,\ \ldots,\ s_{N_T}]^T$ are transmitted in parallel using the N_T transmit antennas as shown in Figure 2-3. Again, all the transmission channels are assumed to be frequency-flat. Then the corresponding parallel outputs of N_R receivers in one signaling interval is given by

$$\mathbf{x} = [x_1, x_2, \ldots, x_{N_R}]^T = \mathbf{H}^T\mathbf{s} + \mathbf{n} \tag{2.5}$$

where x_i and n_i denote the received signal sample and noise sample in i-th receiver, $\mathbf{n} = [n_1,\ n_2,\ \ldots,\ n_{N_R}]^T$, and $\mathbf{H}$ is an $N_T \times N_R$ matrix and contains the complex channel gains with $[\mathbf{H}]_{j,i} = h_{j,i}$ denoting the complex channel gain from transmitter j to receiver i.

This spatial multiplexing scheme can at best achieve a data transmission rate of $N_s = \min\{N_T, N_R\}$ symbols per signaling interval and a maximum diversity order of N_R [31], [68], [102], [114]. Thus it can potentially increase the link capacity by a factor of N_s compared to the corresponding single-antenna system as $C_{erg} \propto \min\{N_T, N_R\} = N_s$ where C_{erg} represents the ergodic capacity of the link [31], [34], [43], [68], [101], [102], [114].

In the above-type spatial multiplexing systems, the parallel transmitted data streams are transmitted from the transmitters to each individual receiver through different radio channels, and from an individual receiver point of view, interfere with each other. This is typically called multi-stream interference (MSI). Thus, in the detection of the transmitted streams on the receiver side, both additive channel noise and MSI should be taken into account. One possible solution here is to use spatial maximum likelihood (ML) receiver. Assuming perfect channel knowledge and spatially uncorrelated Gaussian noise components, the ML-decision on transmitted symbol vector $\mathbf{s}$ is given by [64], [68], [102], [114]

$$\hat{\mathbf{s}}_{ML} = \arg\min_{\mathbf{s}\in\Omega_{\mathbf{s}}} \left\|\mathbf{x} - \mathbf{H}^T\mathbf{s}\right\|^2 \tag{2.6}$$

where Ω_s denotes the set of all the possible signal vectors. From the vector detection performance point of view, assuming all the possible signal vectors are equally likely, the ML detector is the optimum solution for the MSI mitigation [64], [68], [102], [114]. It is generally also able to extract the full diversity order of N_R. Yet its implementation complexity is relatively high, growing exponentially with the number of transmit antennas, and depends also on the order of the symbol alphabet. Therefore, some sub-optimal receivers like the zero-forcing (ZF) receiver of the form

$$\hat{\mathbf{s}}_{ZF} = \mathbf{H}^{-T}\mathbf{x} = \mathbf{s} + \mathbf{H}^{-T}\mathbf{n} \tag{2.7}$$

can be deployed for MSI mitigation, followed by ordinary component-wise minimum distance detector. Other alternatives are, e.g., the corresponding minimum mean-square error (MMSE) receiver and the ordered successive cancellation (OSUC) receiver, providing different trade-offs between receiver performance and implementation complexity [30], [31], [68], [102], [114].

In general, the above multi-antenna waveform principles described in Sections 2.3–2.4 do not assume any explicit channel knowledge on the transmitter side. If such channel knowledge is available at the transmitter, it can be deployed in terms of precoding (additional mapping between the actual data symbols and the transmit variables), in order to, e.g., relieve the MSI mitigation task of the receiver. Such techniques are described in details, e.g., in [68], [102].

2.5 Single-Carrier vs. Multi-Carrier Waveforms

Another important aspect in increasing the data rates in wireless systems is the use of wideband signal waveforms. However, if the signaling bandwidth is clearly wider than the channel coherence bandwidth, the frequency-responses of the transmission channels can not be considered as frequency-flat or one-tap channels any more. Instead, a multipath channel model with frequency-selective frequency-responses becomes a necessity. One typical example of such multipath channel models is the so-called wide-sense stationary-uncorrelated scattering (WSSUS) channel model [16], [58], [70] in which the different multipath components (taps) are statistically uncorrelated. Such WSSUS channels are typically characterized by a power delay profile which defines the average power of different multipath components as a function of the corresponding delay. In addition, the actual fading characteristics due to mobility are characterized by the statistical distribution and the correlation characteristics of the individual multipath components over time. For WSSUS

channels, the correlation properties are independent of the absolute time, as in case of any wide-sense stationary random process. The length of a time window (correlation lag) over which the correlation approaches zero is typically termed coherence time while the Fourier transform of the correlation function is called Doppler spectrum [70]. Since a time-varying multipath (impulse) response maps into a corresponding time-varying frequency response, the correlation characteristics of any frequency "bin" over time can also be used for fading characterization in terms of coherence time and Doppler spectrum.

In general, communication over frequency-selective multipath channels calls for the use of sophisticated equalizers on the receiver side which can dramatically increase the overall system implementation complexity. One efficient way to handle this problem is to use OFDM waveforms [23], [63], [90]. More specifically, by converting the overall frequency-selective radio channel into a collection of parallel frequency-flat subchannels, the equalization problem is simplified, and when combined with proper coding, it is also possible to take advantage of the frequency diversity in multipath environments with reasonable implementation complexity. Therefore, when targeting for link spectral efficiencies in the order of 10 (bits/s)/Hz in the emerging wireless systems [23], [63], [90], the combination of multi-antenna techniques and OFDM generally forms a very attractive choice.

With two transmit antennas and using OFDM waveforms, as shown in Figure 2-4, space-time coding [9] can be applied separately for each subcarrier data stream and transmitted using two parallel OFDM transmitters. Throughout this thesis, the size of the fast Fourier transform (FFT) and inverse FFT used on the receiver and transmitter sides, respectively, is denoted by N_{FFT} , and the corresponding subcarrier indexes are denoted by $k = -N_{FFT}/2 + 1 \ldots N_{FFT}/2$. Then let $s_1(k)$ and $s_2(k)$ represent the two consecutive data samples to be transmitted over the k-th subcarrier. Assuming further that the guard interval (GI) implemented as a cyclic prefix (CP) is longer than the channel delay spread, the corresponding samples $y_1(k)$ and $y_2(k)$ at the outputs of the receiver FFT and combining stages (including appropriate CP removal) are given by

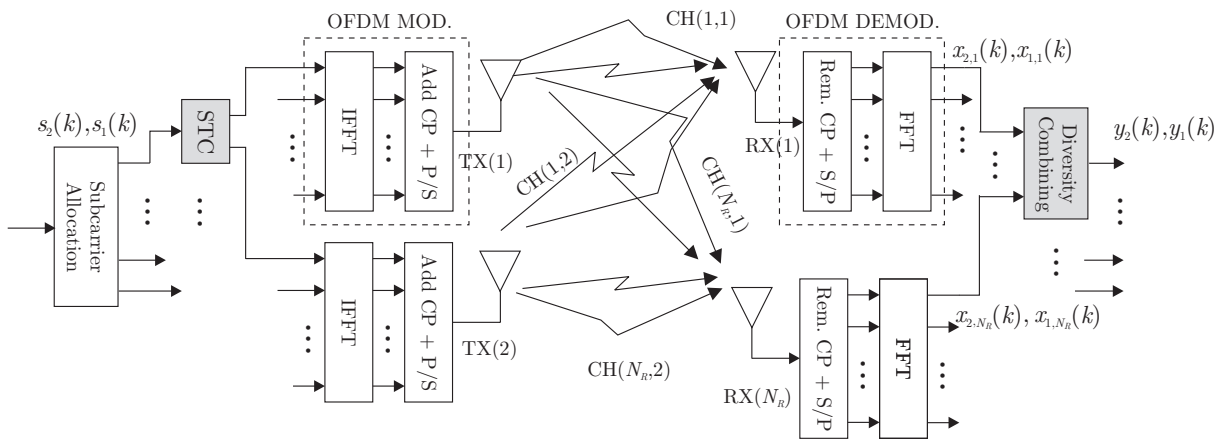

Figure 2-4: $2 \times N_R$ *multi-antenna OFDM transmission system with subcarrier-wise Alamouti transmit diversity coding. (Rem. refers to remove, MOD. and DEMOD. refer to modulation and demodulation respectively.)*

$$
\begin{aligned}
y_1(k) &= \sum_{i=1}^{N_R} (H_{1,i}^*(k) x_{1,i}(k) + H_{2,i}(k) x_{2,i}^*(k)) \\
&= \sum_{i=1}^{N_R} (\left|H_{1,i}(k)\right|^2 + \left|H_{2,i}(k)\right|^2) s_1(k) + \sum_{i=1}^{N_R} (H_{1,i}^*(k) n_{1,i}(k) + H_{2,i}(k) n_{2,i}^*(k)) \\
y_2(k) &= \sum_{i=1}^{N_R} (H_{2,i}^*(k) x_{1,i}(k) - H_{1,i}(k) x_{2,i}^*(k)) \\
&= \sum_{i=1}^{N_R} (\left|H_{1,i}(k)\right|^2 + \left|H_{2,i}(k)\right|^2) s_2(k) + \sum_{i=1}^{N_R} (H_{2,i}^*(k) n_{1,i}(k) - H_{1,i}(k) n_{2,i}^*(k))
\end{aligned}
\tag{2.8}
$$

where $H_{1,i}(k)$ and $H_{2,i}(k)$ denote the channel frequency-responses (TX(1)→RX(i) and TX(2)→RX(i)), $x_{1,i}(k)$ and $x_{2,i}(k)$ are the corresponding received samples after FFT at receiver i, and $n_{1,i}(k)$ and $n_{2,i}(k)$ are noise samples after FFT at receiver i, all at subcarrier k. Based on (2.8), similar diversity interpretations as in Sections 2.2 and 2.3 can be established.

Also the spatial multiplexing principle can be applied separately for each subcarrier [68], [102]. This is illustrated in Figure 2-5. Reflecting the modeling in earlier sections and above, the received spatial signal vector (at subcarrier k) after discarding the CP and taking FFTs can be written as

$$
\mathbf{x}(k) = [x_1(k), x_2(k), ..., x_{N_R}(k)]^T = \mathbf{H}(k)^T \mathbf{s}(k) + \mathbf{n}(k) \tag{2.9}
$$

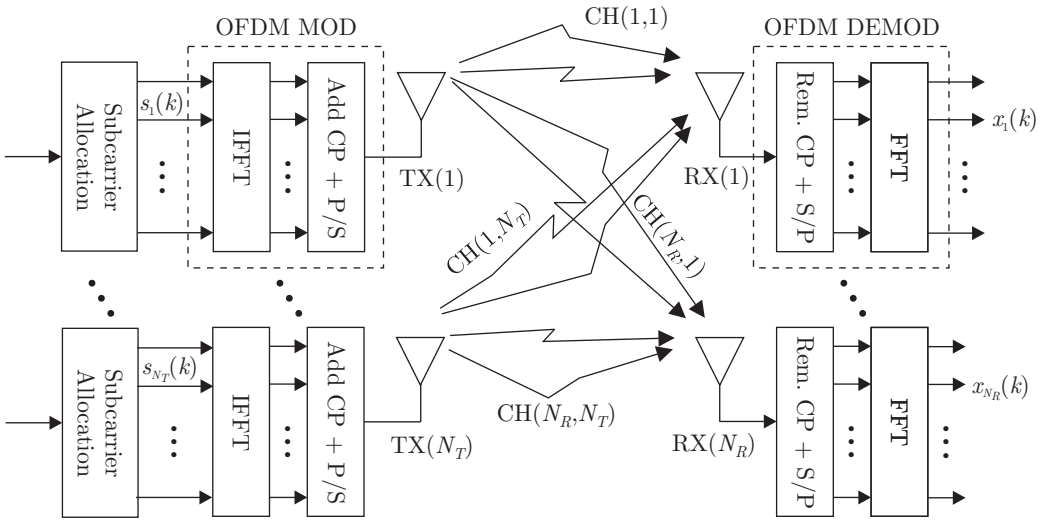

Figure 2-5: $N_T \times N_R$ *multi-antenna OFDM transmission system with subcarrier-wise spatial multiplexing. (Rem. refers to remove, MOD. and DEMOD. refer to modulation and demodulation respectively.)*

where the transmitted sample at j-th transmitter and k-th subcarrier is denoted by $s_j(k)$, the overall transmission vector is $\mathbf{s}(k) = [s_1(k), s_2(k), ..., s_{N_T}(k)]^T$, and $x_i(k)$ denotes the received frequency-domain sample at k-th subcarrier and i-th receiver. The noise vector $\mathbf{n}(k) = \left[n_1(k), n_2(k)...n_{N_R}(k)\right]$ with $n_i(k)$ modeling additive channel noise (after FFT) at k-th subcarrier of i-th receiver and the matrix $\mathbf{H}(k)$ contains the channel responses where $[\mathbf{H}(k)]_{j,i} = H_{j,i}(k)$ denotes the channel frequency-response from transmitter j to receiver i at k-th subcarrier. Now the decision on transmitted signal vector $\mathbf{s}(k)$ can be made by applying, e.g., the earlier ML or ZF principles as

$$\hat{\mathbf{s}}_{ML}(k) = \underset{\mathbf{s}(k)\in\Omega_{\mathbf{s}}}{\arg\min} \left\|\mathbf{x}(k) - \mathbf{H}(k)^T \mathbf{s}(k)\right\|^2 \tag{2.10}$$

and

$$\hat{\mathbf{s}}_{ZF}(k) = \mathbf{H}(k)^{-T}\mathbf{x}(k) = \mathbf{s}(k) + \mathbf{H}(k)^{-T}\mathbf{n}(k). \tag{2.11}$$

The ZF receiver is then followed by ordinary component-wise minimum distance detector.

Chapter 3

I/Q Imbalances and Signal Models

In this chapter, we address the I/Q imbalance modeling in individual transmitters and receivers. For generality, both frequency-independent and frequency-dependent I/Q imbalances are considered to be used with narrowband and wideband waveforms, respectively.

3.1 Frequency-Independent I/Q Imbalance Modeling

Physically the amplitude and phase mismatches between the transceiver I and Q signal branches stem from the relative differences between all the analog components of the I/Q front-end [5], [24], [45], [53], [57], [74], [75], [103], [108]. On the transmitter side, this includes the actual I/Q up-conversion stage as well as the I and Q branch filters and digital-to-analog (D/A) converters. On the receiver side, in turn, the I/Q down-conversion as well as the I and Q branch filtering, amplification, and sampling stages contribute to the effective I/Q imbalances. Here, in the narrowband context, we refer all the mismatches to the I/Q up- and down-conversion stages. Conceptual illustrations of such modulators and demodulators are given in Figure 3-1. Considering then the implications at waveform level, we first write the corresponding complex LO signals as

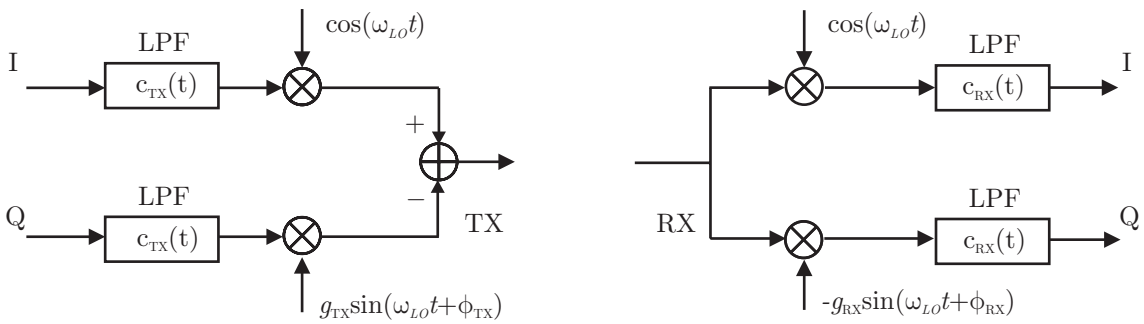

Figure 3-1: *Frequency-independent I/Q imbalance in TX (left) and RX (right).*

$$\begin{aligned} x_{LO}^{TX}(t) &= \cos(\omega_{LO}t) + jg_{TX}\sin(\omega_{LO}t + \phi_{TX}) \\ &= K_{1,TX}e^{j\omega_{LO}t} + K_{2,TX}e^{-j\omega_{LO}t} \end{aligned} \tag{3.1}$$

$$\begin{aligned} x_{LO}^{RX}(t) &= \cos(\omega_{LO}t) - jg_{RX}\sin(\omega_{LO}t + \phi_{RX}) \\ &= K_{1,RX}e^{-j\omega_{LO}t} + K_{2,RX}e^{j\omega_{LO}t} \end{aligned} \tag{3.2}$$

where $\omega_{LO} = 2\pi f_{LO}$, $\{g_{TX}, \phi_{TX}\}$ and $\{g_{RX}, \phi_{RX}\}$ represent the total effective amplitude and phase imbalances of the TX and the RX, respectively, and the coefficients $K_{1,TX}$, $K_{2,TX}$, $K_{1,RX}$, and $K_{2,RX}$ are of the form

$$\begin{aligned} K_{1,TX} &= (1 + g_{TX}e^{j\phi_{TX}})/2, & K_{2,TX} &= (1 - g_{TX}e^{-j\phi_{TX}})/2 \\ K_{1,RX} &= (1 + g_{RX}e^{-j\phi_{RX}})/2, & K_{2,RX} &= (1 - g_{RX}e^{j\phi_{RX}})/2. \end{aligned} \tag{3.3}$$

Then from the individual transmitter and receiver point of views, the above I/Q imbalance models correspond to the following transformations of the effective baseband equivalent signals given by

$$\begin{aligned} z_{TX}(t) &= K_{1,TX}(c_{TX}(t) * z(t)) + K_{2,TX}^{*}(c_{TX}(t) * z(t))^{*} \\ &= c_{TX}(t) * [K_{1,TX}z(t) + K_{2,TX}^{*}z^{*}(t)] \end{aligned} \tag{3.4}$$

$$\begin{aligned} z_{RX}(t) &= c_{RX}(t) * [K_{1,RX}z(t) + K_{2,RX}z^{*}(t)] \\ &= K_{1,RX}(c_{RX}(t) * z(t)) + K_{2,RX}(c_{RX}(t) * z(t))^{*} \end{aligned} \tag{3.5}$$

where $z(t)$ denotes the ideal complex baseband equivalent under perfect I/Q matching and the real-valued impulse responses $c_{TX}(t)$ and $c_{RX}(t)$ denote the common responses of the transmitter and receiver I and Q branch filtering. Based on (3.4) and (3.5), the main effect of I/Q imbalance at complex baseband signal level is that a conjugated version of the ideal signal is showing up. The common responses $c_{TX}(t)$ and $c_{RX}(t)$ do not contribute to the relative strengths of the two signal components ($z(t)$ and $z^{*}(t)$), and are typically dropped, yielding

$$z_{TX}(t) = K_{1,TX}z(t) + K_{2,TX}^{*}z^{*}(t) \tag{3.6}$$

$$z_{RX}(t) = K_{1,RX}z(t) + K_{2,RX}z^{*}(t). \tag{3.7}$$

These are the typical models used in the literature, e.g., [10], [11], [36], [47], [76], [77], [87], [106]–[110], [112]. In link-level developments, on the other hand, the common responses $c_{TX}(t)$ and $c_{RX}(t)$ can also be considered part of the radio channel linking the transmitter and receiver.

In frequency domain, the distortion due to the conjugate signal term corresponds to mirror-frequency interference [106]. This can be seen by taking Fourier transforms (FT) of (3.6) and (3.7) as

$$Z_{TX}(f) = K_{1,TX}Z(f) + K_{2,TX}^{*}Z^{*}(-f) \tag{3.8}$$

$$Z_{RX}(f) = K_{1,RX}Z(f) + K_{2,RX}Z^{*}(-f). \tag{3.9}$$

The corresponding mirror-frequency attenuations L_{TX} and L_{RX} of the individual front-ends are then given by

$$L_{TX} = \frac{\left|K_{1,TX}\right|^2}{\left|K_{2,TX}\right|^2}, \quad L_{RX} = \frac{\left|K_{1,RX}\right|^2}{\left|K_{2,RX}\right|^2} \tag{3.10}$$

which typically range in the order of 25–40dB [5], [26], [58], [74], [75], [108].

3.2 Frequency-Dependent I/Q Imbalance Modeling

In wideband system context, the overall effective I/Q imbalances can easily vary as a function of frequency within the system band, due to e.g. frequency-response differences between the I and Q branch filtering, data conversion and amplification stages. This should also be reflected in the imbalance modeling as well as in imbalance compensation [26], [57], [75]. Using the frequency-independent I/Q imbalance model in (3.3)–(3.9) as a starting point, the frequency-response differences between I and Q branches are modeled here as branch mismatch filters $b_{TX}(t)$ and $b_{RX}(t)$, on the transmitter and receiver sides, respectively, as shown in Figure 3-2. Then if $z(t)$ denotes again the ideal (perfect I/Q balance) complex baseband equivalent signal, the overall baseband equivalent I/Q imbalance models for individual transmitters and receivers appear as

$$\begin{aligned} z_{TX}(t) &= g_{1,TX}(t) * (c_{TX}(t) * z(t)) + g_{2,TX}(t) * (c_{TX}(t) * z(t))^{*} \\ &= c_{TX}(t) * [g_{1,TX}(t) * z(t) + g_{2,TX}(t) * z^{*}(t)] \end{aligned} \tag{3.11}$$

$$\begin{aligned} z_{RX}(t) &= c_{RX}(t) * [g_{1,RX}(t) * z(t) + g_{2,RX}(t) * z^{*}(t)] \\ &= g_{1,RX}(t) * (c_{RX}(t) * z(t)) + g_{2,RX}(t) * (c_{RX}(t) * z(t))^{*}. \end{aligned} \tag{3.12}$$

Here $c_{TX}(t)$ and $c_{RX}(t)$ denote again the common response filtering and the effective impulse responses $g_{1,TX}(t)$, $g_{2,TX}(t)$, $g_{1,RX}(t)$, and $g_{2,RX}(t)$ depend on the actual imbalance properties as

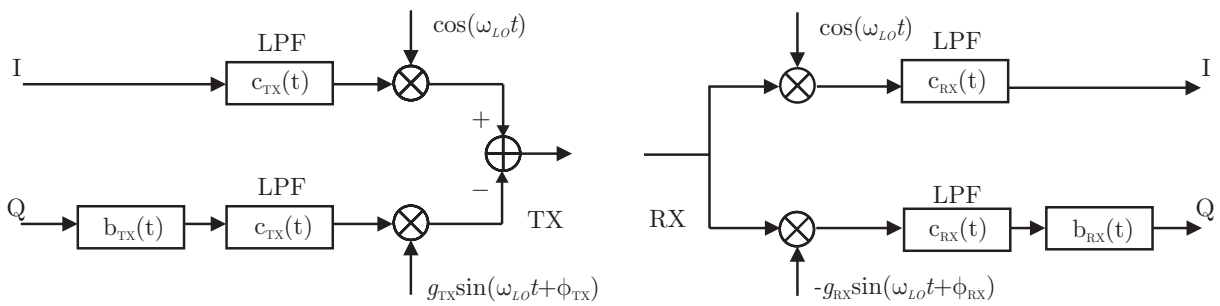

Figure 3-2: *Frequency-dependent I/Q imbalance in TX (left) and RX (right).*

$$\begin{aligned} g_{1,TX}(t) &= (\delta(t) + b_{TX}(t)g_{TX}e^{j\phi_{TX}})/2, \qquad & g_{2,TX}(t) &= (\delta(t) - b_{TX}(t)g_{TX}e^{j\phi_{TX}})/2 \\ g_{1,RX}(t) &= (\delta(t) + b_{RX}(t)g_{RX}e^{-j\phi_{RX}})/2, \qquad & g_{2,RX}(t) &= (\delta(t) - b_{RX}(t)g_{RX}e^{j\phi_{RX}})/2 \end{aligned} \tag{3.13}$$

where $\delta(t)$ denotes impulse function. Similarly as in Section 3.1, the common response does not contribute to the relative strengths of the two signal components, and thus simplified models of the form

$$z_{TX}(t) = g_{1,TX}(t) * z(t) + g_{2,TX}(t) * z^*(t) \tag{3.14}$$

$$z_{RX}(t) = g_{1,RX}(t) * z(t) + g_{2,RX}(t) * z^*(t) \tag{3.15}$$

can be used. Notice that the earlier frequency-independent (instantaneous) I/Q imbalance models of the form $z_{TX}(t) = K_{1,TX}z(t) + K^*_{2,TX}z^*(t)$ and $z_{RX}(t) = K_{1,RX}z(t) + K_{2,RX}z^*(t)$ are obtained as special cases of (3.14) and (3.15) when $b_{TX}(t) = \delta(t)$ and $b_{RX}(t) = \delta(t)$.

Based on the models in (3.14) and (3.15), when viewed in frequency domain, the distortion due to frequency-dependent I/Q imbalance corresponds now to *mirror-frequency interference whose strength varies as a function of frequency*. This can be seen by taking FT of (3.14) and (3.15), yielding [P2]

$$Z_{TX}(f) = G_{1,TX}(f)Z(f) + G_{2,TX}(f)Z^*(-f) \tag{3.16}$$

$$Z_{RX}(f) = G_{1,RX}(f)Z(f) + G_{2,RX}(f)Z^*(-f) \tag{3.17}$$

in which the transfer functions

$$\begin{aligned} G_{1,TX}(f) &= (1 + B_{TX}(f)g_{TX}e^{j\phi_{TX}})\,/\,2, \qquad & G_{2,TX}(f) &= (1 - B_{TX}(f)g_{TX}e^{j\phi_{TX}})\,/\,2 \\ G_{1,RX}(f) &= (1 + B_{RX}(f)g_{RX}e^{-j\phi_{RX}})\,/\,2, \qquad & G_{2,RX}(f) &= (1 - B_{RX}(f)g_{RX}e^{j\phi_{RX}})\,/\,2. \end{aligned} \tag{3.18}$$

Thus, the corresponding mirror-frequency attenuations or image rejection ratios (IRRs) of the individual radio front-ends are now given by

$$L_{TX}(f) = \frac{\left|G_{1,TX}(f)\right|^2}{\left|G_{2,TX}(f)\right|^2}, \quad L_{RX}(f) = \frac{\left|G_{1,RX}(f)\right|^2}{\left|G_{2,RX}(f)\right|^2}. \tag{3.19}$$

With practical analog front-end electronics, these mirror-frequency attenuations are typically in the range of 25–40dB [57], [75], and vary as a function of frequency, when bandwidths in the order of several MHz are considered. An example is given in Figure 3-3 which shows the measured mirror-frequency attenuation characteristics, obtained in comprehensive laboratory test measurements, of state-of-the-art wireless receiver RF-IC operating at 2 GHz. Clearly, for bandwidths in the order of 1–10 MHz, the mirror-frequency attenuation or IRRs (and thus, the effective I/Q imbalances) indeed depend on frequency. Thus the use of frequency-dependent I/Q imbalance modeling is necessary. More detailed information on the IRR measurement setup is given in Appendix.

As a final note, it is illustrative to note already at this stage that the parameterization of the previous models include symmetry of the form

$$\begin{aligned} G_{1,TX}(f) + G_{2,TX}(f) &= 1 \\ G_{1,RX}(f) + G^*_{2,RX}(-f) &= 1. \end{aligned} \tag{3.20}$$

This will be used in some of the forthcoming compensation developments.

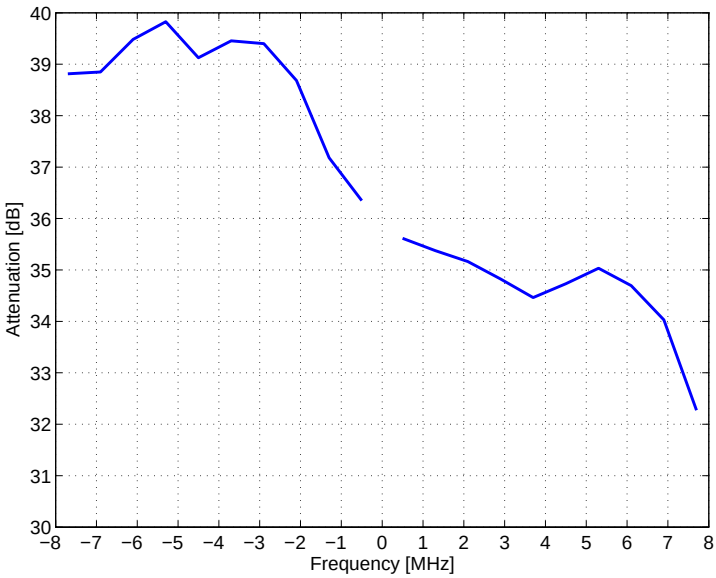

Figure 3-3: *Measured mirror-frequency attenuation of state-of-the-art I/Q receiver RF-IC operating at 2 GHz RF. The x-axis refers to frequencies of the down-converted complex (I/Q) signal, or equivalently, to the frequencies around the LO frequency at RF.*

Chapter 4

Frequency-Independent I/Q Imbalances in Space-Time Coded Single-Carrier Systems

In this chapter, the I/Q imbalance problem is studied in the STC single-carrier system context, focusing on the Alamouti transmit diversity principle [9]. The basic assumption here is that the signal bandwidth is so narrow that both the frequency-responses of transmission channels and the I/Q imbalance properties of individual transmitters and receivers are independent of frequency. In general, this may not be a valid assumption in the future wireless transmission systems where waveform bandwidths in the order of 1–20 MHz are normally assumed [1], [2]. Yet it still forms a good initial study item for understanding the characteristics and behavior of I/Q imbalance in multi-antenna transmission.

4.1 I/Q Signals and System Model

A conceptual block-diagram of the space-time coded single-carrier transmission link used in the following studies is shown in Figure 4-1. For reference and notational convenience, we redefine the ideal combiner output signals given in (2.4) under perfect I/Q balance and zero additive noise as

$$\begin{aligned} y_1^{ideal} &= \sum\nolimits_{i=1}^{N_R} (|h_{1,i}|^2 + |h_{2,i}|^2) s_1 = h_{\text{tot}} s_1 \\ y_2^{ideal} &= \sum\nolimits_{i=1}^{N_R} (|h_{1,i}|^2 + |h_{2,i}|^2) s_2 = h_{\text{tot}} s_2 \end{aligned} \tag{4.1}$$

where $h_{\text{tot}} = \sum\nolimits_{i=1}^{N_R} (|h_{1,i}|^2 + |h_{2,i}|^2)$. Now in order to explore the I/Q mismatch effects on the overall link quality, we apply the I/Q mismatch models of (3.6) and (3.7) to each TX front-end and RX front-end in Figure 4-1. On the transmitter side, the TX symbols are thus effectively distorted according to (3.6). These distorted TX signals propagate then through the channels, and the signals arriving in the receivers are further shaped according to (3.7) in the

individual RX front-ends. Including then also the diversity combining stage (assuming perfect channel knowledge), the overall signal model for the combiner output signals under I/Q imbalance can finally be shown to be [P1], [P4]

$$\begin{aligned} y_1 &= as_1 + bs_1^* + cs_2 + ds_2^* \\ y_2 &= a^*s_2 + b^*s_2^* - c^*s_1 - d^*s_1^* \end{aligned} \tag{4.2}$$

where additive noise has again been ignored for simplicity, and the coefficients a, b, c, d are given by

$$\begin{aligned} a = &\sum\nolimits_{i=1}^{N_R} (\left|h_{1,i}\right|^2 K_{1,RX(i)} K_{1,TX(1)} + \left|h_{2,i}\right|^2 K_{1,RX(i)}^* K_{1,TX(2)}^* \\ &+ (h_{1,i}^*)^2 K_{2,RX(i)} K_{2,TX(1)} + (h_{2,i})^2 K_{2,RX(i)}^* K_{2,TX(2)}^*) \\ b = &\sum\nolimits_{i=1}^{N_R} (\left|h_{1,i}\right|^2 K_{1,RX(i)} K_{2,TX(1)}^* + \left|h_{2,i}\right|^2 K_{1,RX(i)}^* K_{2,TX(2)} \\ &+ (h_{1,i}^*)^2 K_{2,RX(i)} K_{1,TX(1)}^* + (h_{2,i})^2 K_{2,RX(i)}^* K_{1,TX(2)}) \\ c = &\sum\nolimits_{i=1}^{N_R} (h_{1,i}^* h_{2,i} K_{1,RX(i)} K_{1,TX(2)} + h_{1,i}^* h_{2,i}^* K_{2,RX(i)} K_{2,TX(2)} \\ &- h_{1,i}^* h_{2,i} K_{1,RX(i)}^* K_{1,TX(1)}^* - h_{1,i} h_{2,i} K_{2,RX(i)}^* K_{2,TX(1)}^*) \\ d = &\sum\nolimits_{i=1}^{N_R} (h_{1,i}^* h_{2,i} K_{1,RX(i)} K_{2,TX(2)}^* + h_{1,i}^* h_{2,i}^* K_{2,RX(i)} K_{1,TX(2)}^* \\ &- h_{1,i}^* h_{2,i} K_{1,RX(i)}^* K_{2,TX(1)} - h_{1,i} h_{2,i} K_{2,RX(i)}^* K_{1,TX(1)}). \end{aligned} \tag{4.3}$$

Based on (4.2), the I/Q imbalance effect is thus fundamentally different compared to ordinary single-antenna systems. Here the signal is interfered not only by its own complex-conjugate (as in (3.6) and (3.7)) but also by the other information bearing signal (or signals in

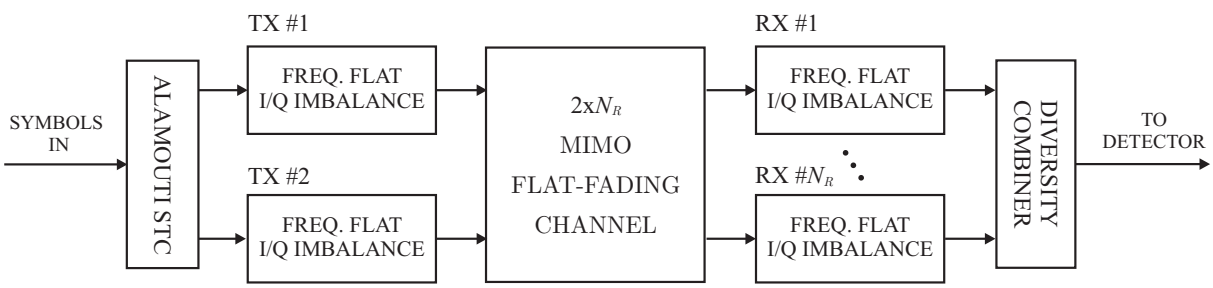

Figure 4-1: *Conceptual model of space-time coded single-carrier transmission link with 2 transmit and N_R receive antennas, including transmitter and receiver front-end I/Q impairments.*

general) in the air during any specific signaling interval. Thus this gives first concrete indication that radio front-end related impairments, such as I/Q imbalance considered here, are likely to play bigger role in multi-antenna systems than in ordinary single-antenna setups.

4.2 Performance Analysis

SIR Analysis

In the following, we analyze the average total SIR at the receiver diversity combiner output due to I/Q imbalance using the signal models of the previous sections. In general, based on (4.2), the total interference consists of the self-interference term as well as of the effect of the other symbol transmitted simultaneously. In the analysis, the natural interference-free reference signals with perfect I/Q balance are $h_{\text{tot}}s_1$ and $h_{\text{tot}}s_2$ as given in (4.1).

Now, consider first the combiner output y_1 in (4.2). We assume that the channel coefficients $h_{1,i}$ and $h_{2,i}$ are mutually statistically independent complex circular Gaussian random variables with zero mean and equal mean power. We also assume that the data symbols s_1 and s_2 are independent of the channel coefficients $h_{1,i}$ and $h_{2,i}$, equal-variance, mutually uncorrelated and circular as well as jointly circular [P1]. In general, these assumptions can be seen rather feasible from the practical data structures (modulation, etc.) point of view. Then based on (4.1) and (4.2), and the above assumptions on the second-order statistics of the data symbols s_1 and s_2, the SIR is defined here as

$$\chi = \frac{E\left[\left|h_{\text{tot}}\right|^2\right]}{E\left[\left|(a-h_{\text{tot}})\right|^2\right] + E\left[\left|b\right|^2\right] + E\left[\left|c\right|^2\right] + E\left[\left|d\right|^2\right]}. \tag{4.4}$$

The idea is that the observation $y_1 = as_1 + bs_1^* + cs_2 + ds_2^* = h_{\text{tot}}s_1 + (a-h_{\text{tot}})s_1 + bs_1^* + cs_2 + ds_2^*$ in which all the other terms except $y_1^{ideal} = h_{\text{tot}}s_1$ are considered interference. Based on (4.1) and (4.2), and the earlier assumptions on s_1, s_2 and $h_{1,i}$, $h_{2,i}$, this is then also the SIR for the second combiner output y_2. Now using the expressions in (4.2) for the system coefficients a, b, c, and d, combined with the previous assumptions on the channel and data statistics, the SIR in (4.4) can finally be written as [P1]

$$\chi = \frac{4{N_R}^2 + 2N_R}{\psi(N_R)} \tag{4.5}$$

in which $\psi(N_R)$ is given by

$$
\begin{aligned}
&\psi(N_R) = \\
&\quad 3\sum_{i=1}^{N_R}\left(\left|K_{1,RX(i)}K_{1,TX(1)}\right|^2 + \left|K^*_{1,RX(i)}K^*_{1,TX(2)}\right|^2 + \left|K_{2,RX(i)}K_{2,TX(1)}\right|^2 + \left|K^*_{2,RX(i)}K^*_{2,TX(2)}\right|^2\right) \\
&+ 3\sum_{i=1}^{N_R}\left(\left|K_{1,RX(i)}K^*_{2,TX(1)}\right|^2 + \left|K^*_{1,RX(i)}K_{2,TX(2)}\right|^2 + \left|K_{2,RX(i)}K^*_{1,TX(1)}\right|^2 + \left|K^*_{2,RX(i)}K_{1,TX(2)}\right|^2\right) \\
&+ 2\sum_{i=1}^{N_R-1}\sum_{j=i+1}^{N_R}\mathrm{Re}[(\left|K_{1,TX(1)}\right|^2 + \left|K_{1,TX(2)}\right|^2 + \left|K_{2,TX(1)}\right|^2 + \left|K_{2,TX(2)}\right|^2)K_{1,RX(i)}K^*_{1,RX(j)}] \\
&+ 2\sum_{i=1}^{N_R}\sum_{\substack{j=1\\ j\neq i}}^{N_R}\mathrm{Re}[K^*_{1,RX(i)}K^*_{1,TX(2)}K^*_{1,RX(j)}K^*_{1,TX(1)} + K_{1,RX(i)}K^*_{2,TX(1)}K_{1,RX(j)}K^*_{2,TX(2)}] \\
&- (4N_R+2)\sum_{i=1}^{N_R}\mathrm{Re}[K_{1,RX(i)}K_{1,TX(1)} + K^*_{1,RX(i)}K^*_{1,TX(2)}] + (4{N_R}^2 + 2N_R).
\end{aligned}
\tag{4.6}
$$

Notice that the SIR in (4.5)–(4.6) is fully determined by the imbalance coefficients and the number of receivers, and can be directly evaluated for any possible imbalance scenario and number of receivers without any link simulations.

Numerical Examples and Simulations

As a simple numerical example (for $N_R = 1$), with 5% and –5º receiver imbalances and transmitter imbalances of 4% and 4º (TX1) and 3% and 3º (TX2), the average SIR at the combiner output is 20.2dB, as can be evaluated using (4.5) and (4.6). Notice that based on (3.10), the individual analog front-end image attenuations are roughly 26.0dB (RX), 27.9dB (TX1), and 30.4dB (TX2). Thus the SIR figure of 20.2dB is really *considerably lower* than what might have been expected by considering the qualities of the individual analog front-ends alone. Especially with higher-order spectrally efficient modulation methods, such as 16 phase shift keying (PSK) or 64 quadrature amplitude modulation (QAM), this results in a severe reduction in the system noise margin.

Closer examination of the previous results in (4.5) and (4.6) indicates some further interesting aspects in assessing the role of I/Q imbalance in multi-antenna systems. One interesting issue is the role of *relative signs* between the phase imbalance values $\phi_{TX(1)}$, $\phi_{TX(2)}$ and $\phi_{RX(i)}$, $i = 1,2,\ldots,N_R$. More specifically, based on (4.5) and (4.6), the resulting SIR does not depend only on the absolute values of the imbalances. As a concrete example with $N_R = 2$, some resulting numerical SIR values are shown in Table 4-1, obtained here with fixed absolute imbalance levels and by just changing the relative signs of $\phi_{TX(1)}$, $\phi_{TX(2)}$, $\phi_{RX(1)}$ and $\phi_{RX(2)}$. Notice that the image attenuations of the individual analog front-ends are identical in all the three cases. It implies that traditional I/Q imbalance analysis using the

image attenuations of the individual front-ends alone is *insufficient* from the overall link quality point of view. More details and illustrations are given in [P1].

Next, to get further visual justification for the reported SIR figures, a link simulator is implemented, with I/Q impairments included, and the achievable link performance is then simulated. The obtained SER as a function of average received SNR at the detector input (defined as the ratio of the average useful signal power and average noise power after diversity combining) is examined in these three imbalance cases described in Table 4-1. As predicted by the SIR values in Table 4-1, the cases with different phase imbalance signs result in considerably different error rate performance. Notice also that since the distribution of the interference is not exactly Gaussian, the derived SIR cannot necessarily be directly mapped to the lowest achievable detection error probability. However, based on the computer simulation results reported in Figure 4-2, the SIR values do indeed predict, especially in cases 2 and 3 with good accuracy, *the error rate floors* when compared against the perfectly matched reference system performance at the corresponding additive white Gaussian noise SNR at detector input. Also, when evaluated at the raw (uncoded) SER levels of 10^{-1} and 10^{-2}, which are of practical interest in most systems before error-control decoding, the degradation due to I/Q imbalance is roughly 1dB to 2.5dB at 10^{-1} and already 2dB to almost 15dB at 10^{-2}. It is obvious that this kind of performance losses are *unacceptable* in any practical system, and thus signal enhancement through efficient compensation processing is needed.

TABLE 4-1: EXAMPLE OF THE INFLUENCE OF PHASE IMBALANCE SIGN ON THE TOTAL AVERAGE SIR DUE TO I/Q IMBALANCE IN A 2X2 STC SINGLE-CARRIER SYSTEMS.

	Imbalance Values				SIR [dB]
	TX1	TX2	RX1	RX2	
Case 1	4%, 4°	3%, 3°	5%, 5°	5%, 5°	26.0
Case 2	4%, 4°	3%, 3°	5%, 5°	5%, –5°	23.8
Case 3	4%, –4°	3%, –3°	5%, 5°	5%, 5°	22.4

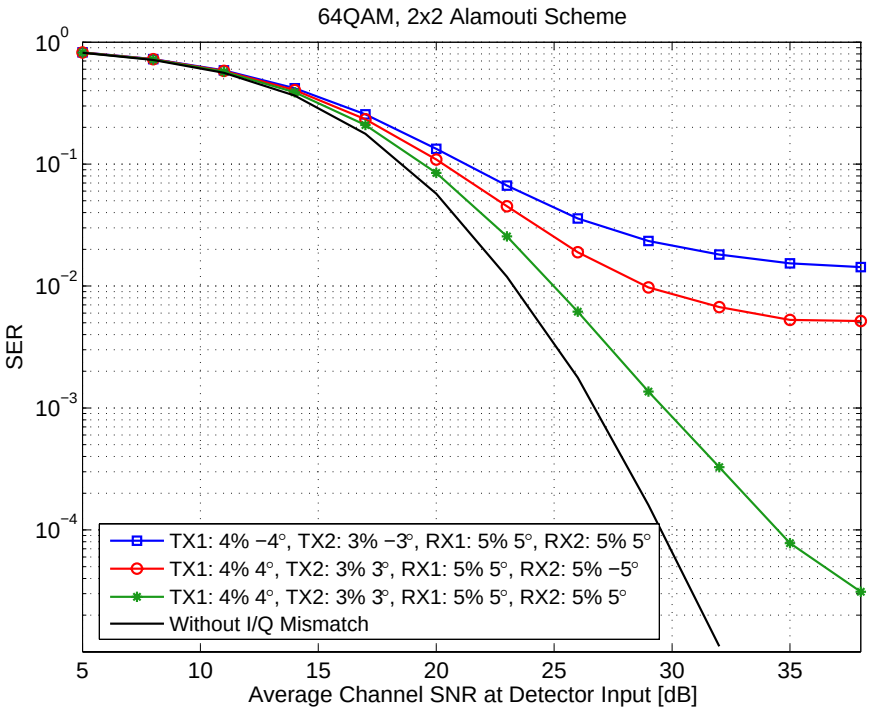

Figure 4-2: *Simulated detection error rate for 64QAM 2x2 Alamouti STC system with three different imbalance values (different phase imbalance signs). Also shown for reference is the corresponding perfectly matched system performance.*

4.3 I/Q Imbalance Compensation Techniques

Compensation Philosophy

One possible way of approaching the imbalance compensation is to consider the I/Q matching of each individual front-end separately. This being the case, any of the earlier proposed compensation techniques targeted for single-antenna systems could basically be applied [10]–[12], [15], [36], [52], [54], [55], [76]–[78], [85], [89], [95], [104]–[110], [112], [113]. However, even with two transmit and two receive antennas, there are already four radio front-ends, thus basically calling for four compensators if treated separately. The implementation complexity may thus grow rapidly with the increased number of antennas. Here, we take an alternative approach and try to mitigate the interference and distortion due to I/Q imbalances of each transmitter and receiver *jointly* on the receiver side, operating on the combiner output signal. As will be shown in the following, this approach has one crucial practical benefit of being able to also compensate for the errors and signal distortion due to channel estimation errors, at zero extra cost. This is seen very important from any practical system point of view, since channel estimation errors are anyway inevitable due to additive channel noise already.

Pilot-Based Compensation

Most of the practical communications systems include certain known data structures in their transmission frames, called training or pilot signals. These are typically used, e.g., for channel estimation and synchronization purposes. Here, we also assume that such a pilot or training period is available. More specifically, for imbalance compensation purposes, we assume that there are at least two known STC blocks (called slots hereafter), over which we set the transmit data according to [P1]

$$s_1^{(1)} = s_P,\, s_2^{(1)} = s_P^*,\, s_1^{(2)} = s_P,\, s_2^{(2)} = s_P. \tag{4.7}$$

Here, s_p refers to the known pilot symbol which is one of the design "parameters" in the continuation and superscripts $^{(1)}$ and $^{(2)}$ refer to the two pilot blocks which as a whole form one pilot slot. Denoting the resulting four observations by $y_{1,p}$, $y_{2,p}$, $y_{3,p}$, and $y_{4,p}$, this yields a well-behaved 4×4 set of linear equations of the form $\mathbf{y}_p = \mathbf{S}_p\boldsymbol{\theta}$ where $\mathbf{y}_p = [y_{1,p},\, y_{2,p}^*,\, y_{3,p},\, y_{4,p}^*]^T$, $\boldsymbol{\theta} = [a\ b\ c\ d]^T$, and

$$\mathbf{S}_p = \begin{bmatrix} s_p & s_p^* & s_p^* & s_p \\ s_p & s_p^* & -s_p^* & -s_p \\ s_p & s_p^* & s_p & s_p^* \\ s_p^* & s_p & -s_p^* & -s_p \end{bmatrix}. \tag{4.8}$$

This follows directly from (4.2) and (4.7). Thus clearly, since $\det(\mathbf{S}_p) = 2(s_p^2 - (s_p^*)^2)^2$, the "system" matrix $\mathbf{S}_p$ in (4.8) is nonsingular and the unknown coefficient vector $\boldsymbol{\theta} = [a\ b\ c\ d]^T$ can be solved uniquely as $\hat{\boldsymbol{\theta}} = \mathbf{S}_p{}^{-1}\mathbf{y}_p$, given that $s_p^2 \neq (s_p^*)^2$. This, in turn, is trivially true given that the training symbol s_p is not purely real or purely imaginary. After estimating the model coefficients $\hat{\boldsymbol{\theta}} = [\hat{a}\ \hat{b}\ \hat{c}\ \hat{d}]^T$, the actual payload (information-bearing) data can then be estimated easily based on (4.2). Within one STC block with data symbols s_1 and s_2, the compensator outputs can formally be solved from $\mathbf{y} = \boldsymbol{\Phi}\mathbf{s}_c$ where $\mathbf{y} = [y_1,\, y_1^*,\, y_2,\, y_2^*]^T$, $\mathbf{s}_c = [s_1,\, s_1^*,\, s_2,\, s_2^*]^T$, and

$$\boldsymbol{\Phi} = \begin{bmatrix} \hat{a} & \hat{b} & \hat{c} & \hat{d} \\ \hat{b}^* & \hat{a}^* & \hat{d}^* & \hat{c}^* \\ -\hat{c}^* & -\hat{d}^* & \hat{a}^* & \hat{b}^* \\ -\hat{d} & -\hat{c} & \hat{b} & \hat{a} \end{bmatrix}. \tag{4.9}$$

In (4.9), $\hat{a}$, $\hat{b}$, $\hat{c}$, and $\hat{d}$ refer to the estimated coefficients. Here, instead of full inversion of $\boldsymbol{\Phi}$ ($\hat{\mathbf{s}}_c = \boldsymbol{\Phi}^{-1}\mathbf{y}$), $\mathbf{y} = \boldsymbol{\Phi}\mathbf{s}_c$ needs to be solved only for $[\mathbf{s}_c]_1 = \hat{s}_1$ and $[\mathbf{s}_c]_3 = \hat{s}_2$, which together

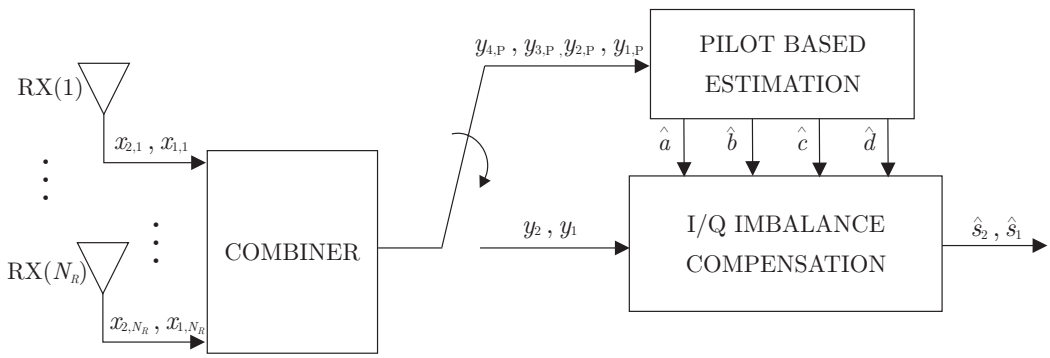

Figure 4-3: *Pilot-based compensation structure.*

with the obvious symmetry in (4.9), results in big savings in the computational complexity [P1]. The overall compensation idea is further illustrated graphically in Figure 4-3 at a conceptual-level. The effects of additive noise together with other practical aspects will be further discussed and addressed in Section 4.4.

Blind Compensation Using Blind Signal Separation (BSS)

Instead of relying on the availability of the known pilot signals, another interesting approach is to address the imbalance compensation using blind signal estimation techniques. In general, the so-called blind signal separation (BSS) task deals with recovering some interesting signals, based on observing their linear mixtures only. Typically the strong assumption of *statistical independence* of the assumed source signals is used, to form the basis for the actual signal estimation algorithms [21], [22], [39].

In our context, as shown in (4.2) the observed data y_1 and y_2 appear as linear combinations of four formal source signals s_1, s_1^*, s_2, and s_2^*. However, this viewpoint does not lend itself very well to the general blind signal estimation since the conjugated signal pairs are obviously statistically dependent. Notice that the circularity assumption ($E[s_i^2(t)] = 0$) actually does imply that s_i and s_i^* are indeed mutually uncorrelated, but this second-order statistics is yet insufficient here alone for blind signal recovery. We can, however, view the observed complex signals y_1 and y_2 in (4.2) in terms of their I and Q components, resulting in four real-valued observations $y_{1,I} = \mathrm{Re}[y_1]$, $y_{1,Q} = \mathrm{Im}[y_1]$, $y_{2,I} = \mathrm{Re}[y_2]$ and $y_{2,Q} = \mathrm{Im}[y_2]$. Using a similar approach for the formal source signals s_1 and s_2, results in the following 4×4 real-valued signal model of the form $\mathbf{y}_{IQ} = \mathbf{H}_{IQ}\mathbf{s}_{IQ}$ [P1] where $\mathbf{y}_{IQ} = [y_{1,I}, y_{1,Q}, y_{2,I}, y_{2,Q}]^T$, $\mathbf{s}_{IQ} = [s_{1,I}, s_{1,Q}, s_{2,I}, s_{2,Q}]^T$, and

$$\mathbf{H}_{IQ} = \begin{bmatrix} \mathrm{Re}(a+b) & -\mathrm{Im}(a-b) & \mathrm{Re}(c+d) & -\mathrm{Im}(c-d) \\ \mathrm{Im}(a+b) & \mathrm{Re}(a-b) & \mathrm{Im}(c+d) & \mathrm{Re}(c-d) \\ -\mathrm{Re}(c+d) & \mathrm{Im}(c-d) & \mathrm{Re}(a+b) & -\mathrm{Im}(a-b) \\ -\mathrm{Im}(c+d) & -\mathrm{Re}(c-d) & \mathrm{Im}(a+b) & \mathrm{Re}(a-b) \end{bmatrix}. \tag{4.10}$$

Now assuming that the I and Q components of the data symbols are all mutually independent, the source signals $\mathbf{s}_{IQ}$ can be blindly estimated based on observed data $\mathbf{y}_{IQ}$. This assumed independence of I and Q, in turn, basically holds for any of the standard QAM type symbol constellations and also up to a certain degree to PSK type constellations (see the discussions in single-input single-output context in [107] and [109]). Notice that since the model $\mathbf{y}_{IQ} = \mathbf{H}_{IQ}\mathbf{s}_{IQ}$ holds for any pair of two consecutive data symbols, any BSS algorithms can basically be applied [P1]. For example, the well-known equivariant adaptive separation via independence (EASI) algorithm [21] can be used in implementing the separation stage. Denoting the separator coefficients at discrete-time index n by $\mathbf{B}_{IQ}(n)$, the formal output of the compensator is simply $\hat{\mathbf{s}}_{IQ}(n) = \mathbf{B}_{IQ}(n)\mathbf{y}_{IQ}(n)$. One iteration of the coefficient adaptation using the EASI algorithm is then given by [21]

$$\begin{aligned} \mathbf{B}_{IQ}(n+1) &= \mathbf{B}_{IQ}(n) \\ &- \mu\Big[\frac{\hat{\mathbf{s}}_{IQ}(n)\hat{\mathbf{s}}_{IQ}(n)^T - \mathbf{I}}{1+\mu\hat{\mathbf{s}}_{IQ}(n)^T\hat{\mathbf{s}}_{IQ}(n)} + \frac{\mathrm{g}(\hat{\mathbf{s}}_{IQ}(n))\hat{\mathbf{s}}_{IQ}(n)^T - \hat{\mathbf{s}}_{IQ}(n)\,\mathrm{g}(\hat{\mathbf{s}}_{IQ}(n))^T}{1+\mu\left|\hat{\mathbf{s}}_{IQ}(n)^T\,\mathrm{g}(\hat{\mathbf{s}}_{IQ}(n))\right|}\Big]\mathbf{B}_{IQ}(n) \end{aligned} \tag{4.11}$$

where μ is the adaptation step-size and $\mathrm{g}(\cdot)$ is a memoryless nonlinear function which is typically selected based on the assumed source statistics. For more details on the algorithm and signal separation in general, refer to [21]. The overall compensation idea is further illustrated graphically in Figure 4-4 at a conceptual-level.

In general, the blind signal separation task has two indeterminacies - the order and scaling of the output signals [21], [22], [39]. Here, however, the structure of the effective mixing matrix in (4.10) is such that the diagonal elements are an order of magnitude larger (in absolute values) compared to the off-diagonal elements, and thus in practice, the separator always converges towards the correct ordering of the source signals. Using (4.11), see also [21], the variance of the output components, in turn, is essentially fixed to unity, and thus proper scaling of the estimated I and Q components can be restored simply based on the known variance of the used data constellation. Thus it can be concluded that the typical permutation and scaling problems related to BSS in general are here avoided, which is seen very important for practical applications [P1].

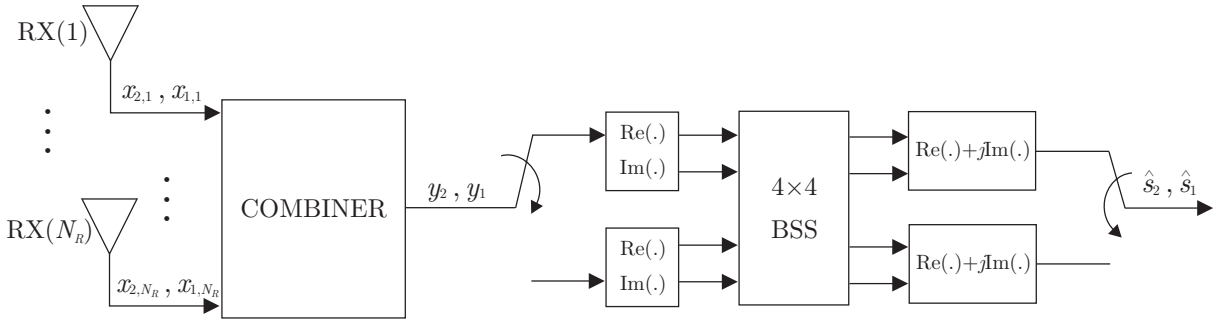

Figure 4-4: *Blind I/Q signal separation based compensation structure.*

4.4 Practical Aspects and Examples

Additive Noise

One important practical aspect in any communication system is the presence of additive noise. This aspect is especially critical for the pilot-based approach, where the coefficient estimation accuracy is obviously affected. However, using simple averaging over a few consecutive training slots can diminish the effects of the noise considerably [P1]. The noise obviously has some influence also on the BSS based compensator, but since the whole idea is based on directly estimating the data signals instead of any parameters of a parametric model, the resulting performance is not expected to be seriously degraded at reasonable noise levels [P1].

Channel Profile and Estimation Errors

Another crucial aspect here is the role of the channel coefficients. The basic starting point in the whole transmission concept is the assumption that the channel is time-invariant at least over two consecutive signaling intervals. In the compensation context, since the model coefficients in (4.3) depend on the channel properties, a time-invariant channel needs to be assumed over a long block of data. Thus a very rapidly fading channel can be seen as one practical limitation of the proposed techniques. In general, this type of "block-fading" assumptions are, however, rather typical in most system and algorithm level developments in the literature.

In practice, with or without imbalance, the accuracy of the channel estimates is also critical from the system performance point of view. In general, both I/Q imbalance and additive noise complicate the channel estimation task, resulting in errors in the estimated channel coefficients. The use of incorrect channel coefficients in the diversity combining, in turn,

results in a formally identical signal model as in (4.2) but with modified values for the system coefficients a , b , c , and d [P1]. However, since both compensators are essentially estimating these coefficients, either explicitly or implicitly, the compensated system performance is not expected to be affected by the errors in channel estimation. Thus, by design, both proposed compensation techniques are not only robust against channel estimation errors but actually also compensate for their effects together with the I/Q impairments [P1].

In practice, the channel coefficients $h_{1,i}$ and $h_{2,i}$ can easily be estimated using the given pilot allocation in (4.7). Under the first pilot block, the individual received signal at receiver *i* is given by (noise ignored for notational simplicity)

$$\begin{aligned} x_{1,i,p}^{(1)} &= h_{1,i}s_P + h_{2,i}s_P^* \\ x_{2,i,p}^{(1)} &= -h_{1,i}s_P + h_{2,i}s_P^* \end{aligned} \tag{4.12}$$

Given that $s_P \neq 0$, this set of linear equations can always be solved for $h_{1,i}$ and $h_{2,i}$, as is easy to verify [P1]. This type of channel estimator will be explored in more details (e.g. estimation performance under noise and imbalances) in [P1] and in Chapter 5 in multi-carrier STC context [P2].

Frequency Offset

One additional practical problem is related to carrier frequency synchronization. This is especially important here since the compensator is operating on the combined front-end signals. In general, the carrier frequency offset (CFO) is stemming from the frequency inaccuracy of the used oscillator(s) and the mobility of the user terminals. As a result, there is a frequency difference between the assumed center-frequency of the received signals and the used LO frequency in the receiver, which can easily degrade the system performance. Under both CFO $\Delta\omega$ and I/Q imbalances, the simple CFO compensation procedure widely used in the literature (first estimating $\Delta\omega$ and then de-rotating the signal with $e^{-j\Delta\omega t}$) is coupled with the imbalance characteristics. As discussed in [P1], after de-rotating the individual receiver signals, the effective system coefficients a , b , c , and d (describing the combiner output under CFO and de-rotation) become time-varying (oscillating). This, of course, complicates then also the actual imbalance compensation task. Thus in this sense, it is fair to say that using separate I/Q imbalance compensators operating individually on each of the transmitters and receivers front-ends would offer more robustness against carrier frequency offsets, compared to the joint compensation approach used here. It should be noted, however, that with practical imbalance levels, the range of the system coefficients a , b , c , and d

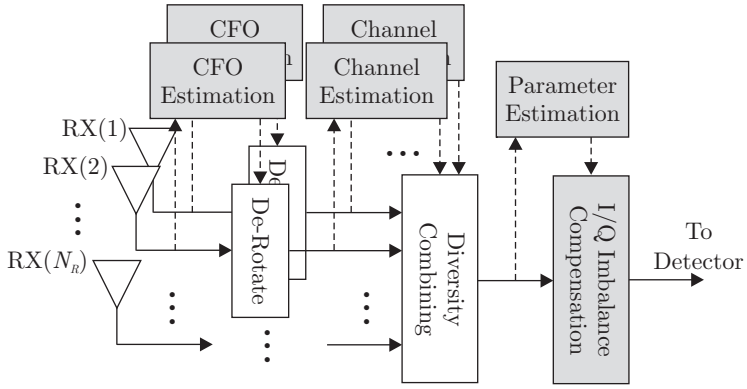

Figure 4-5: *Receiver structure including (i) CFO estimation and de-rotation,(ii) channel estimation and diversity combining, and (iii) I/Q imbalance parameter estimation and compensation, all using the designed pilot structure in (4.7).*

within which the time-variations due to CFO de-rotation occur is fairly limited, and thus with some averaging in the compensator parameter estimation stage, reliable compensation is still obtained [P1]. The overall compensation structure with both CFO compensation and channel estimation is finally illustrated in Figure 4-5. Notice also that a simple yet efficient CFO estimator for individual receivers is developed in [P1], stemming from the used the pilot structure in (4.7).

Numerical Examples and Simulations

Here the detection error rate performance of the compensated system under *additive noise* and *practical channel estimation* is briefly demonstrated using link simulations, including both the training based as well as blind compensation methods. The results are shown in Figure 4-6 and Figure 4-7. The "intermediate" case of the previously demonstrated imbalance values (4% and 4º (TX1), 3% and 3º (TX2), 5% and 5º (RX1), 5% and –5º (RX2)) is used to model a typical example case. In the legends, the terms "w/o" and "w/" are abbreviations of "without" and "with", respectively. Different numbers of pilot slots are tested in Figure 4-6 and the upper-right corner symbol ("$7 + 7j$") from the 64QAM constellation is selected as the used pilot symbol. In Figure 4-7, the adaptation step-size μ of the blind algorithm (BSS-based compensator) is selected such that convergence is established in 3 000–4 000 iterations when updated using (4.11). At the input of the BSS stage, the average received signal level is normalized to unit power. For both simulations, a quasi-static system model is also assumed in the sense that the channels are assumed fixed over 10000 consecutive symbol intervals, after which new channel coefficients are drawn independently. In general, virtually all the signal distortion due to I/Q imbalance can be efficiently removed using either of the proposed

techniques, the error rate performance being within 0.2dB of the perfectly matched reference. Both algorithms are also rather robust to the channel estimation errors since the perfectly matched reference performance is obtained with perfect channel estimation.

Additional link simulations are carried out with CFO of roughly 1% of the symbol rate included in the receiver front-ends. The obtained results are shown in Figure 4-8 and Figure 4-9. In the pilot-based compensator, averaging over multiple pilot slots results in compensator coefficients corresponding to the average system coefficients. Similar averaging effect is also taking place implicitly in the BSS compensator since the dynamics of the EASI algorithm with the used step-size is much slower than the time-variation rate of the system coefficients. Processing the received data then with these "average" coefficients cannot, of course, yield perfect compensation but is clearly seen to work, the performance difference being within 1dB or so when compared to the previous simulations without carrier offsets.

Overall, the computer simulation results demonstrate that the proposed principles can provide good compensation performance under very realistic signaling assumptions. Also the computational complexity of both techniques is feasible for already today's state-of-the-art digital signal processing implementations. Thus, they are generally feasible compensation approaches in practical signal environments.

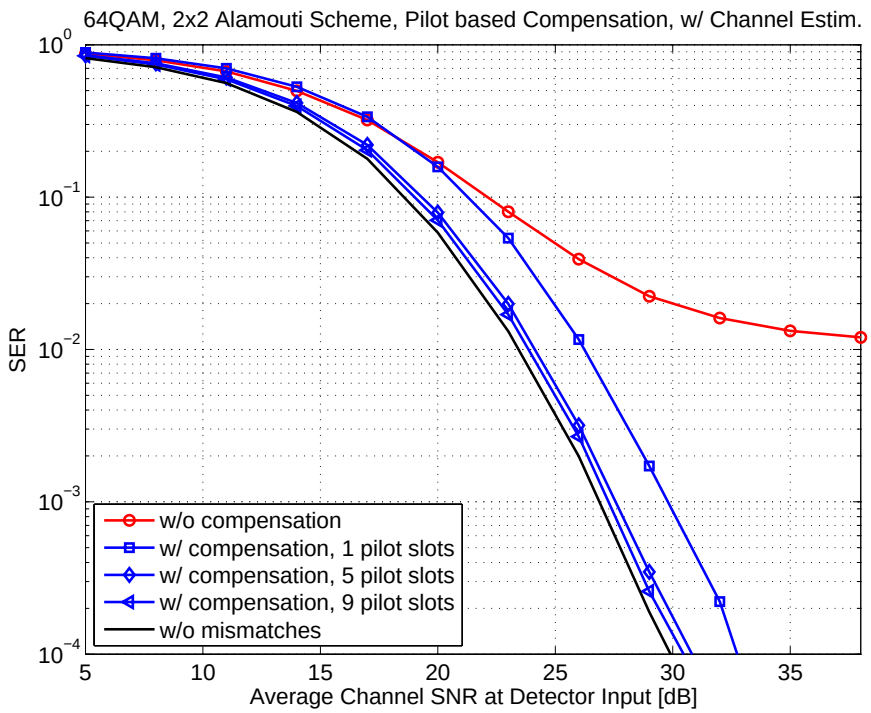

Figure 4-6: *Average symbol error rate (SER) performance of the pilot-based imbalance compensator including practical channel estimation for diversity combining. Perfectly matched reference curve is also shown assuming no I/Q imbalances and perfect channel estimation.*

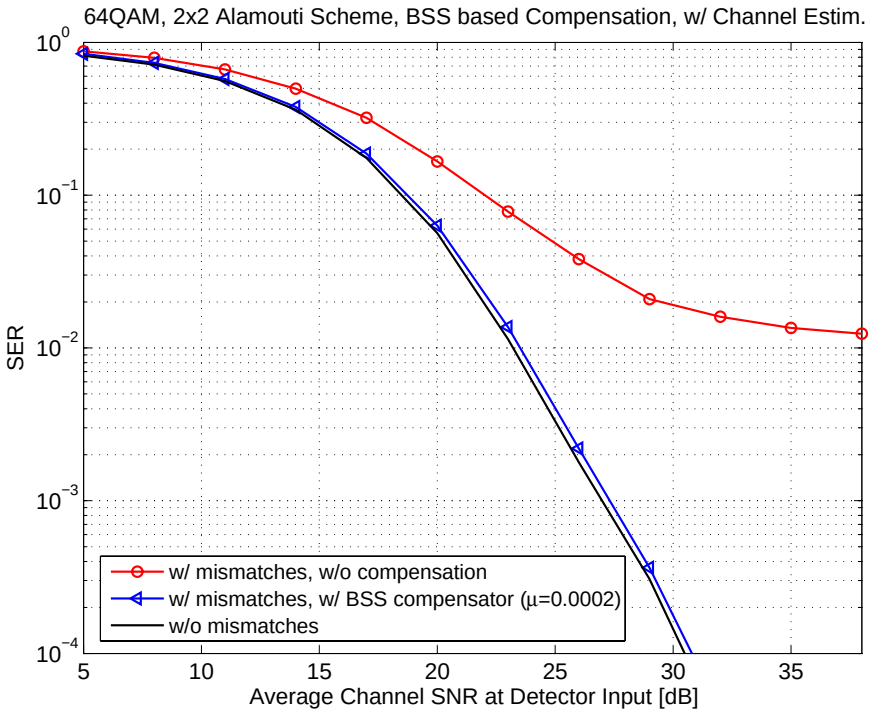

Figure 4-7: *Average symbol error rate (SER) performance of the blind signal separation based imbalance compensator including practical channel estimation for diversity combining. Perfectly matched reference curve is also shown assuming no I/Q imbalances and perfect channel estimation.*

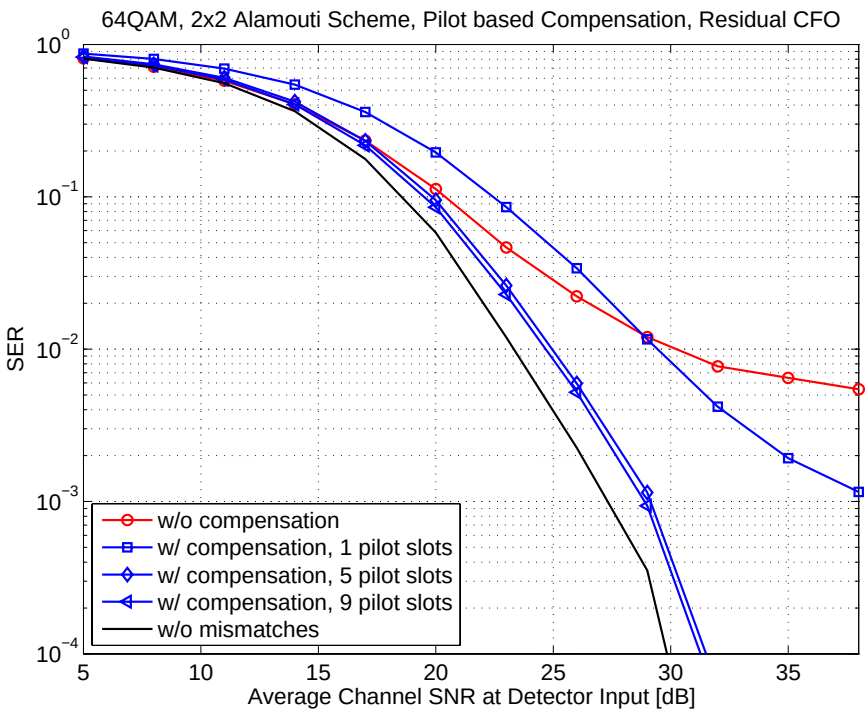

Figure 4-8: *Average symbol error rate (SER) performance of the pilot-based imbalance compensator with ~1% carrier frequency offset in the receivers. Perfectly matched reference curve is also shown assuming no I/Q imbalances and perfect synchronization.*

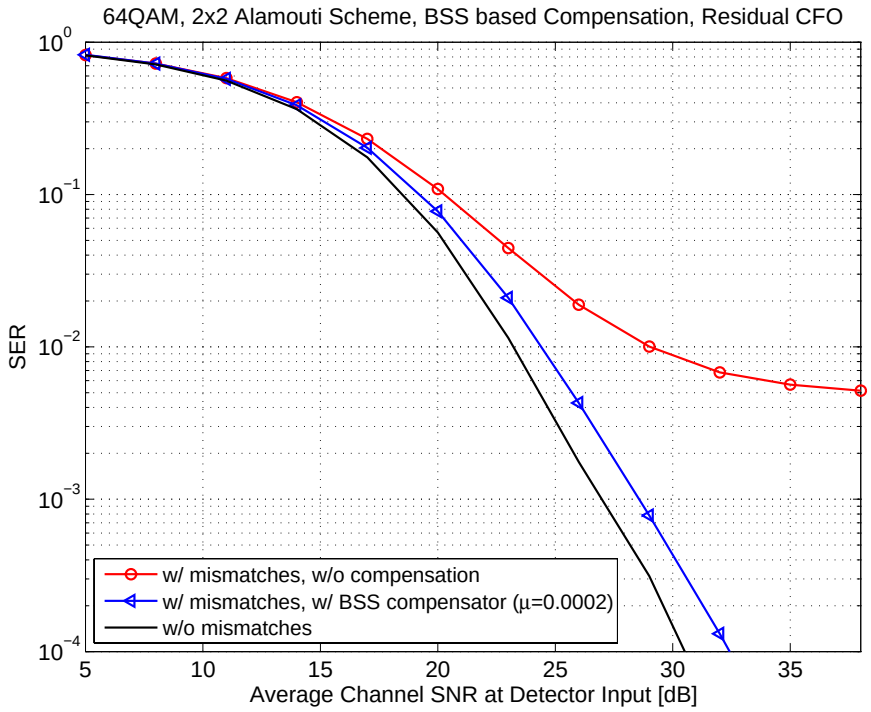

Figure 4-9: *Average symbol error rate (SER) performance of the blind signal separation based imbalance compensator with ~1% carrier frequency offset in the receivers. Perfectly matched reference curve is also shown assuming no I/Q imbalances and perfect synchronization.*

Chapter 5

Frequency-Selective I/Q Imbalances in Space-Time Coded Multi-Carrier Systems

The combination of multi-antenna transmission and multi-carrier modulation is generally seen as one of the most important physical layer techniques for future wireless systems. However with waveform and radio bandwidths in the order of 1–20 MHz and beyond [1], [2], not only the frequency-responses of physical radio channels but also the I/Q imbalances of radio transceivers are likely to be frequency-selective. Thus, both performance analysis and digital compensation of the resulting link performance degradation due to I/Q imbalances should reflect this frequency-selectivity as well.

5.1 I/Q Signals and System Model

Conceptual-level block-diagram of a space-time coded multi-carrier transmission link under study with 2 transmit antennas and N_R receive antennas is depicted in Figure 5-1. The OFDM MOD and OFDM DEMOD blocks implement OFDM waveform generation and demodulation operations illustrated earlier in Figure 2-4. The overall data transmission at any specific subcarrier k is described by (2.8), assuming ideal radio transmitters and receivers. For readability, this is reproduced here as

$$\begin{aligned} y_1^{ideal}(k) &= \sum_{i=1}^{N_R}(\left|H_{1,i}(k)\right|^2 + \left|H_{2,i}(k)\right|^2)s_1(k) = H_T(k)s_1(k) \\ y_2^{ideal}(k) &= \sum_{i=1}^{N_R}(\left|H_{1,i}(k)\right|^2 + \left|H_{2,i}(k)\right|^2)s_2(k) = H_T(k)s_2(k) \end{aligned} \tag{5.1}$$

where $s_1(k)$ and $s_2(k)$ denote the two consecutive data symbols transmitted over the k-th subcarrier, $H_{1,i}(k)$ and $H_{2,i}(k)$ denote the channel frequency-responses (TX(1)→RX(i) and TX(2)→RX(i)) at subcarrier k, $H_T(k) = \sum_{i=1}^{N_R}(\left|H_{1,i}(k)\right|^2 + \left|H_{2,i}(k)\right|^2)$ and additive channel

noise has been ignored for notational simplicity. Incorporating next the general frequency-selective TX and RX I/Q impairment models in (3.16) and (3.17) into the considered STC-OFDM system setup, the corresponding observations at the output of the receiver diversity combining stage at subcarrier k can be shown to be of the form [P2]

$$\begin{aligned} y_1(k) &= a(k)s_1(k) + b(k)s_1^*(-k) + c(k)s_2(k) + d(k)s_2^*(-k) \\ y_2(k) &= a^*(k)s_2(k) + b^*(k)s_2^*(-k) - c^*(k)s_1(k) - d^*(k)s_1^*(-k). \end{aligned} \tag{5.2}$$

The exact expressions for the imbalanced system coefficients $a(k)$, $b(k)$, $c(k)$ and $d(k)$, as functions of the individual transmitter and receiver imbalance properties ($G_{1,TX(j)}(k)$, $G_{2,TX(j)}(k)$, $j = 1,2$ and $G_{1,RX(i)}(k)$, $G_{2,RX(i)}(k)$, $i = 1,2,...,N_R$) are given in (5.2) below by combining (3.16), (3.17) and (2.8) as

$$\begin{aligned} a(k) = \sum_{i=1}^{N_R} (&\left|H_{1,i}(k)\right|^2 G_{1,RX(i)}(k)G_{1,TX(1)}(k) + H_{1,i}^*(k)H_{1,i}^*(-k)G_{2,RX(i)}(k)G_{2,TX(1)}^*(-k) \\ &+\left|H_{2,i}(k)\right|^2 G_{1,RX(i)}^*(k)G_{1,TX(2)}^*(k) + H_{2,i}(k)H_{2,i}(-k)G_{2,RX(i)}^*(k)G_{2,TX(2)}(-k)) \end{aligned}$$

$$\begin{aligned} b(k) = \sum_{i=1}^{N_R} (&\left|H_{1,i}(k)\right|^2 G_{1,RX(i)}(k)G_{2,TX(1)}(k) + H_{1,i}^*(k)H_{1,i}^*(-k)G_{2,RX(i)}(k)G_{1,TX(1)}^*(-k) \\ &+\left|H_{2,i}(k)\right|^2 G_{1,RX(i)}^*(k)G_{2,TX(2)}^*(k) + H_{2,i}(k)H_{2,i}(-k)G_{2,RX(i)}^*(k)G_{1,TX(2)}(-k)) \end{aligned}$$

$$\begin{aligned} c(k) = \sum_{i=1}^{N_R} (&H_{1,i}^*(k)H_{2,i}(k)G_{1,RX(i)}(k)G_{1,TX(2)}(k) + H_{1,i}^*(k)H_{2,i}^*(-k)G_{2,RX(i)}(k)G_{2,TX(2)}^*(-k) \\ &-H_{1,i}^*(k)H_{2,i}(k)G_{1,RX(i)}^*(k)G_{1,TX(1)}^*(k) - H_{1,i}(-k)H_{2,i}(k)G_{2,RX(i)}^*(k)G_{2,TX(1)}(-k)) \end{aligned}$$

$$\begin{aligned} d(k) = \sum_{i=1}^{N_R} (&H_{1,i}^*(k)H_{2,i}(k)G_{1,RX(i)}(k)G_{2,TX(2)}(k) + H_{1,i}^*(k)H_{2,i}^*(-k)G_{2,RX(i)}(k)G_{1,TX(2)}^*(-k) \\ &-H_{1,i}^*(k)H_{2,i}(k)G_{1,RX(i)}^*(k)G_{2,TX(1)}^*(k) - H_{1,i}(-k)H_{2,i}(k)G_{2,RX(i)}^*(k)G_{1,TX(1)}(-k)). \end{aligned} \tag{5.3}$$

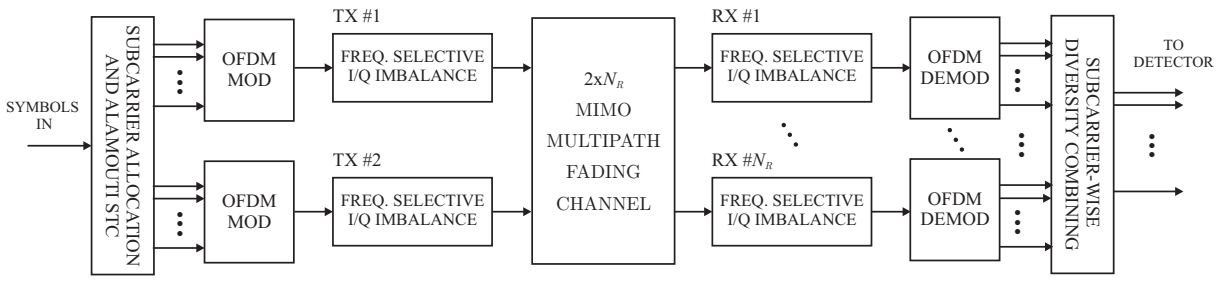

Figure 5-1: *Conceptual model of space-time coded multi-carrier transmission link with 2 transmit and N_R receive antennas, including transmitter and receiver front-end I/Q impairments.*

In general, based on (5.2), the observations at any individual subcarrier k are interfered by the conjugate of the data at the corresponding mirror-carrier $-k$ as well as by the other data symbol within the STC block at subcarriers k and $-k$. Assuming independent subcarrier data streams, the combiner outputs thus appear as weighted linear combinations of 4 independent data symbols, while in the corresponding STC single-carrier system addressed in Section 4.1, there are only two independent data symbols and their own complex-conjugates. This has rather big impact on the distribution of the overall interference, and is thus important when carrying out the statistical interference analysis in the following. Another difference lies in the structure of the coefficients $a(k)$, $b(k)$, $c(k)$ and $d(k)$ which, for any subcarrier k, are influenced also by the channel frequency-responses and I/Q imbalance properties at the mirror-subcarrier $-k$. These aspects will be quantified and demonstrated in details by both analysis as well as computer simulations in the next sections.

5.2 Performance Analysis

SIR Analysis

In the following, we analyze and quantify the amount of signal distortion due to I/Q imbalance in terms of SIR at the receiver diversity combiner output using the signal models of the previous section. Again, opposed to traditional imbalance analysis focusing on individual radios, this SIR represents a link-level performance measure describing *the combined impact* of individual imperfections to the overall data transmission (from TX symbols to RX detector input) in the STC-OFDM context.

In the analysis, stemming from the WSSUS channel modeling discussed in Section 2.5, L-tap frequency-selective multipath radio channels are assumed, with the individual taps being modeled as independent circular complex Gaussian random variables with zero mean and power-delay profile $\mathbf{P} = [P(0), P(1), ..., P(L-1)]^T$ in which $P(l)$ denotes the average power of the l-th tap. Based on this, it is easy to show that the channel frequency-responses $H_{1,i}(k)$ and $H_{2,i}(k)$ at any subcarrier k are also complex circular Gaussian random variables with zero mean and equal mean power $E[|H_{1,i}(k)|^2] = E[|H_{2,i}(k)|^2] = P_H$ and derive further statistical properties (addressed in detail in [P2]) which simplify the following analysis. Now consider the first combiner output $y_1(k)$ in (5.2) consisting of the four signal terms. The ideal interference-free reference signal given in (5.1) is $y_1^{ideal}(k) = H_T(k)s_1(k)$. Including then amplitude restoration by $1 / H_T(k)$ to both $y_1(k)$ and $y_1^{ideal}(k)$, and assuming that the symbols $s_1(k)$, $s_2(k)$, $s_1(-k)$ and $s_2(-k)$ are all equal-variance ($E[|s_1(k)|^2] = E[|s_2(k)|^2] = \sigma_s^2$), uncorrelated, circular complex random variables, and

independent of the channel coefficients ($H_{1,i}(k)$ and $H_{2,i}(k)$), the SIR at subcarrier k is here defined as [P2]

$$\chi(k) = \frac{E[|s_1(k)|^2]}{E[\left|\frac{y_1(k)}{H_T(k)} - s_1(k)\right|^2]} = \frac{1}{E[\left|\frac{a(k)}{H_T(k)} - 1\right|^2] + E[\left|\frac{b(k)}{H_T(k)}\right|^2] + E[\left|\frac{c(k)}{H_T(k)}\right|^2] + E[\left|\frac{d(k)}{H_T(k)}\right|^2]}. \tag{5.4}$$

Essentially the SIR in (5.4) represents the power ratio of the transmit symbol $s_1(k)$ and the undesired signal components due to I/Q imbalance at the detector input. Based on (5.2) and the above assumptions, the SIR in (5.4) holds also for the second combiner output $y_2(k)$.

As shown below in more details, this SIR *varies* as a function of the subcarrier index k and *depends on the exact power-delay profile of the radio channels* as well as on the overall imbalance properties of the transmitters and receivers. Without additional assumptions on the frequency-correlation of the radio channels, analytic simplification of the above SIR expression is, however, somewhat tedious, due to the intercarrier interference (ICI) between the mirror-subcarriers (k and $-k$). Thus to carry out the analysis further and to get some general understanding on the role of the radio channel type and TX/RX imbalance characteristic on the SIR behavior, we examine next the following two extreme cases:

(i) frequency-flat (single-tap, $L = 1$) fading channels, implying maximum subcarrier frequency-response correlation

(ii) frequency-selective fading channels with independent fading characteristics at each subcarrier

At any subcarrier k, this results in *a range of SIR values* within which the actual SIR in (5.4) is then confined with practical mobile radio channels. After some rather involved yet relatively straight-forward manipulations, these SIR bounds corresponding to the previous cases can be written as [P2]

$$\chi_{(i)}(k) \approx \chi_{def}(2,1,k), \quad \chi_{(ii)}(k) \approx \chi_{def}(\beta_{N_R}, \beta_{N_R}, k) \tag{5.5}$$

where

$$\chi_{\text{def}}(\alpha_1, \alpha_2, k) = \frac{2N_R + 4N_R^2}{A(\alpha_1, \alpha_2, k)}, \tag{5.6}$$

$$
\begin{aligned}
&A(\alpha_1,\alpha_2,k) = \\
&\sum_{i=1}^{N_R}\sum_{j=1}^{2}[3\left|G_{1,RX(i)}(k)G_{1,TX(j)}(k)\right|^2 + (\alpha_1+\alpha_2)\left|G_{2,RX(i)}(k)G_{2,TX(j)}(-k)\right|^2 \\
&+ 3\left|G_{1,RX(i)}(k)G_{2,TX(j)}(k)\right|^2 + (\alpha_1+\alpha_2)\left|G_{2,RX(i)}(k)G_{1,TX(j)}(-k)\right|^2] \\
&+ 2\,\mathrm{Re}[\sum_{i_1=1}^{N_R}\sum_{i_2\neq i_1}^{N_R} G_{1,RX(i_1)}(k)G_{1,RX(i_2)}(k)(G_{1,TX(2)}(k)G_{1,TX(1)}(k) + G^*_{2,TX(1)}(k)G^*_{2,TX(2)}(k)\ )] \\
&+ 2\,\mathrm{Re}[\sum_{i_1=1}^{N_R-1}\sum_{i_2=i_1+1}^{N_R}(\left|G_{1,TX(1)}(k)\right|^2 + \left|G_{1,TX(2)}(k)\right|^2 + \left|G_{2,TX(1)}(k)\right|^2 + \left|G_{2,TX(2)}(k)\right|^2) \\
&\qquad G_{1,RX(i_1)}(k)G^*_{1,RX(i_2)}(k))] \\
&+ (4{N_R}^2 + 2N_R) - (4N_R+2)\textstyle\sum_{i=1}^{N_R}\mathrm{Re}[G_{1,RX(i)}(k)G_{1,TX(1)}(k) + G^*_{1,RX(i)}(k)G^*_{1,TX(2)}(k)]
\end{aligned}
\tag{5.7}
$$

and

$$
\beta_{N_R} = E[\left|\frac{H^{(ii)}_{j,i}(k)}{H^{(ii)}_{T}(k)}\right|^2] \Bigg/ (\frac{E[\left|H^{(ii)}_{j,i}(k)\right|^2]}{E[\left|H^{(ii)}_{T}(k)\right|^2]}). \tag{5.8}
$$

Here $H^{(ii)}_T(k) = \sum_{i=1}^{N_R}(\left|H^{(ii)}_{1,i}(k)\right|^2 + \left|H^{(ii)}_{2,i}(k)\right|^2)$ and $H^{(ii)}_{j,i}(k)$ is the frequency-response of the radio channel between transmitter j and receiver i with channel profile (*ii*) (independent subcarrier fading). Then, it is interesting to notice that the parameter β_{N_R} defined in (5.8) depends essentially on only the number of receivers N_R and is practically independent of the considered subcarrier k. For practically interesting numbers of receivers, the values of β_{N_R} are given in Table 5-1.

TABLE 5-1: VALUES OF THE PARAMETER β_{N_R} WITH DIFFERENT NUMBER OF RECEIVERS N_R.

N_R	1	2	3	4	8
β_{N_R}	3	1.66	1.40	1.28	1.133

Impact of I/Q Imbalances on Channel Estimation

The previous SIR analysis operates on the subcarrier data samples after diversity combining. This implies that some form of channel estimation is needed prior to the combining stage. The previous derivations assumed ideal diversity combining with perfectly estimated channels, which is of course unrealistic. Both additive noise as well as I/Q imbalance result in erroneous channel estimates in practice.

As a concrete practical example, the pilot allocation of the form $\forall k : s_1(k) = s_P,\, s_2(k) = s_P^*$ is assumed for channel estimation [P2]. Similar pilot allocation is used later on also for imbalance parameter estimation and compensation. Under this pilot design, with perfect I/Q balance and no additive noise, the outputs of the i-th receiver FFT stage after CP removal are given by

$$\begin{aligned} {x_{1,i,p}}^{(1)}(k) &= H_{1,i}(k)s_P + H_{2,i}(k)s_P^* \\ {x_{2,i,p}}^{(1)}(k) &= -H_{1,i}(k)s_P + H_{2,i}(k)s_P^*. \end{aligned} \tag{5.9}$$

Then, the channel coefficients can be directly estimated as

$$\begin{aligned} \hat{H}_{1,i}(k) &= ({x_{1,i,p}}^{(1)}(k) - {x_{2,i,p}}^{(1)}(k))/(2s_P) \\ \hat{H}_{2,i}(k) &= ({x_{1,i,p}}^{(1)}(k) + {x_{2,i,p}}^{(1)}(k))/(2s_P^*) \end{aligned} \tag{5.10}$$

which follows directly from (5.9). Now incorporating also the transmitter and receiver I/Q imbalances, together with additive noise, the resulting channel estimation errors $E_{1,i}(k) = \hat{H}_{1,i}(k) - H_{1,i}(k)$ and $E_{2,i}(k) = \hat{H}_{2,i}(k) - H_{2,i}(k)$ at the k-th subcarrier in the i-th receiver can be shown to be of the form

$$\begin{aligned} E_{1,i}(k) = {} & H_{1,i}(k)[G_{1,RX(i)}(k)G_{1,TX(1)}(k) - 1] + H_{1,i}^*(-k)G_{2,RX(i)}(k)G_{2,TX(1)}^*(-k) \\ & +[H_{1,i}(k)G_{1,RX(i)}(k)G_{2,TX(1)}(k) + H_{1,i}^*(-k)G_{2,RX(i)}(k)G_{1,TX(1)}^*(-k)](s_P^* \,/\, s_P) \\ & +[G_{1,RX(i)}(k)(n_{1,i}(k) - n_{2,i}(k)) + G_{2,RX(i)}(k)(n_{1,i}^*(-k) - n_{2,i}^*(-k))]/(2s_P) \\ E_{2,i}(k) = {} & H_{2,i}(k)[G_{1,RX(i)}(k)G_{1,TX(2)}(k) - 1] + H_{2,i}^*(-k)G_{2,RX(i)}(k)G_{2,TX(2)}^*(-k) \\ & +[H_{2,i}(k)G_{1,RX(i)}(k)G_{2,TX(2)}(k) + H_{2,i}^*(-k)G_{2,RX(i)}(k)G_{1,TX(2)}^*(-k)](s_P \,/\, s_P^*) \\ & +[G_{1,RX(i)}(k)(n_{1,i}(k) + n_{2,i}(k)) + G_{2,RX(i)}(k)(n_{1,i}^*(-k) + n_{2,i}^*(-k))]/(2s_P^*) \end{aligned} \tag{5.11}$$

where $n_{1,i}(k)$ and $n_{2,i}(k)$ are the noise samples at the FFT output (k-th bin) of the i-th receiver. Then with realistic I/Q imbalance values and similar assumptions on the channel statistics described in previous subsection, the impact of noise and I/Q imbalances on the quality of the channel estimation can be assessed analytically. The so-called channel-to-interference-plus-noise ratio (CINR) at the k-th subcarrier of the i-th receiver, defined below, can now be shown to be of the form [P2]

$$\xi_{1,i}(k) = \frac{E[|H_{1,i}(k)|^2]}{E[|E_{1,i}(k)|^2]} = 1/\{\left|G_{1,RX(i)}(k)(G_{1,TX(1)}(k) + (s_P^* / s_P)G_{2,TX(1)}(k)) - 1\right|^2$$
$$+\left|G_{2,RX(i)}(k)(G_{2,TX(1)}^*(-k) + (s_P^* / s_P)G_{1,TX(1)}^*(-k))\right|^2$$
$$+(\left|G_{1,RX(i)}(k)\right|^2 + \left|G_{2,RX(i)}(k)\right|^2)/(\gamma_{RX} \times \sigma_p)\}$$

(5.12)

$$\xi_{2,i}(k) = \frac{E[|H_{2,i}(k)|^2]}{E[|E_{2,i}(k)|^2]} = 1/\{\left|G_{1,RX(i)}(k)(G_{1,TX(2)}(k) + (s_P / s_P^*)G_{2,TX(2)}(k)) - 1\right|^2$$
$$+\left|G_{2,RX(i)}(k)(G_{2,TX(2)}^*(-k) + (s_P / s_P^*)G_{1,TX(2)}^*(-k))\right|^2 + (\left|G_{1,RX(i)}(k)\right|^2$$
$$+\left|G_{2,RX(i)}(k)\right|^2)/(\gamma_{RX} \times \sigma_p)\}$$

respectively. Here $\gamma_{RX} = 2\sigma_s^2 P_H / \sigma_n^2$ is the average receiver input signal-to-noise ratio where $P_H = E[|H_{1,i}(k)|^2] = E[|H_{2,i}(k)|^2]$, σ_n^2 refers to the average noise power, σ_s^2 is the average data symbol power, and σ_p is ratio of the used pilot data power to the average data symbol power. These expressions clearly indicate that, in addition to traditional additive noise effect, the I/Q imbalances in transmitter and receiver radio front-ends are also having a clear impact on the channel estimation quality. In effect, with zero additive noise, the CINRs in (5.12) are *upper-bounded* due to I/Q imbalances alone by

$$\xi_{1,i}^{\max}(k) = 1/[\left|G_{1,RX(i)}(k)(G_{1,TX(1)}(k) + \frac{s_P^*}{s_P}G_{2,TX(1)}(k)) - 1\right|^2$$
$$+\left|G_{2,RX(i)}(k)(G_{2,TX(1)}^*(-k) + \frac{s_P^*}{s_P}G_{1,TX(1)}^*(-k))\right|^2]$$

(5.13)

$$\xi_{2,i}^{\max}(k) = 1/[\left|G_{1,RX(i)}(k)(G_{1,TX(2)}(k) + \frac{s_P}{s_P^*}G_{2,TX(2)}(k)) - 1\right|^2$$
$$+\left|G_{2,RX(i)}(k)(G_{2,TX(2)}^*(-k) + \frac{s_P}{s_P^*}G_{1,TX(2)}^*(-k))\right|^2].$$

Numerical Examples and Simulations

To give some illustrations about the derived SIR and CINR expressions, we consider a 2×1 STC-OFDM system ($N_R = 1$) with 256 subcarriers. The quadrature mixer I/Q imbalance values as well as the branch difference filters are 4%, $-4°$, $[1, 0.04, -0.03]$ (TX1), 3%, $3°$, $[1, -0.04, -0.03]$ (TX2), and 5%, $5°$, $[1, 0.05]$ (RX). Using (3.19), the individual TX and RX front-end image attenuations are then ranging between 23.3dB–49.8dB

(TX1), 25dB–43.5dB (TX2), and 22.5dB–32dB (RX), varying rather smoothly as a function of frequency from subcarrier to another.

Then, the resulting SIR due to I/Q imbalances is evaluated using (5.5)–(5.7), assuming both frequency-flat (case (*i*)) and independent subcarrier fading (case (*ii*)) radio channels. The results are shown in Figure 5-2, together with the corresponding simulated SIRs obtained using full link simulations with 64QAM as the subcarrier data modulation. Clearly, based on Figure 5-2, the link simulation results for the obtainable SIR fully match with the derived analytical results, confirming the validity and correctness of the analysis. It also demonstrates that the achievable SIR *heavily depends on the channel conditions* (in terms of channel power-delay profile). Stemming from the mild frequency-selectivity in the actual I/Q imbalances, as in this example, the subcarrier-wise SIRs are also frequency-selective varying from one subcarrier to another. As an example of the impact of the fading characteristics, say at subcarriers $k_1 = 40$ and $k_2 = -111$, the SIR ranges corresponding to frequency-flat and independent subcarrier fading cases are 18.9dB–19.7dB (k_1) and 20.8dB–22.8dB (k_2), respectively. Notice also that the overall SIR levels for both cases are again *considerably lower* than what might have been expected considering the qualities (IRRs) of the individual radios alone as defined in (3.19). Similar conclusion was also drawn in the STC single-carrier system context already in Chapter 4. Thus with higher-order spectrally efficient modulation methods, such as 16PSK or 64QAM, the I/Q imbalance is expected to play a big role in multi-antenna multi-carrier link performance.

Further examples and illustrations on upper and lower bounds for the SIRs at each subcarrier, together with actual detection error rate simulations, using Extended Vehicular A type practical radio channels (P_{dB}) described in [88] are given in Figure 5-3 and Figure 5-4 respectively. Clearly, as shown in Figure 5-3, the analytical calculations are predicting and bounding the actual SIR behavior with realistic radio channels very accurately, whereas these calculations themselves *do not need* any information on the used channel power-delay profile. Notice also that, even though the interference due to I/Q imbalance is not exactly Gaussian, the derived SIR values do indeed predict the high-SNR behavior of the detection error rates at example subcarriers #40 and # –111 very accurately as shown in Figure 5-4. Thus altogether, the SIR analysis results can be used for thorough link-level impairment analysis without actually running lengthy link simulations.

Next, with the given numerical example, the resulting CINRs are evaluated using both the analytical expression in (5.12) as well as using actual link simulations. In the simulations, the used radio channels are again random realizations of the Extended Vehicular A model [88], and channel estimation is implemented as given in (5.9). The used pilot data value s_P is the

right upper corner symbol ($7 + j7$) of the used 64QAM constellation, corresponding to roughly 3.5dB pilot "boost" compared to average symbol power. The obtained results for the channel estimation quality are presented in Figure 5-5 and Figure 5-6. Figure 5-5 shows both the simulated and analytical CINRs for different subcarriers at a fixed received SNR of 20dB, while Figure 5-6 presents the CINR behavior at an example subcarrier #40 as a function of additive noise SNR. Altogether these results demonstrate clearly that the CINR figures obtained using link simulations match again the analytical analysis very accurately.

It is also very interesting to notice that in this example, the channel estimation qualities are relatively different for the two channels (TX(1)-to-RX and TX(2)-to-RX) due to different I/Q imbalances, even though the additive noise SNRs are identical at the receiver input. Thus, in general, the above CINR analysis shows that I/Q imbalances can easily become a limiting factor also from the channel estimation point of view in future multi-antenna OFDM systems. Thus devising techniques that can compensate also for channel estimation inaccuracies are seen generally an important and interesting task.

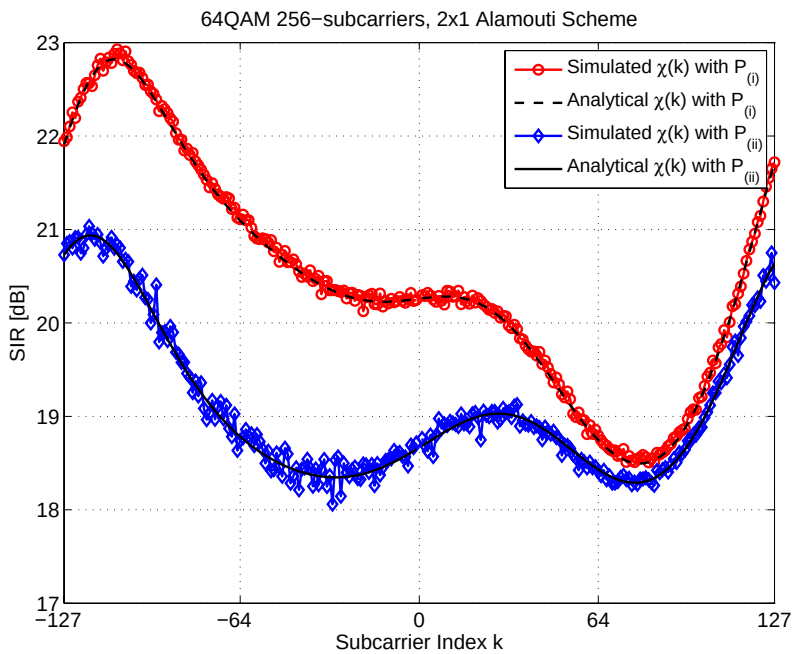

Figure 5-2: *Obtained SIR as a function of the subcarrier index k in a 2x1 STC-OFDM system with realistic frequency-selective I/Q imbalances at both transmitter and receiver analog front-ends, assuming (i) frequency-flat and (ii) frequency-selective (independent subcarrier fading) radio channels. Both analytical and simulated SIRs are shown.*

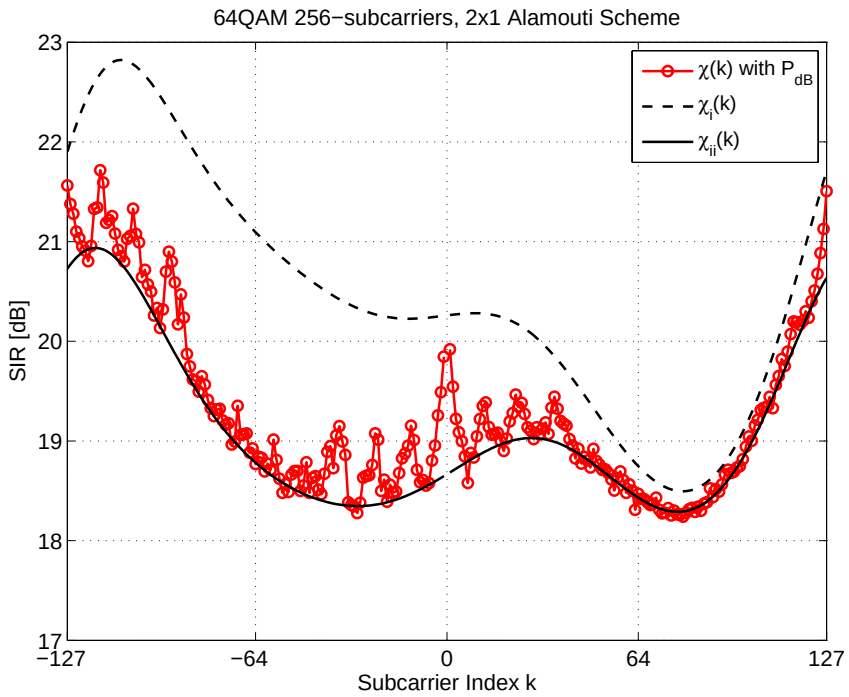

Figure 5-3: *SIR as a function of the subcarrier index k in a 2x1 STC-OFDM system with realistic frequency-selective I/Q imbalances at both transmitter and receiver analog front-ends, Extended vehicular A radio channels. The dashed and solid lines show the analytical SIR values corresponding to (i) frequency-flat and (ii) arbitrarily frequency selective fading cases, respectively.*

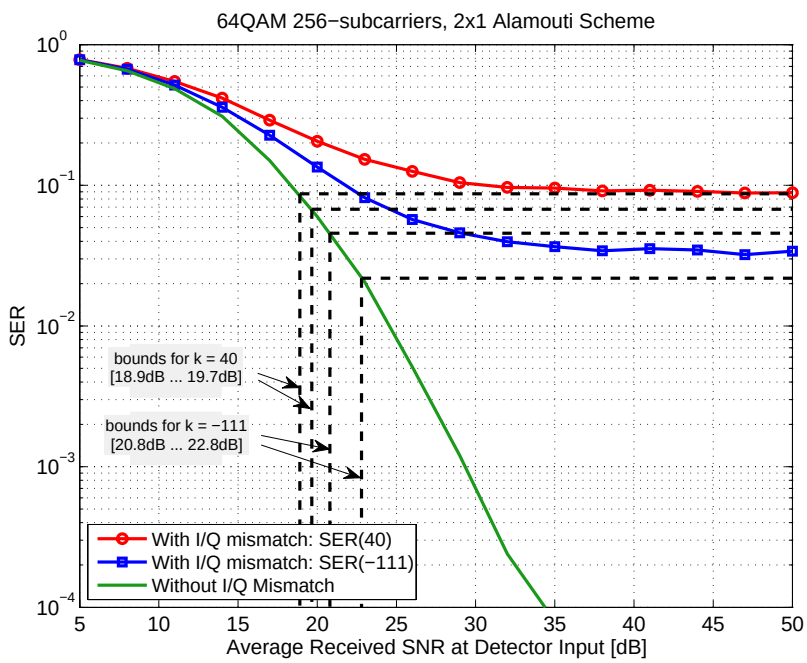

Figure 5-4: *Simulated 64QAM symbol error rates at example subcarriers #40 and #-111. 2x1 STC-OFDM system with 256 subcarriers and realistic frequency-selective I/Q imbalances at both TX and RX analog front-ends. The figure also shows the high-SNR error floors obtained using the SIR analysis results in (5.5)–(5.8). Extended vehicular A radio channels.*

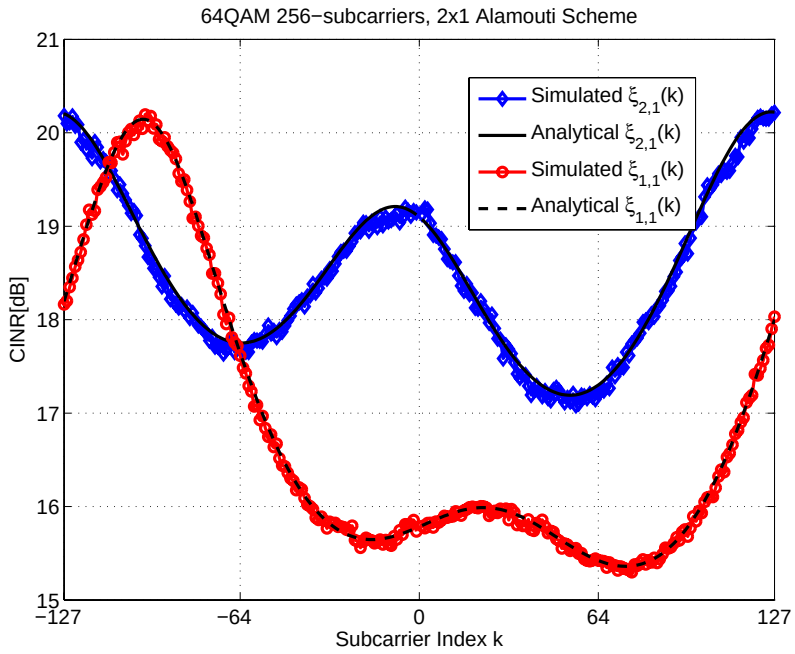

Figure 5-5: *Channel estimation error figure of merits, with realistic transmitter and receiver I/Q imbalances and received SNR of 20dB, as a function of subcarrier index k in a 2x1 256-subcarrier STC-OFDM system. Extended vehicular A radio channels.*

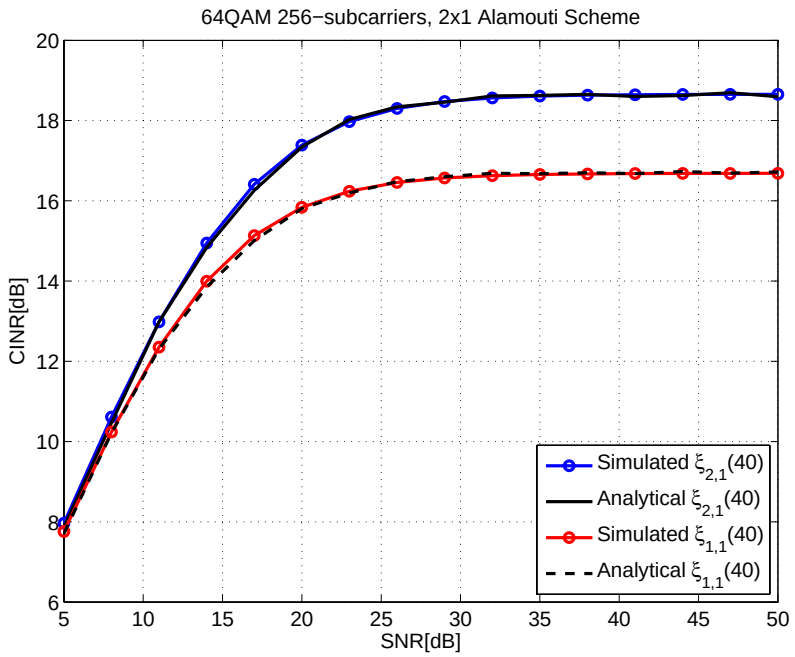

Figure 5-6: *Channel estimation error figure of merits at subcarrier #40, with realistic transmitter and receiver I/Q imbalances, as a function of received SNR in a 2x1 256-subcarrier STC-OFDM system. Extended vehicular A radio channels.*

5.3 I/Q Imbalance Compensation Technique

Compensation Philosophy

In this section, the I/Q imbalance effects due to all the OFDM transmitters and receivers are *jointly* compensated on the receiver side. Only frequency-domain based approach is deployed here such that the compensation is carried out subcarrier-wise. In general, both pilot-based and BSS based compensators could in principle be deployed, as was done in the previous chapter. However, with practical numbers of subcarriers, running subcarrier-wise blind algorithms is most likely not feasible from the computational complexity point of view, thus only pilot-subcarrier based structures are considered here.

Pilot-Based Compensation

All practical OFDM and MIMO-OFDM systems include some known pilot data for channel estimation purposes. Here we also assume that such pilot signal is available. More specifically, we assume that four consecutive OFDM symbol periods (two STC blocks) are used for pilot purposes, during which the subcarrier data are allocated as [P2]

$$\forall k : {s_1}^{(1)}(k) = s_P,\ \ {s_2}^{(1)}(k) = s_P^*,\ \ {s_1}^{(2)}(k) = s_P,\ \ {s_2}^{(2)}(k) = s_P. \tag{5.14}$$

Here s_P denotes again the pilot data value (which can be considered as one of the design "parameters") and superscripts $^{(1)}$ and $^{(2)}$ refer to the two pilot blocks. Again, one pilot slot consists of two pilot blocks as specified in (5.14). With the above pilot allocation, the resulting subcarrier observations $y_{1,p}(k)$, $y_{2,p}(k)$, $y_{3,p}(k)$, $y_{4,p}(k)$ can be shown (see (5.2)) to yield a well-behaving 4×4 set of linear equations [P2]. Writing this in vector-matrix form yields

$$\mathbf{y}_P(k) = \mathbf{S}_P \boldsymbol{\theta}(k) \tag{5.15}$$

where $\mathbf{y}_P(k) = [y_{1,p}(k),\, y_{2,p}(k)^*,\, y_{3,p}(k),\, y_{4,p}(k)^*]^T$, $\boldsymbol{\theta}(k) = [a(k),\, b(k),\, c(k),\, d(k)]^T$, and

$$\mathbf{S}_P = \begin{bmatrix} s_P & s_P^* & s_P^* & s_P \\ s_P & s_P^* & -s_P^* & -s_P \\ s_P & s_P^* & s_P & s_P^* \\ s_P^* & s_P & -s_P^* & -s_P \end{bmatrix}. \tag{5.16}$$

Then the coefficients $a(k)$, $b(k)$, $c(k)$, and $d(k)$ can be easily solved from (5.15) as

$$\hat{\boldsymbol{\theta}}(k) = {\mathbf{S}_P}^{-1} \mathbf{y}_P(k) \tag{5.17}$$

given that $\det(\mathbf{S}_P) = 2(s_P^2 - (s_P^*)^2)^2 \neq 0$ or $s_P^2 \neq (s_P^*)^2$. This, in turn, holds for any purely complex-valued training symbol s_P (i.e., both real and imaginary parts being nonzero). Notice also that the obvious symmetric structure of $\mathbf{S}_P$ in (5.16) yields great computational savings in solving (5.15) for $\boldsymbol{\theta}(k)$ in (5.17). If the pilot symbol s_P is "designed" (selected) such that its real and imaginary parts are identical (e.g., $3 + j3$), the inversion in (5.17) becomes actually almost trivial. Denoting such pilot symbol as $s_P = p + jp$, direct substitution and manipulations yield

$$\mathbf{S}_P{}^{-1} = \frac{1}{4p}\begin{bmatrix} 1 & -j & 0 & 1+j \\ 1 & j & 0 & 1-j \\ j & -1 & 1-j & 0 \\ -j & -1 & 1+j & 0 \end{bmatrix}. \tag{5.18}$$

So the parameter estimation in (5.17) is close to trivial in terms of the needed computational complexity. Notice that the above estimation steps in (5.14)–(5.18) are structurally similar to the I/Q imbalance estimation approach used in (4.7)–(4.8). The difference is, of course, that the estimation is carried out here in a *subcarrier-wise* manner.

Now having estimated the model coefficients for all the active subcarriers during the pilot slots, these estimates are then used during the actual data transmission phase for removing the interfering signal terms due to I/Q imbalance. As discussed in Section 5.1, the combiner output appears here as a weighted linear combination of two data symbols and their mirror-frequency counterparts, while in STC single-carrier systems the observation consists of the two data symbols and their own complex-conjugates. This in turn imposes that in the multi-carrier transmission context, the impaired signals at each *mirror-frequency pair* should indeed be processed *jointly*. During one STC data block, this can be done by collecting the observations $y_1(k)$, $y_2(k)$, $y_1(-k)$, and $y_2(-k)$ into $\mathbf{y}(k) = [y_1(k), y_1^*(-k), y_2(k), y_2^*(-k)]^T$ which, based on (5.2), yields

$$\mathbf{y}(k) = \boldsymbol{\Phi}(k)\mathbf{s}_c(k) \tag{5.19}$$

where $\mathbf{s}_c(k) = [s_1(k), s_1^*(-k), s_2(k), s_2^*(-k)]^T$ and

$$\boldsymbol{\Phi}(k) = \begin{bmatrix} \hat{a}(k) & \hat{b}(k) & \hat{c}(k) & \hat{d}(k) \\ \hat{b}^*(-k) & \hat{a}^*(-k) & \hat{d}^*(-k) & \hat{c}^*(-k) \\ -\hat{c}^*(k) & -\hat{d}^*(k) & \hat{a}^*(k) & \hat{b}^*(k) \\ -\hat{d}(-k) & -\hat{c}(-k) & \hat{b}(-k) & \hat{a}(-k) \end{bmatrix}. \tag{5.20}$$

In (5.19)–(5.20), the hat notation ($\hat{a}(k)$, etc.) refers to the estimated coefficients obtained during the pilot phase. Since the vector $\mathbf{s}_c(k)$ includes the data symbols (or their conjugates) at both mirror-carriers k and $-k$, it is obvious that (5.19) needs to be solved only for each mirror-carrier pair. Assuming symmetric subcarrier deployment, which is the typical case, the overall compensator is given by [P2]

$$\hat{\mathbf{s}}_c(k) = \mathbf{\Phi}(k)^{-1}\mathbf{y}(k), \quad k \in \Omega_+ \tag{5.21}$$

in which Ω_+ denotes the set of positive subcarrier indexes. Notice that again, the inherent symmetric structure of the matrix $\mathbf{\Phi}(k)$ in (5.20) yields great computational savings in practice, opposed to full matrix inversion in (5.21).

5.4 Practical Aspects and Examples

Additive Noise

This issue has been thoroughly discussed in Section 4.4 in single-carrier STC context. Here, similar principles still apply, namely a few consecutive training slots can be allocated and averaged, yielding compensation performance virtually identical to the perfectly matched case. Some examples will be given in the continuation.

Channel Profile and Estimation Errors

Again, the same principles discussed in Section 4.4 are still applicable here. With imperfect channel knowledge, the derived system model above is structurally identical to the one with perfect channel knowledge [P2]. The only difference is in the more detailed and complicated structure of the system coefficients ($a(k)$, $b(k)$, $c(k)$ and $d(k)$). This, in turn, shows that the mirror-subcarrier-wise estimation-compensation processing described in (5.14)–(5.21) can, by design, simultaneously compensate the effects of both I/Q imbalance and channel estimation inaccuracies. This is a very important practical benefit and will be illustrated and demonstrated in more details in the following using computer simulations [P2].

Frequency Offset

One essential element in the design and implementation of any multi-carrier system is the frequency synchronization. Here, since the estimator-compensator is operating after the receiver FFTs, it is clear that relatively accurate carrier synchronization is needed, prior to FFT. This can be seen as one practical limitation. It should be noticed, however, that accurate carrier synchronization is needed in the considered STC-OFDM system context anyway, even with

perfect I/Q balance, so in this sense the requirements for carrier synchronization are coming mainly from the transmission technique itself, not from the compensation principle as such.

Pilot Interpolation

In multi-carrier systems, one practical scheme to reduce the amount of needed pilot data is to use interpolation techniques in frequency-domain. This is typically used in pilot-based channel estimation in OFDM systems, since the channel response values between neighboring subcarriers are typically correlated. Similarly here, in imbalance estimation, the frequency-selectivity of the imbalances is expected to be relatively smooth in practical circuit implementations, and thus also the model coefficients $a(k)$, $b(k)$, $c(k)$, and $d(k)$ should vary rather mildly from subcarrier to another. Based on this, interpolating across the subcarriers should in general be feasible.

One practical interpolation approach can be devised as follows. Given that the basic pilot allocation in (5.14) is implemented at every J_f-th positive and negative mirror-subcarrier pair, the previous estimation scheme in (5.15)–(5.17) is still directly applicable at those subcarriers [P6]. This yields thus estimates of the model coefficients $a(k)$, $b(k)$, $c(k)$, and $d(k)$ at these pilot subcarriers, and then estimates for the corresponding model coefficients at the active data subcarriers are obtained using interpolation. The I/Q imbalance effects in the active data subcarriers can then be compensated using the interpolated model coefficients in (5.20)–(5.21). The achievable compensation performance is obviously heavily dependent on the used interpolating technique (e.g., linear interpolation, cubic spline interpolation, etc. [46]) as well as on the selected pilot spacing J_f and the radio channel coherence bandwidth [P6]. The overall compensation structure with both channel estimation and pilot interpolation is then illustrated in Figure 5-7. Notice that the pilot patterns defined in the standards of the existing or emerging wireless systems, such as 3GPP-LTE [1], [2], do not exactly match with the pilot patterns discussed in this thesis. Thus it is fair to say that direct applicability of the proposed techniques to existing radio systems is not feasible without some changes in the pilot structures (i.e., mirror-frequency nature of the pilots in the frequency domain). The main focus in the thesis work is, however, on the future radio systems still under planning phase, and through the research results like the one reported in this thesis, better interaction between the waveform design and standardization, and the usable radio electronics, is one possible direction.

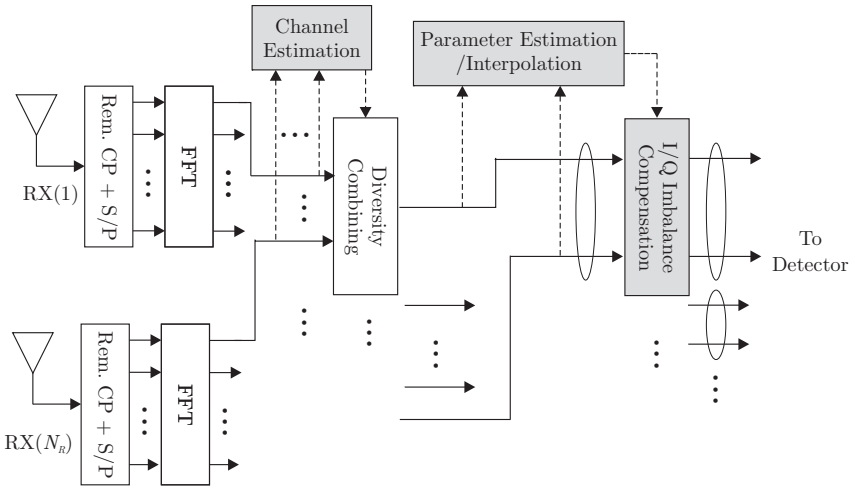

Figure 5-7: *Overall receiver structure including (i) channel estimation and diversity combining, (ii) I/Q imbalance parameter estimation, and (iii) imbalance parameter interpolation and compensation, all using the designed pilot structure in (5.14). Imbalance parameter estimation and compensation are carried out in mirror-subcarrier wise manner. (Rem. refers to remove)*

Mobility

Another important issue is the application of the proposed pilot-based approach in scenarios with clear mobility. As an example, if one terminal is moving with speed of, e.g., 30 km/h, the wireless channel may already vary from one symbol duration to another. Then the basic assumptions in the whole Alamouti transmit diversity scheme (channels are time-invariant during two consecutive OFDM symbols) as well as in the proposed pilot approach (channels are time-invariant during four consecutive OFDM symbols) are not valid any more. In addition, from imbalance compensation point of view, the system coefficients $a(k)$, $b(k)$, $c(k)$, and $d(k)$ which depend on the channel frequency-responses, will also be time-variant accordingly, especially when viewed between consecutive pilot slots as a whole. Thus certain performance degradation due to mobility is expected, especially with high mobilities and/or high-order subcarrier alphabets.

One widely applied approach to track time-variant features between pilot instants is to use interpolation along the time direction. More specifically, given the pilot slot in (5.14) is implemented every J_t-th slot of four consecutive OFDM symbols, then the corresponding channel and imbalance coefficients are estimated based on (5.10) and (5.17) respectively. Next, a time domain interpolator is applied for obtaining all the channel responses and imbalance coefficients at the data transmission slots. With the interpolated channel responses

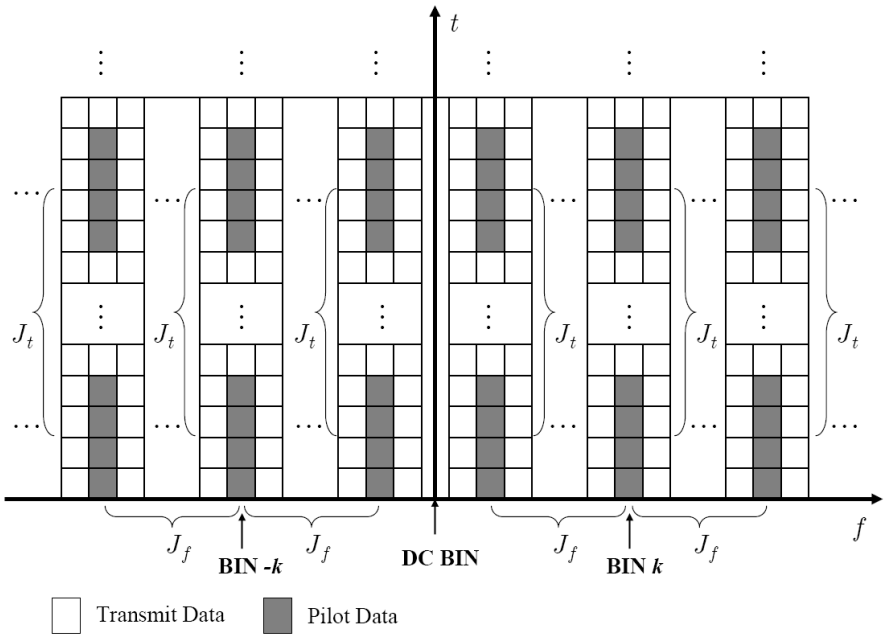

Figure 5-8: *Conceptual-level diagram of proposed pilot structure for imbalance estimation and interpolation in both time and frequency domains. J_f measures the spacing of mirror-frequency pilot subcarrier pairs in frequency domain (measured in subcarriers), while J_t measures the spacing the pilot slots of 4 OFDM symbols in time direction (measured in slots).*

and imbalance coefficients, diversity combining and I/Q imbalance compensation are then carried out as described in (2.8) and (5.21), respectively. The pilot density J_t should generally be designed according to the assumed coherence time of the radio channels t_c [102]. Then the conceptual-level description of above-mentioned pilot structure taking both time and frequency domain pilot interpolation is briefly illustrated in Figure 5-8.

Numerical Examples and Simulations

Here the overall link performance with the proposed imbalance compensation scheme under practical considerations is evaluated in terms of the detection error rates. 3GPP-LTE type [1], [2] multi-carrier system is assumed with subcarrier spacing of 15 kHz and FFT size of 1024. The transmitter and receiver sampling rate is then 1024 x 15 kHz = 15.36 MHz. The radio channels linking the transmitters and receivers are random realizations from the Extended Vehicular A power-delay profile described in [88]. A quasi-static system model is first assumed such that the channel coefficients are assumed fixed over 1000 consecutive OFDM symbol intervals after which new channel realizations are drawn. The upper right corner symbol "$7 + j7$" of the used 64QAM constellation is used as the pilot data s_P. Figure 5-9 shows the system SER performance with different numbers of pilot slots, averaged over all the

subcarriers. Here one slot refers to a pair of pilot blocks allocated as given in (5.14). With multiple slots, averaging is used over the individual parameter estimates to decrease the additive noise effects. Clearly, with just a few pilot slots, SER performance practically *identical* to the reference system can be obtained using the proposed approach [P2].

Figure 5-10 shows the corresponding SER performance when also the channel frequency-responses are estimated using (5.9)–(5.10), together with the model coefficients, using the given pilot allocation in (5.14). Due to noise and I/Q imbalance, this obviously results in errors in the estimated channel coefficients used in the combining stage. However, as shown by Figure 5-10, the overall system performance remains practically *unchanged* in the compensated case. This is generally seen a very important practical asset, related to the proposed estimation-compensation scheme.

Next the detection error rate with the proposed imbalance compensation scheme combined with pilot-based channel estimation and pilot-interpolation in frequency-domain is evaluated. The delay spread of the Extended Vehicular A channel is in the order of 2.5 microseconds, corresponding to a coherence bandwidth of around ten subcarriers or so, depending on the definition. Then linear interpolation [46] is deployed and the SER performances with different pilot-spacings $J_f = \{2, 3, ..., 6\}$ are then shown in Figure 5-11. It is very interesting to observe that even with such simple interpolation technique, the system can still achieve very good performance. Then a more sophisticated interpolation technique, cubic spline interpolation [46], is deployed and the resulting SER performance with different values of the pilot-spacing J_f is illustrated in Figure 5-12. The simulation shows that the system performance using the proposed algorithm and cubic spline interpolation approaches the ideal reference system performance very closely.

Next, in Figure 5-13, the impact of receiver mobility on the proposed compensation approach is briefly demonstrated. As a practical example, we assume a carrier frequency range of 2 GHz and receiver mobilities of 10km/h and 30km/h. The exact fading statistics is following the widely-applied Jakes' model described, e.g., in [25] and [102]. Combined with subcarrier spacing of 15 kHz, this implies coherence times in the order of one hundred OFDM symbols. The pilot-spacings in frequency and time domains are then set to $J_f = 6$ and $J_t = 3$, respectively. As shown in Figure 5-13, the overall link performance is somewhat degraded due to mobility, even without any I/Q imbalance, as discussed in Section 5.4. Yet the figure also demonstrates that the proposed compensation approach is still able to mitigate most signal distortion due to I/Q imbalance also under reasonable mobility. Thus, it generally forms a *practical and feasible solution* for efficient mitigation of frequency-selective I/Q imbalances in the STC-OFDM transmission context.

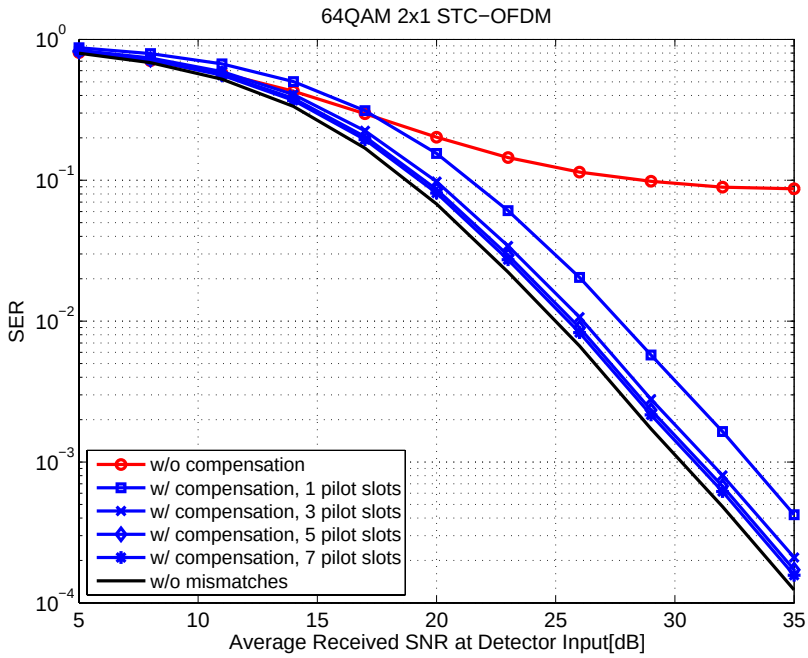

Figure 5-9: *Simulated 64-QAM symbol error rates, averaged for all the subcarriers, with and without the proposed compensation technique, with different amounts of pilot symbols used for imbalance parameter estimation in the receiver. Channel estimation is assumed perfect.*

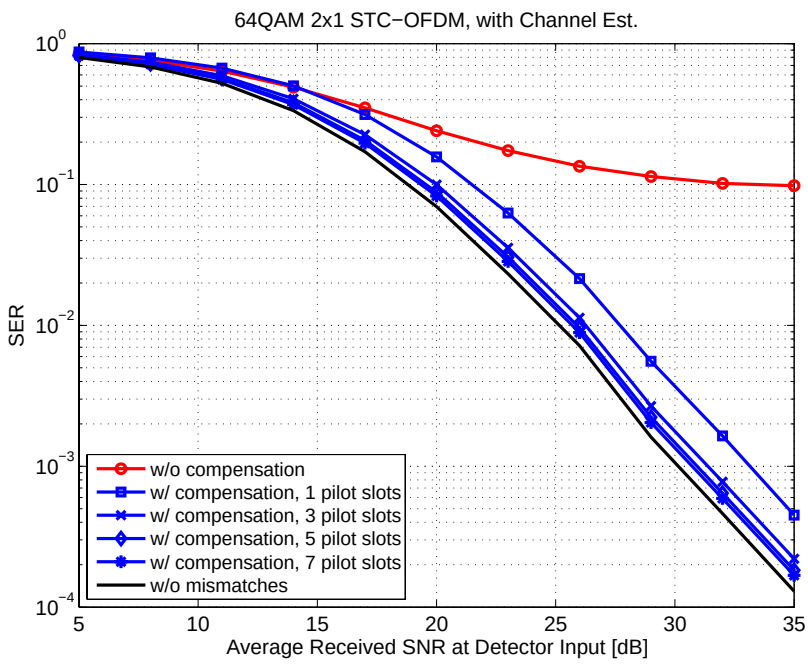

Figure 5-10: *Simulated 64QAM symbol error rates, averaged for all the subcarriers, with and without the proposed compensation technique, with different amounts of pilot symbols used for imbalance parameter as well as for channel response estimation in the receiver.*

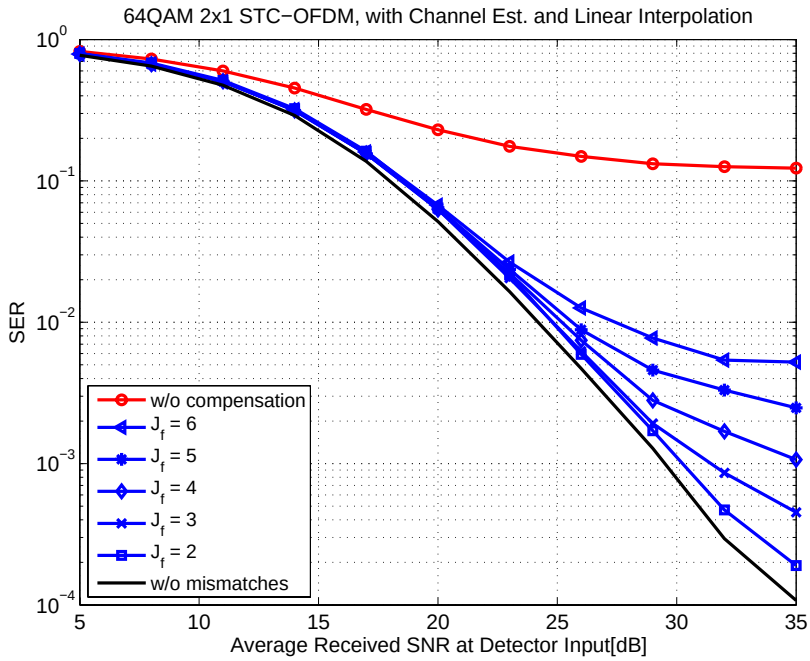

Figure 5-11: *Simulated system performance with 7 pilot slots for channel response and imbalance parameter estimation and with different pilot-subcarrier spacings* J_f. *Linear interpolation is used to interpolate channel responses as well as imbalance compensation parameters for active data subcarriers. Extended vehicular A radio channels.*

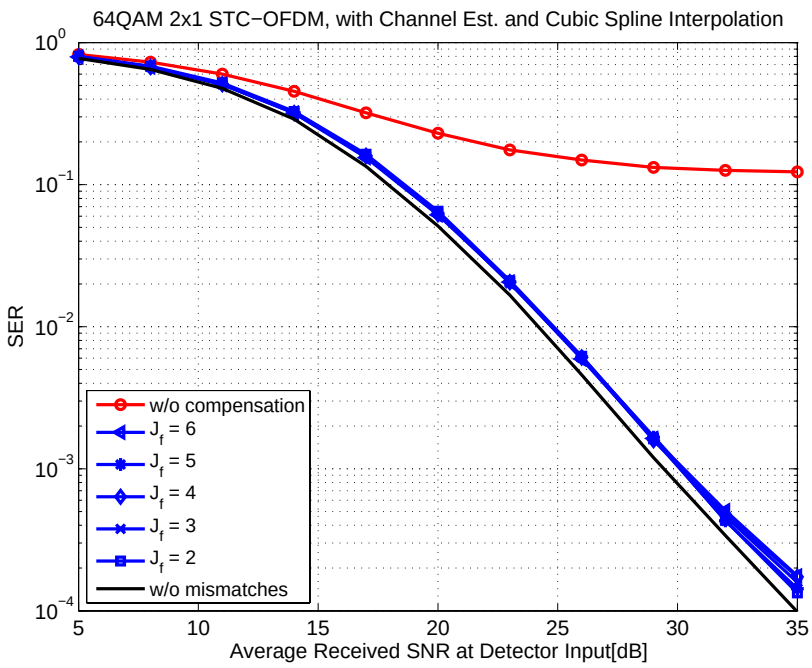

Figure 5-12: *Simulated system performance with 7 pilot slots for channel response and imbalance parameter estimation and with different pilot-subcarrier spacings* J_f. *Cubic spline interpolation is used to interpolate channel responses as well as imbalance compensation parameters for active data subcarriers. Extended vehicular A radio channels.*

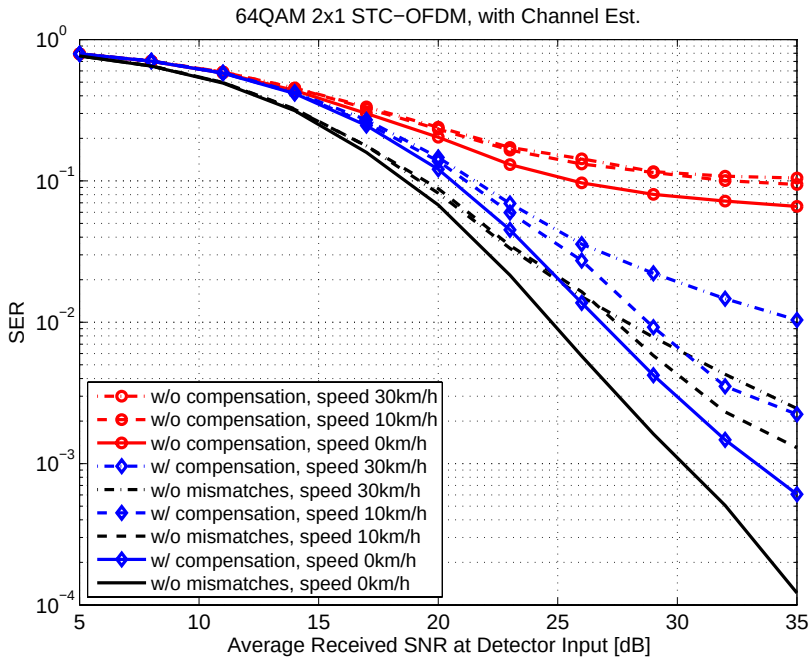

Figure 5-13: *Simulated system performance under different receiver mobilities with pilot slot –based estimation of channel response and imbalance parameters. Pilot spacing* $J_f = 6$ *and* $J_t = 3$. *Cubic spline interpolation is used to interpolate channel responses as well as imbalance compensation parameters in both time domain and frequency domains. Extended vehicular A radio channels.*

Chapter 6

Frequency-Selective I/Q Imbalances in Spatial Multiplexing Multi-Carrier Systems

In this chapter, we focus on the analysis and compensation of frequency-selective I/Q imbalances in spatial multiplexing MIMO-OFDM transmission systems.

6.1 I/Q Signals and System Model

A conceptual block-diagram of the overall spatial multiplexing MIMO-OFDM link under study is depicted in Figure 6-1. Again, OFDM MOD and DEMOD blocks refer to OFDM waveform generation and demodulation operations, respectively, shown in Figure 2-5. For reference, the ideal link model under perfect I/Q balance in all the radios is reproduced below as (c.f. (2.9))

$$\mathbf{x}^{ideal}(k) = \mathbf{H}(k)^T \mathbf{s}(k) + \mathbf{n}(k). \tag{6.1}$$

where the transmit vector $\mathbf{s}(k) = [s_1(k), s_2(k), ..., s_{N_T}(k)]^T$, $\mathbf{n}(k) = \left[n_1(k), n_2(k)...n_{N_R}(k)\right]$ denotes the noise vector and the matrix $\mathbf{H}(k)$ contains the channel responses where $[\mathbf{H}(k)]_{j,i} = H_{j,i}(k)$ denotes the channel frequency-response from transmitter j to receiver i, all at k -th subcarrier. Then similar to the previous developments in Chapter 5, the I/Q imbalance properties in individual transceivers are here expected to be varying as a function of frequency within the overall waveform bandwidth. Thus, the basic signal models given in (3.16) and (3.17) describing the frequency-selective transmitter and receiver I/Q imbalances can be directly applied here as well. Combining now (3.16) and (3.17) with the given system model in (2.9), the overall link-level model for SM-MIMO-OFDM system under frequency-selective I/Q imbalances can then be written as

$$\begin{aligned}\mathbf{x}(k) &= [x_1(k),\, x_2(k),\, \ldots,\, x_{N_R}(k)]^T \\ &= [\mathbf{R}_1(k)\mathbf{H}(k)^T\mathbf{T}_1(k) + \mathbf{R}_2(k)\mathbf{H}(-k)^H\mathbf{T}_2^*(-k)]\mathbf{s}(k) \\ &\quad +[\mathbf{R}_1(k)\mathbf{H}(k)^T\mathbf{T}_2(k) + \mathbf{R}_2(k)\mathbf{H}(-k)^H\mathbf{T}_1^*(-k)]\mathbf{s}^*(-k) \\ &\quad +\mathbf{R}_1(k)\mathbf{n}(k) + \mathbf{R}_2(k)\mathbf{n}^*(-k) \\ &= \mathbf{H}_{\mathrm{TOT},1}(k)\mathbf{s}(k) + \mathbf{H}_{\mathrm{TOT},2}(k)\mathbf{s}^*(-k) + \mathbf{R}_1(k)\mathbf{n}(k) + \mathbf{R}_2(k)\mathbf{n}^*(-k)\end{aligned} \tag{6.2}$$

where

$$\begin{aligned}\mathbf{H}_{\mathrm{TOT},1}(k) &= \mathbf{R}_1(k)\mathbf{H}(k)^T\mathbf{T}_1(k) + \mathbf{R}_2(k)\mathbf{H}(-k)^H\mathbf{T}_2^*(-k) \\ \mathbf{H}_{\mathrm{TOT},2}(k) &= \mathbf{R}_1(k)\mathbf{H}(k)^T\mathbf{T}_2(k) + \mathbf{R}_2(k)\mathbf{H}(-k)^H\mathbf{T}_1^*(-k)\end{aligned}, \tag{6.3}$$

$$\begin{aligned}\mathbf{R}_m(k) &= diag\{G_{m,RX(1)}(k),\ G_{m,RX(2)}(k),\ \ldots,\ G_{m,RX(N_R)}(k)\} \\ \mathbf{T}_m(k) &= diag\{G_{m,TX(1)}(k),\ G_{m,TX(2)}(k),\ \ldots,\ G_{m,TX(N_T)}(k)\}\end{aligned},\ m = 1,2. \tag{6.4}$$

in which $G_{m,RX(i)}(k)$ and $G_{m,TX(j)}(k)$ represent the I/Q imbalance responses at k -th subcarrier of i-th receiver and j-th transmitter, respectively. Compared to the individual TX and RX models in (3.16) and (3.17) as well as the ideal link model in (2.9), the observed signal vector at subcarrier k is interfered due to I/Q imbalance by the conjugate of the data vector at the corresponding mirror carrier $-k$. Then, similar to the ideal case in (2.10) and (2.11), and assuming again perfect channel knowledge, the decision on transmitted symbol vector $\mathbf{s}(k)$ can be made by applying, e.g., the ML or ZF detection principles written below as

$$\hat{\mathbf{s}}_{ML}(k) = \underset{\mathbf{s}(k)\in\Omega_{\mathbf{s}}}{\arg\min}\left\|\mathbf{x}(k) - \mathbf{H}(k)^T\mathbf{s}(k)\right\|^2 \tag{6.5}$$

$$\hat{\mathbf{s}}_{ZF}(k) = \mathbf{H}(k)^{-T}\mathbf{x}(k). \tag{6.6}$$

Here it is assumed that the detector has perfect knowledge on the transmission channels but has no knowledge on the I/Q imbalances of the radios.

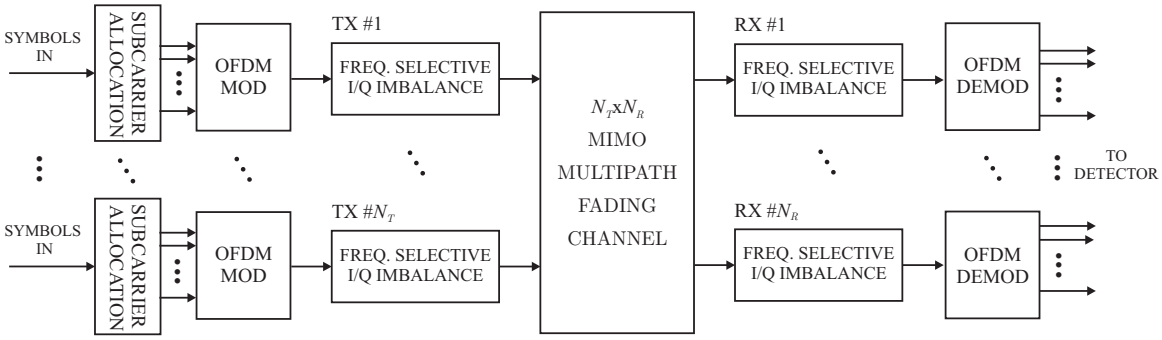

Figure 6-1: *Conceptual model of spatial multiplexing multi-carrier transmission link with N_T transmit and N_R receive antennas, including transmitter and receiver front-end I/Q impairments.*

6.2 Performance Analysis

In the following, the target is to again analyze the link-level signal degradation due to I/Q imbalances. In general, the performance analysis for evaluating I/Q imbalance effects in SM-MIMO-OFDM systems is somewhat more challenging compared to the earlier STC-OFDM case. This is due to the fact that there is no structural symmetry in the basic signal models describing the reception in the SM-MIMO-OFDM case. Also the deployed detector or MSI mitigation solution has a clear impact on the nature of the interference at detector input. Here, as a performance baseline study, we focus on the ML detector case described in (6.5).

Signal-to-Interference-plus-Noise Ratio (SINR) Analysis

Here we analyze and quantify the amount of signal distortion due to I/Q imbalances in terms of signal-to-interference-plus-noise ratio (SINR). Compared to the SIR analyses given in Chapters 4 and 5, the effect of additive channel noise is also taken into account in the analysis here. Based on (6.1)–(6.3), the ideal desired signal term at the detector input is $\mathbf{H}(k)^T\mathbf{s}(k)$ while the overall interference plus noise term is then

$$\begin{aligned}&\mathbf{x}(k) - \mathbf{H}(k)^T\mathbf{s}(k) = \\ &\quad (\mathbf{H}_{\mathrm{TOT},1}(k) - \mathbf{H}(k)^T)\mathbf{s}(k) + \mathbf{H}_{\mathrm{TOT},2}(k)\mathbf{s}^*(-k) + \mathbf{R}_1(k)\mathbf{n}(k) + \mathbf{R}_2(k)\mathbf{n}^*(-k).\end{aligned} \tag{6.7}$$

Thus the SINR at the detector input at k-th subcarrier and i-th receiver is formally given by

$$\rho_i(k) = \frac{E[\left|\sum_{j=1}^{N_T} s_j(k) H_{j,i}(k)\right|^2]}{E[\left|x_i(k) - \sum_{j=1}^{N_T} s_j(k) H_{j,i}(k)\right|^2]}. \tag{6.8}$$

Further assumptions on the transmission environment are made similar to those in Section 5.2. We also assume that the transmitted symbols $s_j(k)$ and additive noise variables $n_i(k)$ are all mutually uncorrelated, circular complex random variables, with variances $E[|s_j(k)|^2] = \sigma_s^2$ and $E[|n_i(k)|^2] = \sigma_n^2$, and independent of the channel coefficients at all subcarriers. After straight-forward manipulations, the SINR in (6.8) for i-th receiver at k-th subcarrier can now be further written as [P8]

$$\rho_i(k) = \frac{N_T}{A_i(k) + B_i(k) + C_i(k)} \tag{6.9}$$

where

$$\begin{aligned} A_i(k) &= \sum_{j=1}^{N_T} \{ \left|G_{1,TX(j)}(k) G_{1,RX(i)}(k)\right|^2 + \left|G_{2,TX(j)}(-k) G_{2,RX(i)}(k)\right|^2 \\ &\quad -2\,\mathrm{Re}[G_{1,TX(j)}(k) G_{1,RX(i)}(k)] + 1\} \\ B_i(k) &= \sum_{j=1}^{N_T} [\left|G_{1,TX(j)}(-k) G_{2,RX(i)}(k)\right|^2 + \left|G_{2,TX(j)}(-k) G_{2,RX(i)}(k)\right|^2] \\ C_i(k) &= N_T(\left|G_{1,RX(i)}(k)\right|^2 + \left|G_{2,RX(i)}(k)\right|^2) / \gamma_{RX} \end{aligned} \tag{6.10}$$

with

$$\gamma_{RX} = \frac{N_T \sigma_s^2 P_H}{\sigma_n^2} \tag{6.11}$$

denoting the average signal-to-noise ratio per receiver antenna where $P_H = E[|H_{j,i}(k)|^2]$. Notice that the obtained analytical SINR in (6.9)–(6.11) above is fully determined by the imbalance values of the N_T transmitters and N_R receivers and the signal-to-noise ratio at receiver input, and thus can be directly evaluated for any possible imbalance scenario and SNR value without any system simulations. Furthermore, with bandwidths in the order of several MHz, these SINR values are varying as a function of frequency through the assumed frequency-selectivity of the I/Q imbalance responses.

SIR Analysis

With zero additive noise, the SINRs in (6.9)–(6.11) are *upper-bounded* due to I/Q imbalances alone by

$$\rho_i^{max}(k) = \frac{N_T}{A_i(k) + B_i(k)} \tag{6.12}$$

which corresponds to the achievable SIR of the given SM-MIMO-OFDM system due to I/Q imbalances. Yet the obtained SIR values in (6.12) can not be directly mapped to the achievable detection error rate floor due to I/Q imbalances as was done earlier in the STC-OFDM system case. More specifically, when viewing the ideal received signal $\mathbf{H}(k)^T\mathbf{s}(k)$ as the desired signal at subcarrier k, this interference is composed of two parts. The first part consists of the term $\mathbf{H}_{\mathrm{TOT},2}(k)\mathbf{s}^*(-k)$ which can be seen as the interference due to spatially multiplexed transmit symbols at the mirror-subcarrier. With i.i.d. transmit data, this interference can be assumed *statistically independent of the target signal*. Even though this interference is not exactly Gaussian distributed with practical symbol alphabets, its impact on the achievable SER can still be reliably approximated as being additional channel noise. The second part of the overall interference is then kind of self-interference. Based on (6.7), this self-interference is formally given by $[\mathbf{H}(k)^T - \mathbf{H}_{\mathrm{TOT},1}(k)]\mathbf{s}(k)$. Due to strong statistical dependence on the ideal received signal $\mathbf{H}(k)^T\mathbf{s}(k)$, the impact of this self-interference on the achievable SER is rather different compared to other error sources (additive channel noise and interference due to mirror-carrier). There are some brief discussions on this issue in [82]. Yet it is not exactly a trivial issue to analyze analytically, even if the desired signal in [82] has much simpler form (a single data symbol) than the desired signal here (a signal vector). Thus, a closed-form detection error rate analysis for the impact of self-interference on the overall SM-MIMO-OFDM system performance is generally very complicated. It is, however, possible to approximate the contribution of the self-interference through an additional, modulation-specific parameter α, linking the self-interference contribution to the other error sources. As a result, a modified SIR derivation, based on (6.12), is given by [P8]

$$\overline{\rho}_i^{max}(k) \simeq \frac{N_T}{\alpha A_i(k) + B_i(k)} \tag{6.13}$$

where $A_i(k)$ and $B_i(k)$ are given in (6.10). In general, this parameter α can be obtained by computer simulations. As a practical numerical example, the value of α in a 2 transmit 2 receive antenna system with 64QAM symbol alphabet is $\alpha = 0.5$. Furthermore, as shown in [64], [68], [102], with ML detection, the achievable detection error rate of SM transmission

systems is generally proportional to ${\gamma_{RX}}^{-N_R}$ at high SNR regime. Thus incorporating this and the above derivation in (6.13), an equivalent overall link-level SIR can be given as [P8]

$$\overline{\rho}_{all}^{max}(k) = \sqrt[N_R]{\prod_{i=1}^{N_R} \overline{\rho}_i^{max}(k)} \tag{6.14}$$

This can now be directly mapped to the system detection error rate floor under given I/Q imbalance values, similarly as in STC transmit diversity systems in (4.5) and (5.5). Notice that the self-interference issue could almost be neglected in the earlier STC transmit diversity analysis since the power of self-interference in STC reception is relatively low compared to the power of the interference coming from the mirror-subcarriers. Here in spatial multiplexing case, however, this is not the case but the powers of the two interference parts are actually comparable to each other, and thus the impact of self-interference cannot be neglected.

Numerical Examples and Simulations

In this subsection, the previous analysis results are illustrated and verified using extensive computer simulations. As a practical example, we consider a 2×2 spatial multiplexing MIMO-OFDM system with the total number of subcarriers being 1024 out of which 600 central subcarriers are active (excluding the DC-bin). The subcarrier spacing is assumed to be 15kHz conforming with basic 3GPP LTE specifications [1] and [2]. The quadrature mixer I/Q imbalance values as well as the branch difference filters for the two transmitters and two receivers are 3%, $-3°$, $[1, 0.04, -0.03]$ (TX1), 1%, $1°$, $[1, -0.04, -0.03]$ (TX2), 2%, $2°$, $[1, 0.05]$ (RX1), and -3%, $-3°$, $[1, -0.03, 0.04]$(RX2), representing practical example values. The sample spacing in the I/Q branch difference filter models above is 1024x15kHz = 15.36MHz. The corresponding individual TX/RX front-end image attenuations evaluated using (3.19) are ranging between 25dB–50dB (TX1), 28dB–38dB (TX2), 27dB–46dB (RX1) and 26dB–40dB (RX2) varying rather smoothly as a function of frequency from subcarrier to another. 64QAM is used as the subcarrier data modulation. The radio channels linking the transmitters and receivers follow the Extended Vehicular A power-delay profile described in [88], with the delay spread being in the order of $2.5\,\mu s$. Proper CP is always used on the transmitter side and discarded in the receiver prior to the FFT as in any OFDM system.

As a first verification exercise, we evaluate the subcarrier-wise SINR assuming (*i*) infinite received SNR and (*ii*) received SNR of 20dB. Received signals are generated with 200,000 independent channel realizations (for each of the 2x2 = 4 radio channels) and are used to evaluate the SINR numerically. The obtained SINR behavior is shown in Figure 6-2 (infinite received SNR) and in Figure 6-3 (received SNR 20dB), together with the analytical results

evaluated using (6.9)–(6.11). As demonstrated by the figures, the proposed analysis results are capable of predicting the actual SINR behavior with realistic radio channels very accurately. Notice also that the absolute achievable SINR values are again *considerably lower* than what might have been expected considering the qualities (IRRs) of the individual front-ends alone. Thus this gives further evidence that the RF impairments like I/Q mismatch will in general play a more critical role in the future multi-antenna wireless system than in current single-antenna systems.

Next, the detection error performance is examined at example subcarriers #199 and #-249 where, based on (6.10), (6.13) and (6.14), the corresponding equivalent overall SIRs ($\overline{\rho}_{all}^{max}(k)$) are 23.3dB and 24.9dB, respectively. As shown in Figure 6-4, the analysis predicts very accurately the subcarrier-wise high-SNR behavior and the resulting SER floor due to I/Q imbalances.

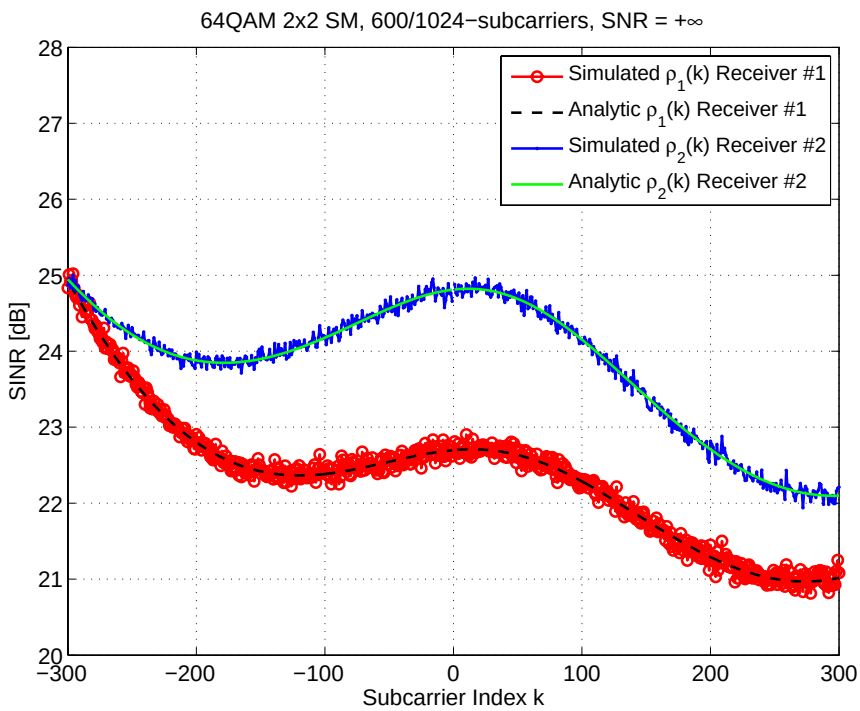

Figure 6-2: *SINR as a function of the subcarrier index k in a 2x2 SM-MIMO-OFDM system with realistic frequency-selective I/Q imbalances at both transmitter and receiver analog front-ends, Extended vehicular A radio channels, infinite received SNR per antenna.*

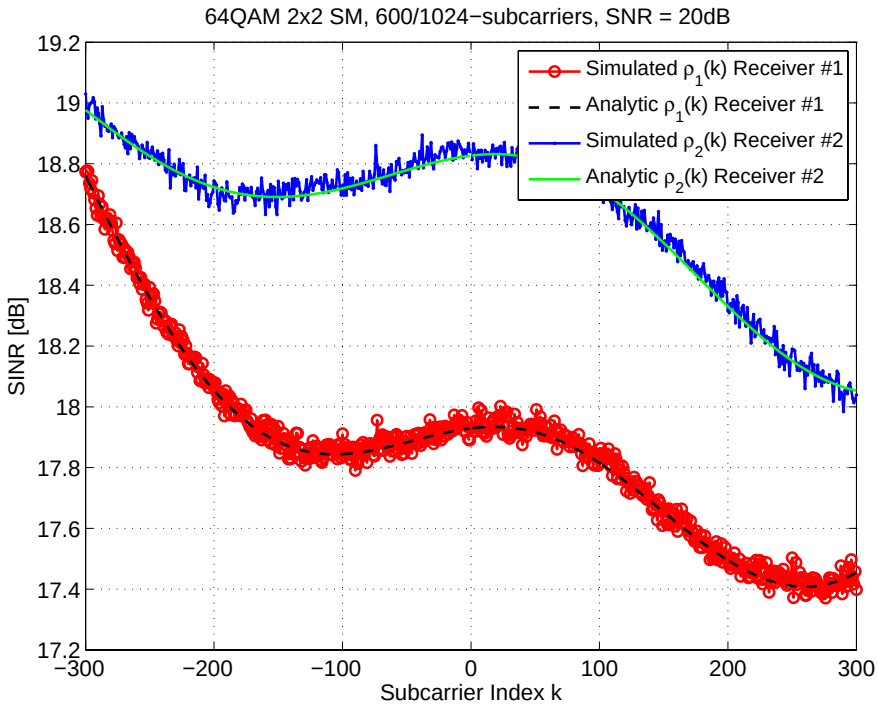

Figure 6-3: *SINR as a function of the subcarrier index k in a 2x2 SM-MIMO-OFDM system with realistic frequency-selective I/Q imbalances at both transmitter and receiver analog front-ends, Extended vehicular A radio channels, average received SNR per antenna is 20dB.*

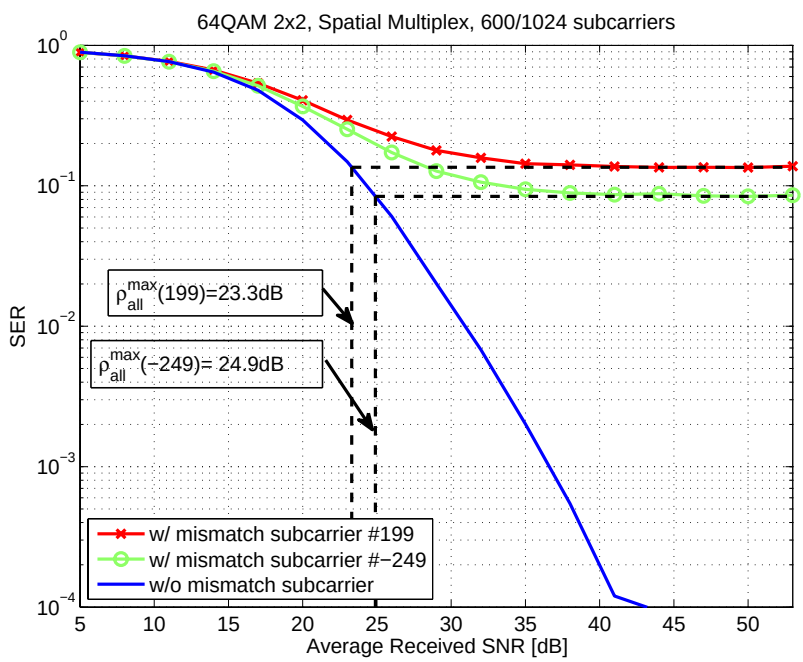

Figure 6-4: *Simulated 64QAM symbol error rates at example subcarriers #199 and #-249 in a 2x2 SM-MIMO-OFDM system. Extended vehicular A radio channels. The figure also shows the high-SNR error floors using the SINR analysis results in (6.10), (6.13) and (6.14).*

6.3 I/Q Imbalance Compensation Technique

Compensation Philosophy

Here we consider compensating the I/Q imbalance effects in all transmitters and receivers jointly on the receiver side. In general, like discussed in Chapter 1, there has been some related studies in the literature (see, e.g., [33], [44], [61], [72], [73], [80]–[82], [91], [92], [96]) addressing the I/Q imbalance compensation in spatial multiplexing MIMO-OFDM. Most of the reported work focus on either frequency-independent imbalance case or consider receiver imbalances only. Here, assuming the 2×2 case for simplicity and illustration purposes, we propose a pilot-based estimation-compensation method, stemming from similar pilot-allocation discussed earlier in Chapter 5. The proposed technique is specifically designed to handle the frequency-selective imbalance case. Also, for reducing the implementation complexity, both I/Q imbalance compensation and MSI mitigation are carried out at the same time. This is done by building a detector which takes both the MSI and mirror-carrier interference into account. Notice that no separate channel estimation stage is needed in the proposed detector but the combined effects of the radio channels and I/Q imbalances of all the radios are essentially estimated jointly.

Pilot-Based Compensation

For simplicity, we focus on the 2 transmit, 2 receive antenna case. First, we rewrite the signal reception under I/Q imbalances (assuming zero channel noise to simplify the notations again) in (6.2) as

$$\begin{aligned}\mathbf{x}(k) &= [x_1(k),\ x_2(k)]^T \\ &= \mathbf{H}_{\mathrm{TOT},1}(k)\mathbf{s}(k) + \mathbf{H}_{\mathrm{TOT},2}(k)\mathbf{s}^*(-k) \\ &= \begin{bmatrix} a_1(k)s_1(k) + b_1(k)s_1^*(-k) + c_1(k)s_2(k) + d_1(k)s_2^*(-k) \\ a_2(k)s_1(k) + b_2(k)s_1^*(-k) + c_2(k)s_2(k) + d_2(k)s_2^*(-k) \end{bmatrix}^T\end{aligned} \tag{6.15}$$

where

$$\mathbf{H}_{\mathrm{TOT},1}(k) = \begin{bmatrix} a_1(k) & c_1(k) \\ a_2(k) & c_2(k) \end{bmatrix}, \quad \mathbf{H}_{\mathrm{TOT},2}(k) = \begin{bmatrix} b_1(k) & d_1(k) \\ b_2(k) & d_2(k) \end{bmatrix}. \tag{6.16}$$

The coefficients $a_1(k)$, $a_2(k)$, $b_1(k)$, $b_2(k)$, $c_1(k)$, $c_2(k)$, $d_1(k)$, $d_2(k)$ are given below as

$$\begin{aligned}
a_i(k) &= G_{1,RX(i)}(k)G_{1,TX(1)}(k)H_{1,i}(k) + G_{2,RX(i)}(k)G^*_{2,TX(1)}(-k)H^*_{1,i}(-k) \\
b_i(k) &= G_{1,RX(i)}(k)G_{2,TX(1)}(k)H_{1,i}(k) + G_{2,RX(i)}(k)G^*_{1,TX(1)}(-k)H^*_{1,i}(-k) \\
c_i(k) &= G_{1,RX(i)}(k)G_{1,TX(2)}(k)H_{2,i}(k) + G_{2,RX(i)}(k)G^*_{2,TX(2)}(-k)H^*_{2,i}(-k) \\
d_i(k) &= G_{1,RX(i)}(k)G_{2,TX(2)}(k)H_{2,i}(k) + G_{2,RX(i)}(k)G^*_{1,TX(2)}(-k)H^*_{2,i}(-k)
\end{aligned} \tag{6.17}$$

$i \in \{1,2\}$. Now, we assume that four consecutive OFDM symbol periods are used as a pilot slot for estimation and synchronization purposes, during which the subcarrier data are allocated as

$$\begin{aligned}
\forall k : s_1^{(1)}(k) = s_1^{(2)}(k) = s_1^{(3)}(k) = s_2^{(3)}(k) = s_P, \\
s_2^{(1)}(k) = -s_2^{(2)}(k) = -s_2^{(4)}(k) = s_1^{(4)}(k) = s_P^*
\end{aligned} \tag{6.18}$$

where s_P denotes the pilot data value (which can again be considered as one of the design "parameters") and superscripts $^{(1)}$, $^{(2)}$, $^{(3)}$and $^{(4)}$ refer to the multi-carrier symbol index inside the pilot slot. With the above pilot allocation, the resulting subcarrier observations $x_{1,p,i}(k)$, $x_{2,p,i}(k)$, $x_{3,p,i}(k)$, $x_{4,p,i}(k)$ for i-th receiver ($i \in \{1,2\}$) can be shown see (6.15)) to yield a well-behaving 4×4 set of linear equations. Writing this in vector-matrix form yields

$$\mathbf{x}_{P,i}(k) = \mathbf{S}_P \boldsymbol{\theta}_i(k),\ i \in \{1,2\} \tag{6.19}$$

where the subcarrier observation vector $\mathbf{x}_{P,i}(k) = [x_{1,p,i}(k),\ x_{2,p,i}(k),\ x_{3,p,i}(k),\ x_{4,p,i}(k)]^T$, parameter vector $\boldsymbol{\theta}_i(k) = [a_i(k), b_i(k), c_i(k), d_i(k)]^T$, and

$$\mathbf{S}_P = \begin{bmatrix} s_P & s_P^* & s_P^* & s_P \\ s_P & s_P^* & -s_P^* & -s_P \\ s_P & s_P^* & s_P & s_P^* \\ s_P^* & s_P & -s_P^* & -s_P \end{bmatrix}. \tag{6.20}$$

Notice that the pilot structure in (6.18) is designed in such a way that the resulting pilot matrix $\mathbf{S}_P$ in (6.20) is identical to the $\mathbf{S}_P$ in (5.16). In general, like discussed earlier, this matrix $\mathbf{S}_P$ is invertible given that the training symbol s_P is purely complex-valued (i.e., both real and imaginary parts are nonzero). Then the coefficients $a_i(k)$, $b_i(k)$, $c_i(k)$, and $d_i(k)$ at k-th subcarrier and i-th receiver can be easily solved from (6.15) as

$$\hat{\boldsymbol{\theta}}_i(k) = \mathbf{S}_P{}^{-1}\mathbf{x}_{P,i}(k),\ i \in \{1,2\}. \tag{6.21}$$

Now having estimated the model coefficients for all the active subcarriers and all receiver branches during the pilot slots, these estimates are then used during the actual data

transmission for removing the interfering signal terms due to I/Q imbalance. Again, the received signals located at a mirror frequency pair should be processed *jointly*. During one multi-carrier symbol interval, this can be done by collecting the observations $x_1(k)$, $x_2(k)$, $x_1^*(-k)$, and $x_2^*(-k)$ into $\overline{\mathbf{x}}(k) = [x_1(k), x_1^*(-k), x_2(k), x_2^*(-k)]^T$ which, based on (6.15), yields (additive noise ignored again)

$$\overline{\mathbf{x}}(k) = \mathbf{\Phi}(k)\overline{\mathbf{s}}(k) \tag{6.22}$$

where $\overline{\mathbf{s}}(k) = [s_1(k), s_1^*(-k), s_2(k), s_2^*(-k)]^T$ and

$$\mathbf{\Phi}(k) = \begin{bmatrix} \hat{a}_1(k) & \hat{b}_1(k) & \hat{c}_1(k) & \hat{d}_1(k) \\ \hat{b}_1{}^*(-k) & \hat{a}_1{}^*(-k) & \hat{d}_1^*(-k) & \hat{c}_1^*(-k) \\ \hat{a}_2(k) & \hat{b}_2(k) & \hat{c}_2(k) & \hat{d}_2(k) \\ \hat{b}_2{}^*(-k) & \hat{a}_2{}^*(-k) & \hat{d}_2^*(-k) & \hat{c}_2^*(-k) \end{bmatrix}. \tag{6.23}$$

In (6.22)–(6.23), the hat –notation ($\hat{a}_i(k)$, etc.) refers to the estimated coefficients obtained during the pilot phase. Then the decision on transmitted symbol vector $\overline{\mathbf{s}}(k)$ can be made by applying the ML principle as

$$\hat{\overline{\mathbf{s}}}_{ML}(k) = \underset{\overline{\mathbf{s}}(k)\in\Omega_{\overline{\mathbf{s}}}}{\arg\min} \left\| \overline{\mathbf{x}}(k) - \mathbf{\Phi}(k)\overline{\mathbf{s}}(k) \right\|^2. \tag{6.24}$$

Another alternative is to do joint MSI and mirror-carrier spatial equalization using the ZF principle as

$$\hat{\overline{\mathbf{s}}}_{ZF}(k) = \mathbf{\Phi}(k)^{-1}\overline{\mathbf{x}}(k) \tag{6.25}$$

after which ordinary element-wise detection is applied.

6.4 Practical Aspects and Examples

In general, the pilot grouping and I/Q imbalance estimation principles described in Section 6.3 are in many sense conceptually similar to the earlier developments in Section 5.3. Therefore, we can expect that the discussions on practical aspects raised in Section 5.4 are applicable to the proposed imbalance compensation approach in SM-MIMO-OFDM case as well. Thus no further discussion regarding the practical aspects will be given here. Instead, as a concrete example, the performance of the proposed compensator with ZF detector in (6.25) is examined using extensive computer simulations.

Numerical Examples and Simulations

For examining the performance of the proposed I/Q imbalance compensation algorithm, the same system setup deployed in Section 6.2 is used here. In general, the radio channels are random realizations from the Extended Vehicular A model [88]. A quasi-static system model is assumed such that the channel coefficients are assumed fixed over 1000 consecutive OFDM symbol intervals after which new channel realizations are drawn. The upper right corner symbol "$7 + j7$" of the used 64QAM subcarrier constellation is used as the pilot data s_P. Figure 6-6 shows the system SER performance with different numbers of pilot slots, averaged over all the active subcarriers. With multiple slots, averaging is used over the individual parameter estimates to decrease the additive noise effects. Clearly, with just a few pilot slots, the proposed pilot-based estimator-compensator can still achieve SER performance practically identical to the reference system.

Next, the pilot interpolation idea is examined by allocating the data of only every J_f-th mirror subcarrier pair as given in (6.18). The overall compensation structure with parameter interpolation is then illustrated in Figure 6-5. With cubic spline interpolation [46] and pilot spacing of $J_f = 6$, the resulting SER performance with different number of pilot slots is illustrated in Figure 6-7. The results show that with rather low pilot overhead, the proposed pilot-based compensation algorithm can still achieve very good SER performance. Again, as the error rate performance of the proposed technique is within 0.2dB from the perfectly matched reference, no further comparisons against possible other compensation techniques (other than the perfectly matched reference system) are carried out.

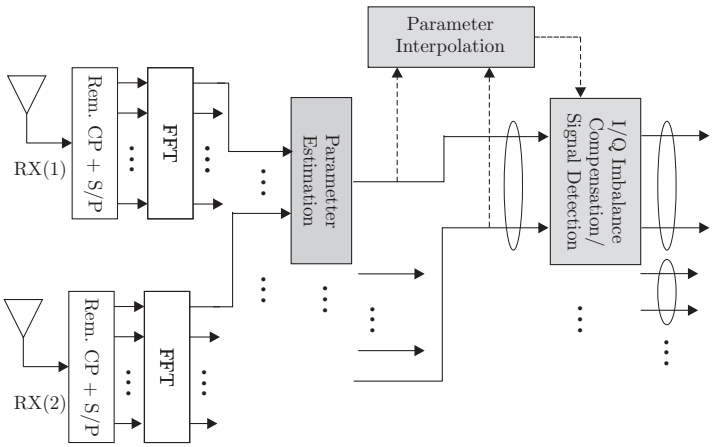

Figure 6-5: *Overall receiver structure including (i) I/Q imbalance parameter estimation, (ii) imbalance parameter interpolation, and (iii) imbalance compensation and signal detection, all using the designed pilot structure in (6.18). Imbalance parameter estimation and compensation are carried out in mirror-subcarrier wise manner. (Rem. refers to remove)*

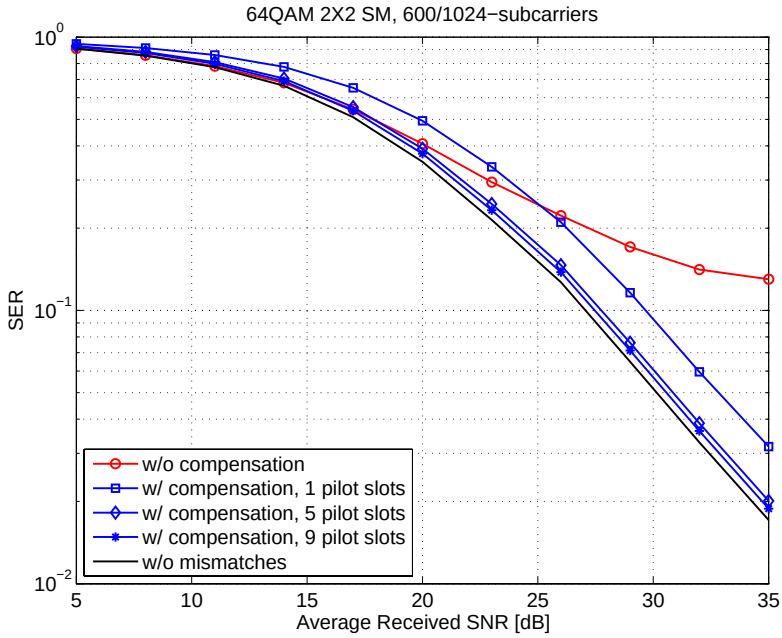

Figure 6-6: *Simulated 64-QAM symbol error rates, averaged for all the active subcarriers, with and without the proposed compensation technique, with different amounts of pilot symbols used for imbalance parameter estimation in the receiver. Perfectly matched reference curve is also shown assuming no I/Q imbalances and perfect channel knowledge. Extended Vehicular A radio channels.*

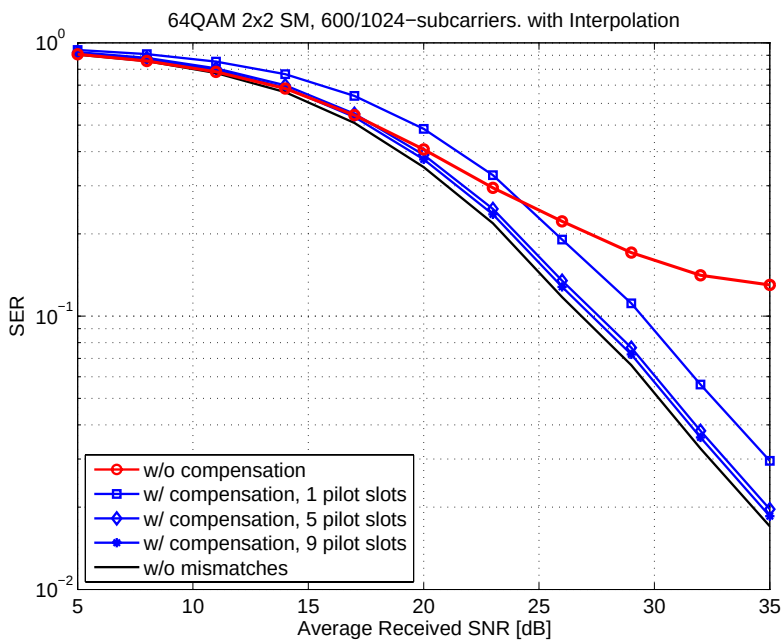

Figure 6-7: *Simulated 64-QAM symbol error rates, averaged for all the active subcarriers, with and without the proposed compensation technique, with different amounts of pilot symbols used for imbalance parameter estimation in the receiver. Cubic spline interpolation is used to interpolate estimated coefficients in (6.21) for active data subcarriers. Perfectly matched reference curve is also shown assuming no I/Q imbalances and perfect channel knowledge. Extended Vehicular A radio channels.*

Chapter 7

Frequency-Selective I/Q Imbalance Compensation in Individual Radios

In this chapter, instead of trying to mitigate the overall link distortion due to I/Q imbalances jointly on the receiver side, we address the imbalance mitigation problem from another point of view and try to compensate the I/Q imbalance effects within each radio transceiver. A pilot-based transmitter imbalance calibration scheme and a pilot-based receiver imbalance compensation method are proposed in Sections 7.1 and 7.2, respectively, targeted for OFDM radios. As will be shown later in Section 7.3, with proper arrangement, these two algorithms can then be used to calibrate the I/Q impairments of all the transmitters and receivers in individual multi-radio devices. In addition, different from conventional algorithms developed for single-antenna systems in the literature [10]–[12], [15], [36], [52], [54], [55], [76]–[78], [85], [89], [95], [104]–[110], [112], [113], the proposed algorithms extract the I/Q imbalance properties using a differential approach by essentially comparing the effects of impairments on consecutive pilot symbols. Together with the concept of inner loop calibration, this approach is shown to be robust against many practical aspects, making the proposed digital compensator a feasible solution for practical implementations.

7.1 Pilot-Based Transmitter Calibration

In the following, the effects of I/Q imbalance on the transmit waveform (mirror-subcarrier interference) in an OFDM transmitter are mitigated using proper baseband predistortion. The starting point is the mirror-subcarrier interference model (3.11) and (3.16).

Transmitter I/Q Imbalance Calibration Through Predistortion

Assume first that the frequency-selective I/Q imbalance properties in (3.16) over the subcarriers (i.e., $G_{1,TX}(k)$ and $G_{2,TX}(k)$) are known. Then, to remove mirror-subcarrier interference, the baseband complex data to be transmitted is predistorted by combining the signals at mirror-subcarriers k and $-k$ as

$$Z_c(k) = a_{TX,c}(k)Z(k) + b_{TX,c}(k)Z^*(-k). \tag{7.1}$$

In above, the combination coefficients $a_{TX,c}(k)$ and $b_{TX,c}(k)$ are selected such that when the predistorted signal goes through the actual transmitter analog sections, the generated RF waveform is free from I/Q imbalance. In terms of baseband equivalents, this can be stated as

$$\begin{aligned} Z_{TX,c}(k) &= C_{TX}(k)\Big(G_{1,TX}(k)Z_c(k) + G_{2,TX}(k)Z_c^*(-k)\Big) \\ &= C_{TX}(k)(G_{1,TX}(k)a_{TX,c}(k) + G_{2,TX}(k)b_{TX.c}^*(-k))Z(k) \\ &\quad + C_{TX}(k)(G_{2,TX}(k)a_{TX.c}^*(-k) + G_{1,TX}(k)b_{TX,c}(k))Z^*(-k) \\ &= C_{TX}(k)Z(k) \end{aligned} \tag{7.2}$$

where $C_{TX}(k)$ denotes the transmitter common response. This, in turn, implies that for perfect cancellation of mirror-frequency-interference, the following conditions of the form $G_{1,TX}(k)a_{TX,c}(k) + G_{2,TX}(k)b_{TX.c}^*(-k) = 1$ and $G_{2,TX}(k)a_{TX.c}^*(-k) + G_{1,TX}(k)b_{TX,c}(k) = 0$ need to be fulfilled. These can be now directly solved for $a_{TX,c}(k)$ and $b_{TX,c}(k)$ as

$$\begin{aligned} a_{TX,c}(k) &= \frac{{G_{1,TX}}^*(-k)}{{G_{1,TX}}^*(-k)G_{1,TX}(k) - {G_{2,TX}}^*(-k)G_{2,TX}(k)} \\ b_{TX,c}(k) &= \frac{-G_{2,TX}(k)}{{G_{1,TX}}^*(-k)G_{1,TX}(k) - {G_{2,TX}}^*(-k)G_{2,TX}(k)}. \end{aligned} \tag{7.3}$$

Thus, the predistortion coefficients $a_{TX,c}(k)$ and $b_{TX,c}(k)$ at k-th subcarrier depend on I/Q imbalance properties at subcarriers k and $-k$. This is fairly obvious based on (7.1) and (7.2) already.

Pilot-Based Estimation of Predistortion Coefficients

In practical implementations, the exact I/Q imbalance characteristics ($G_{1,TX}(k)$ and $G_{2,TX}(k)$ in (3.16)) are of course unknown and thus need to be estimated somehow. One simple but very efficient way to do the estimation is then to use feedback from RF back to lower frequencies inside the transmitter. As illustrated in Figure 7-1, real down-conversion from RF to a low-IF is used here in the feedback loop implementation (instead of direct I/Q down-conversion to baseband) to avoid excess I/Q imbalances due to feedback inaccuracies. Similar approach is deployed also, e.g., in [10]. Final I/Q down-conversion from IF to baseband in the feedback branch can then be carried out in the digital domain. We further assume that a training or calibration period is available during which the transmit signal can

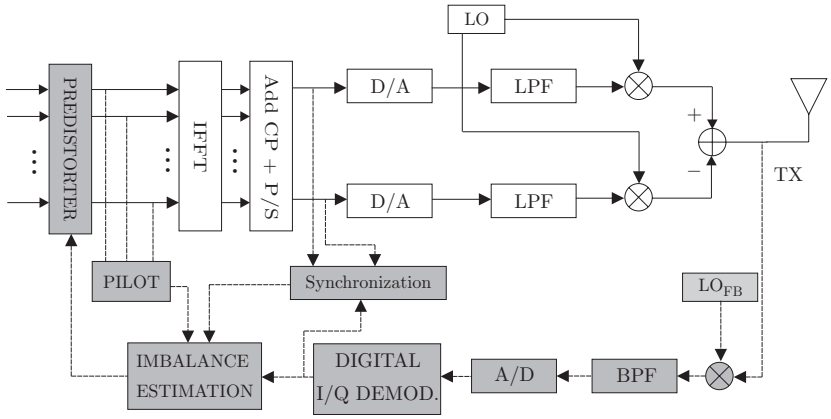

Figure 7-1: *The overall predistortion based transmitter calibration scheme where I/Q imbalances are estimated using a feedback loop.*

be allocated or designed purely for parameter estimation purposes, as will be explained in more details below. The overall imbalance estimation scheme is depicted in Figure 7-1.

We assume that two OFDM pilot symbols, $Z_p^{(m)}(k)$, $m = \{1,2\}$, are implemented for calibration and estimation purposes. Assuming further that proper pre-/post-fixing is used, as in any practical OFDM system, intersymbol interference between the pilot symbols is avoided. Then, the frequency domain observations (after feedback loop FFT) for the two pilot symbols are given by

$$X_{m,fb}(k) = C_{TX}(k)H_{FB}(k)(G_{1,TX}(k)Z_p^{(m)}(k) + G_{2,TX}(k)Z_p^{*(m)}(-k)), \tag{7.4}$$

$m = \{1,2\}$. Here $H_{FB}(k)$ denotes the total effective feedback response due to feedback branch filtering and down-converter gain and phase offset [P7]. Normally, the exact frequency-responses of the feedforward branch (common response) and the feedback loop are not known. Thus the two observations $X_{1,fb}(k)$ and $X_{2,fb}(k)$ cannot be used for estimation directly. However, it is very interesting to observe that the ratio of the feedback loop subcarrier observations $X_{1,fb}(k)$ and $X_{2,fb}(k)$ is independent of the *loop response* as well as of the *common feedforward response*, and can be used to extract the imbalance behavior. To see this more explicitly, we write this ratio as [P7]

$$\begin{aligned} Y_{fb}(k) &= \frac{X_{1,fb}(k)}{X_{2,fb}(k)} \\ &= \frac{C_{TX}(k)H_{FB}(k)(G_{1,TX}(k)Z_p^{(1)}(k) + G_{2,TX}(k)Z_p^{*(1)}(-k))}{C_{TX}(k)H_{FB}(k)(G_{1,TX}(k)Z_p^{(2)}(k) + G_{2,TX}(k)Z_p^{*(2)}(-k))} \\ &= \frac{G_{1,TX}(k)Z_p^{(1)}(k) + G_{2,TX}(k)Z_p^{*(1)}(-k)}{G_{1,TX}(k)Z_p^{(2)}(k) + G_{2,TX}(k)Z_p^{*(2)}(-k)}. \end{aligned} \tag{7.5}$$

Now, if the pilot symbols are designed such that $Z_p^{(1)}(k) \neq Z_p^{*(1)}(-k)$, $Z_p^{(1)}(k) / Z_p^{(2)}(k) \neq Z_p^{*(1)}(-k) / Z_p^{*(2)}(-k)$ and $Z_p^{(2)}(k) \neq Z_p^{*(2)}(-k)$, the I/Q imbalance coefficients can be estimated directly as [P7]

$$\hat{G}_{1,TX}(k) = \frac{Y_{fb}(k)Z_p^{*(2)}(-k) - Z_p^{*(1)}(-k)}{(Z_p^{(1)}(k) - Z_p^{*(1)}(-k)) - Y_{fb}(k)(Z_p^{(2)}(k) - Z_p^{*(2)}(-k))} \tag{7.6}$$

and

$$\hat{G}_{2,TX}(k) = 1 - \hat{G}_{1,TX}(k). \tag{7.7}$$

This can be easily verified by directly substituting the expression in (7.5) into (7.6). After estimating $G_{1,TX}(k)$ and $G_{2,TX}(k)$ for all the active subcarriers, the actual predistortion coefficients are then obtained as given in (7.3). One easily applicable practical scheme for pilot design is to set the subcarrier data according to $Z_p^{(1)}(k) = Z_p^{(1)}(-k)$ and $Z_p^{(2)}(k) = Z_p^{(2)}(-k) = Z_p^{*(1)}(k)$ where $Z_p^{(1)}(k)$ can basically be an arbitrary complex number (from the used symbol constellation).

7.2 Pilot-Based Compensation in Receivers

In the following, the digital calibration task continues to the receiver side. Here we assume that the transmitter I/Q imbalance has been mitigated such that the signal entering the receiver is originally free from mirror-frequency interference. Also, for analysis purposes, any possible common responses of transmitter and receiver are assumed to be lumped into the radio channel response. Then an efficient pilot-based digital estimation-compensation algorithm, being able to deal with frequency-selective I/Q imbalances, is developed and applied at the receiver.

Basic Compensation Principle

Assuming first that the I/Q imbalance properties $G_{1,RX}(k)$ and $G_{2,RX}(k)$ in (3.17) of the used radio receiver are known, digital imbalance compensation can basically be carried out by

linearly combining the received data at mirror frequency pairs (subcarriers k and $-k$). More formally, we write this as [P3]

$$\begin{aligned} Z_{RX,c}(k) &= a_{RX,c}(k)Z_{RX}(k) + b_{RX,c}(k)Z^*_{RX}(-k) \\ &= (G_{1,RX}(k)a_{RX,c}(k) + G^*_{2,RX}(-k)b_{RX.c}(k))Z(k) \\ &\quad +(G_{2,RX}(k)a_{RX,c}(k) + G^*_{1,RX}(-k)b_{RX,c}(k))Z^*(-k) \end{aligned} \tag{7.8}$$

with the idea of finding the two combination coefficients $a_{RX,c}(k)$ and $b_{RX,c}(k)$ such that the compensator output equals the received signal with perfect I/Q balance, i.e., $Z_{RX,c}(k) = Z(k)$. Combining then (7.8) and (3.17) with the target setting $Z_{RX,c}(k) = Z(k)$ yields directly

$$\begin{aligned} a_{RX,c}(k) &= \frac{{G_{1,RX}}^*(-k)}{G_{1,RX}(k){G_{1,RX}}^*(-k) - {G_{2,RX}}^*(-k)G_{2,RX}(k)} \\ b_{RX,c}(k) &= \frac{-G_{2,RX}(k)}{G_{1,RX}(k){G_{1,RX}}^*(-k) - {G_{2,RX}}^*(-k)G_{2,RX}(k)}. \end{aligned} \tag{7.9}$$

Notice that both $a_{RX,c}(k)$ and $b_{RX,c}(k)$ are only dependent on the I/Q imbalance coefficients at subcarriers k and $-k$. Again, it implies that proper I/Q imbalance estimation is then the key for efficient imbalance compensation.

Pilot-Based I/Q Imbalance Estimation

We assume that a pilot slot composed of two OFDM pilot symbols is transmitted from a perfectly matched transmitter. We assume further that the actual radio channel is time-invariant over a few consecutive symbol intervals. Then, based on the previous signal models, and assuming ideal synchronization and proper use of CP, the FFT output samples at subcarrier k ($Z^{(1)}_{RX}(k)$ and $Z^{(2)}_{RX}(k)$) and the corresponding conjugated samples at mirror subcarrier $-k$ ($Z^{(1)*}_{RX}(-k)$ and $Z^{(2)*}_{RX}(-k)$), measured over the two pilot symbol intervals, can be written as [P3]

$$\begin{aligned} \mathbf{r}_{RX}(k) &= \left[Z^{(1)}_{RX}(k) \;\; Z^{(2)}_{RX}(k) \right]^T = \mathbf{\Phi}(k)\mathbf{g}(k) \\ \mathbf{r}^*_{RX}(-k) &= [Z^{(1)*}_{RX}(-k) \;\; Z^{(2)*}_{RX}(-k)]^T = \mathbf{\Phi}(k)\overline{\mathbf{g}}(k) \end{aligned} \tag{7.10}$$

where

$$\begin{aligned}\mathbf{g}(k) &= \begin{bmatrix} G_{1,RX}(k) & G_{2,RX}(k) \end{bmatrix}^T \\ \overline{\mathbf{g}}(k) &= [G^*_{2,RX}(-k) \quad G^*_{1,RX}(-k)]^T\end{aligned} \tag{7.11}$$

and

$$\mathbf{\Phi}(k) = \begin{bmatrix} H(k)S_p^{(1)}(k) & H^*(-k)S_p^{*(1)}(-k) \\ H(k)S_p^{(2)}(k) & H^*(-k)S_p^{*(2)}(-k) \end{bmatrix}. \tag{7.12}$$

In (7.12), $S_p^{(m)}(k)$, $m = 1,2$, denote the two pilot symbol values at subcarrier k and $H(k)$ denotes channel frequency-response. Based on above, if the 2×2 matrix $\mathbf{\Phi}(k)$ at k -th subcarrier is known and invertible, the I/Q imbalance properties in terms of $\mathbf{g}(k)$ and $\overline{\mathbf{g}}(k)$ can be obtained by solving the linear equations in (7.10)–(7.12). Thus, at this point, the problem of I/Q imbalance estimation can be further translated to the problem of proper pilot "design" enabling efficient estimation of the matrix $\mathbf{\Phi}(k)$.

To emphasize simple implementation, the following pilot construction of the form

$$S_p^{(2)}(k) = jS_p^{(1)}(k) \tag{7.13}$$

is proposed here. The corresponding "system" matrix $\mathbf{\Phi}(k)$ is then given simply by

$$\mathbf{\Phi}(k) = \begin{bmatrix} 1 & 1 \\ j & -j \end{bmatrix} \begin{bmatrix} H(k)S_p^{(1)}(k) & 0 \\ 0 & H^*(-k)S_p^{*(1)}(-k) \end{bmatrix} \tag{7.14}$$

which is obviously invertible by-design (given that $S_p^{(1)}(k)$, $H(k)$ and $H(-k)$ are nonzero) and depends on both the known transmitted pilot symbols and the presumably unknown frequency-response of transmission channel. Now, it is interesting to note that this matrix $\mathbf{\Phi}(k)$ is still essentially identifiable, despite the possible lack of channel knowledge. More specifically, by using the earlier-established feature of the I/Q imbalance parameterization, reproduced here as $G_{1,RX}(k) + G^*_{2,RX}(-k) = 1$ and $G_{2,RX}(k) + G^*_{1,RX}(-k) = 1$, the sum of the received pilot data samples in (7.10) can be written as

$$\begin{aligned}\mathbf{r}_\Sigma(k) &= \mathbf{r}_{RX}(k) + \mathbf{r}^*_{RX}(-k) \\ &= \mathbf{\Phi}(k)\left[G_{1,RX}(k) + G^*_{2,RX}(-k) \quad G_{2,RX}(k) + G^*_{1,RX}(-k)\right]^T \\ &= \begin{bmatrix} 1 & 1 \\ j & -j \end{bmatrix}\left[H(k)S_p^{(1)}(k) \quad H^*(-k)S_p^{*(1)}(-k)\right]^T.\end{aligned} \tag{7.15}$$

Thus, the system matrix $\mathbf{\Phi}(k)$ at k -th subcarrier can be obtained directly as

$$\hat{\mathbf{\Phi}}(k) = \begin{bmatrix} 1 & 1 \\ j & -j \end{bmatrix} \mathrm{diag}_{2\mathrm{x}2}\left(\begin{bmatrix} 1 & 1 \\ j & -j \end{bmatrix}^{-1} \mathbf{r}_{\Sigma}(k) \right) \tag{7.16}$$

where $\mathbf{r}_{\Sigma}(k) = \mathbf{r}_{RX}(k) + \mathbf{r}_{RX}^{*}(-k)$ and $\mathrm{diag}_{2\mathrm{x}2}(.)$ denotes a 2x2 diagonal matrix of the input vector. With this estimated system matrix $\hat{\mathbf{\Phi}}(k)$, the actual I/Q imbalance properties at subcarriers k and $-k$ can then be obtained as

$$\hat{\mathbf{g}}(k) = \hat{\mathbf{\Phi}}(k)^{-1} \left[Z_{RX}^{(1)}(k) \;\; Z_{RX}^{(2)}(k) \right]^{T} \tag{7.17}$$

and

$$\hat{\bar{\mathbf{g}}}(k) = \hat{\mathbf{\Phi}}(k)^{-1} [Z_{RX}^{(1)*}(-k) \;\; Z_{RX}^{(2)*}(-k)]^{T} \tag{7.18}$$

as can easily be verified.

7.3 Application in Multi-Radio Transceivers

In general, the I/Q imbalance calibration and compensation algorithms formulated in Sections 7.1 and 7.2 are basically applicable and valid in any direct-conversion OFDM transmitter and receiver, respectively. While the focus in Sections 7.1 and 7.2 was initially mostly on a single transmitter and a single receiver, working on two sides of a communication link, the previous methods can also be directly applied within a multi-radio transceiver having multiple transmitters and receivers in a single device. As a concrete example, a sequential estimation and calibration procedure for a multi-transmitter device is illustrated in Figure 7-2. Here the pilot-based estimation-calibration flow is applied for one transmitter at a time. After all the transmitters have been calibrated, then they can be used to create mirror-frequency interference -free pilot reception for the corresponding receiver units of the device as shown in Figure 7-3. Thereon, the receiver I/Q imbalance estimation procedure developed in Section 7.2 is applied sequentially at each receiver. Compared to the notations in Section 7.2, the effective “radio” channel contains only the possible common responses of the transmit and receive units.

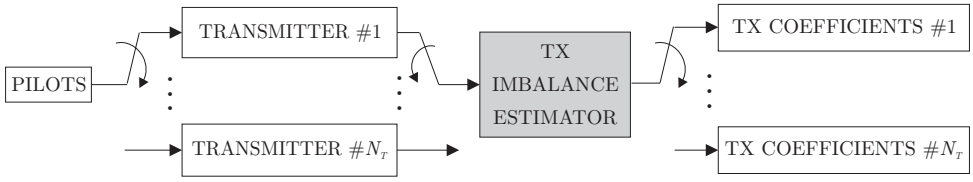

Figure 7-2: *Sequential transmitter I/Q imbalance estimation-calibration flow in a multi-transmitter device.*

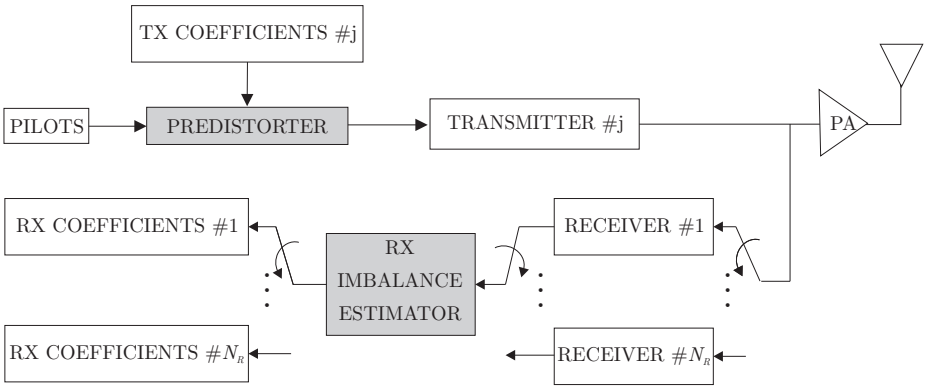

Figure 7-3: *Sequential receiver I/Q imbalance estimation-compensation flow in a multi-receiver device.*

7.4 Practical Aspects and Examples

Additive Noise

One important issue here is the unavoidable noise in the circuits. In both compensator derivations, only two OFDM pilot symbols were assumed. In order to get more reliable operation, e.g., in the presence of circuit noise, this basic pilot structure can be repeated. Then the individual imbalance estimates for each pilot slot can be averaged over time, assuming of course that the imbalance properties do not change in time (or at least vary very slowly) which should be a reasonable assumption in practice [75]. It should also be noted that the initial calibration is intended to be implemented at the start-up phase, while further monitoring of possible time-variant features can then also be implemented between the actual data slots or bursts in practice [P3], [P7].

Timing Synchronization

Assume that sufficiently long cyclic prefix used in the transmission phase, and this CP can cover the essential time-dispersion due to the feedback loop and the receiver itself (which are

typically short compared to actual radio channel delay spread). Then any residual timing error within the CP duration is only seen as additional phase rotations (complex exponentials) for different subcarriers, whose effects will cancel out similarly as those of other phase rotations when carrying out the previous estimation-compensation procedure. Based on this, it can be concluded that timing synchronization, within the CP duration, does not pose any essential limitation in the proposed techniques [P3], [P7].

Frequency Synchronization

In OFDM based transmission systems, correct and precise carrier synchronization is crucial. Here, as a single mother oscillator can be used to derive all the needed oscillator signals (actual up-converter, down-converter and the feedback loop down-converter), obtaining accurate frequency synchronization in both transmitter I/Q imbalance estimation and receiver I/Q imbalance estimation stages is then straight-forward. Thus the CFO problem can be generally avoided here.

Implementation Complexity

In general, with proposed approach, a feedback loop including a bandpass analog-to-digital converter (ADC) need to be implemented for the transmitter I/Q imbalance estimation. This in turn introduces extra implementation cost compared to the joint compensation approaches which were discussed in Chapter 5 and Chapter 6. Yet, on the other hand, the transmitter imbalance estimation and feedback signal processing are fully implemented inside the transmitter, so the dynamic range of the processed signals are expected to be really modest compared to actual received signals. Thus in this sense, the requirements for the ADC quality are fairly relaxed in practice.

Numerical Examples and Simulations

To give some illustrations about the performance of the proposed compensators, we consider an example multi-user multi-antenna transmission scenario below. As shown in Figure 7-4 and Figure 7-5, there are two mobile users in the system, each of which has only one antenna. During uplink transmission, both of them send signals to the same base-station which has 2 receive and 2 transmit antennas. Without any transmit precoding, this uplink forms a 2×2 SM multi-user MIMO-OFDM scenario [102]. On the other hand, during downlink transmission, 2×1 STC-OFDM transmission scheme is deployed for each user and time division multiple access (TDMA) is used as the multiple access scheme. The number of subcarriers is assumed to be 256. The quadrature mixer I/Q imbalance values as well as the

branch difference filters on the base station side are 4%, -4°, $[1, 0.04, -0.03]$ (TX1), 3%, 3°, $[1, -0.04, -0.03]$ (TX2), and 2%, 2°, $[1, 0.05]$ (RX1), and -3%, -3°, $[1, -0.03, 0.04]$(RX2). The corresponding parameters on the mobile users sides are 3%, -3°, $[1, 0.04, -0.03]$ (TX of user #1) 5%, 5°, $[1, 0.05]$ (RX of user #1), 1%, 1°, $[1, -0.04, -0.03]$ (TX of user #2), and -4%, 5°, $[1, 0.02, -0.05]$ (RX of user #2). In general, the radio channels of both links are random realizations of the Extended Vehicular A model [88]. A quasi-static system model is assumed such that the channel coefficients are assumed fixed over 1000 consecutive OFDM symbol intervals after which new channel realizations are drawn. The previous transceiver I/Q imbalance calibration procedures are carried out before the actual data transmission phase, on both mobile transmitters and the two base-station receivers in the uplink case and both mobile receivers and the two base-station transmitters in the downlink case. During the calibration, the effective SNR due to circuit noise inside the transceivers is assumed to be 35dB as an example value. During calibration, the pilot interpolation idea is applied with an example pilot spacing of $J_f = 5$ along the frequency axis. In time-direction, only 3 pilot slots are used here, over which the estimated quantities are averaged at each subcarrier. Cubic spline interpolator is used as an example interpolation technique and the upper right-corner symbol $7 + 7j$ of the used 64QAM alphabet is used as the pilot symbol at all the pilot subcarriers. After calibration period, in order to actually detect the received data during link operation, ideal knowledge of the channel frequency-responses is assumed to be available and ZF detector is deployed.

The resulting detection error performances are then finally evaluated with and without compensation. As shown in Figure 7-6 and Figure 7-7, with a fairly small amount of available pilot data, in both uplink and downlink transmission, the SER performance for both users approach the ideal reference system performance. Thus, taking into account its practical advantages, this inner loop calibration approach discussed in this chapter provide a rather feasible way to cope with the I/Q imbalance effects in multi-user, multi-antenna scenario.

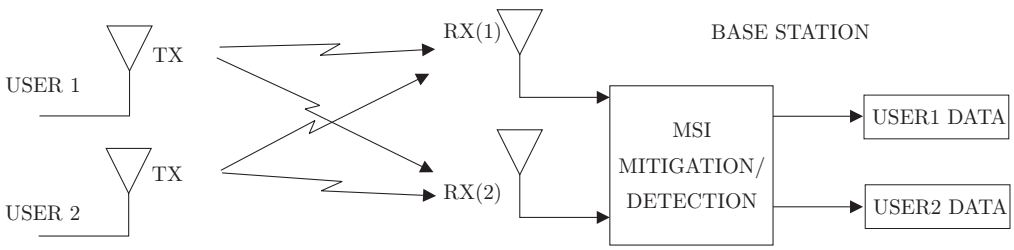

Figure 7-4: *An example 2x2 multi-user multi-antenna transmission system uplink.*

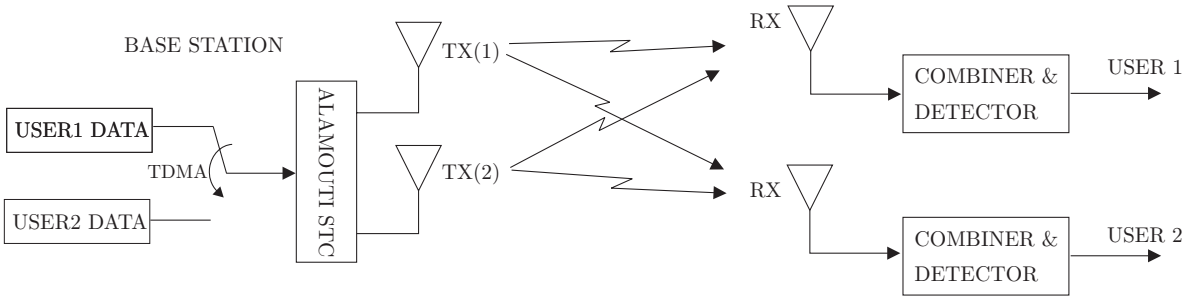

Figure 7-5: *An example 2x2 multi-user multi-antenna transmission system downlink.*

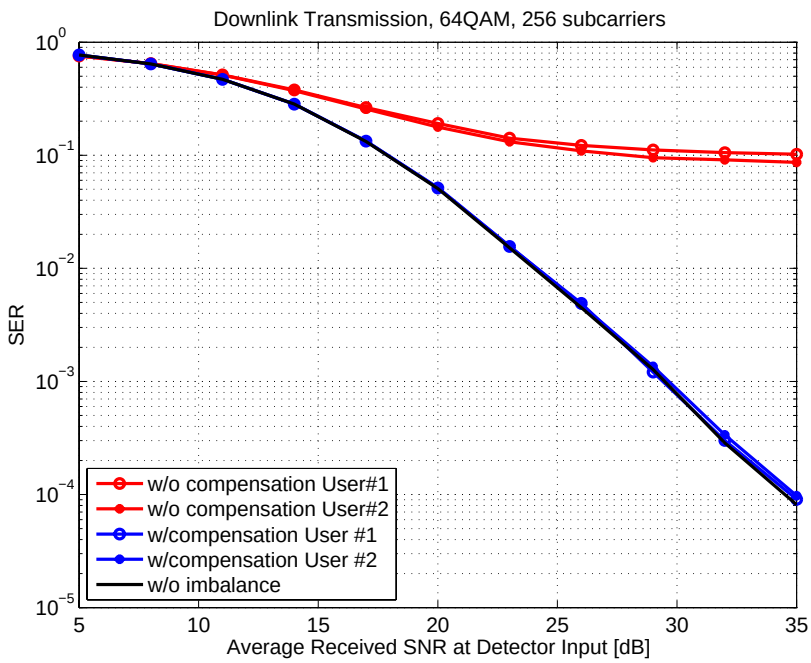

Figure 7-6: *Simulated system performance of the example 2-user multi-antenna downlink transmission system. 3 pilot slots are used in the transmitter and receiver I/Q imbalance estimation stages, respectively. In the actual data detection, perfect channel knowledge is assumed. Perfectly matched reference curve is also shown assuming no I/Q imbalances.*

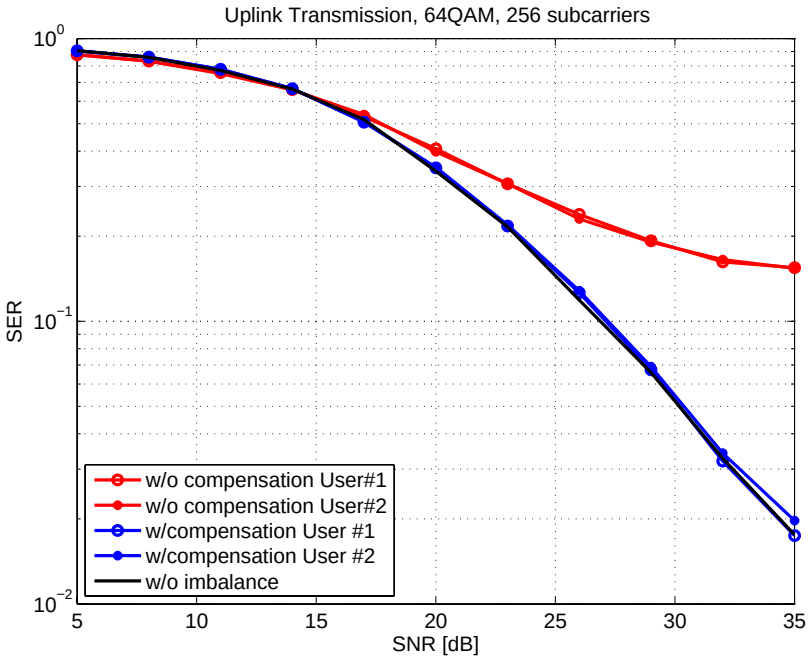

Figure 7-7: *Simulated system performance of the example 2-user multi-antenna uplink transmission system. 3 pilot slots are used in the transmitter and receiver I/Q imbalance estimation stages, respectively. In the actual data detection, perfect channel knowledge is assumed. Perfectly matched reference curve is also shown assuming no I/Q imbalances.*

Chapter 8

Conclusions

Current focus in the development of new wireless communication systems is on increasing the system capacity, spectral efficiency and coverage as well as improving the flexibility and efficiency of the radio spectrum use. Lots of attention and efforts have been paid in the recent years by both academy and telecommunications industry to developing enabling technologies at waveform and digital signal processing levels. The use of multiple antennas and advanced signal processing techniques on the transmitter and receiver sides has drawn most interest and is currently seen as the main physical layer technology. However, the actual radio implementation aspect, which is of major concern especially on the terminal side has not been thoroughly investigated yet in multi-antenna multi-radio context.

In a multi-antenna radio device, multiple transmitters and receivers need to be implemented. This is generally a challenging task calling for a proper compromise and trade-off between the size, cost and performance of the individual radio equipment. Therefore, to minimize the size and cost as well as to emphasize radio re-configurability, rather simple radio architectures and RF front-ends, such as the direct-conversion radio topology, are likely to be deployed. In such radios, the quality of the remaining analog RF modules is one key element from the overall radio performance point of view. More specifically, any nonidealities in the used electronics can easily distort the transmitted and received waveforms in a considerable manner. With wideband modulated communication waveforms and high-order symbol alphabets, this problem is even further emphasized and can eventually degrade the whole wireless link performance, if not properly understood and combated through proper analog or digital signal processing.

In this thesis, one example of such implementation nonidealities in direct-conversion transceivers, namely the I/Q imbalance, was thoroughly studied in a multi-antenna communication system context. Different from the traditional approach of evaluating and mitigating the I/Q imbalance effects in each individual radio, the overall signal distortion and waveform degradation were studied from the overall link performance point of view, taking

both transmitter and receiver sides as well as the transmission channels into account. As the main contribution, the challenging yet practical case of having frequency-dependent I/Q imbalances in all the radios was considered, which is essential in the future system developments with bandwidths in the order of tens of MHz. Then the overall signal distortion due to the I/Q imbalances was analyzed, in terms of resulting SIR, in STC single-carrier transmission systems, STC-OFDM transmission systems and SM-MIMO-OFDM transmission systems, respectively. The derived SIR values form an upper bound on the achievable overall SINR in the link prior to the data detection. Thus the SIR analysis results can be used to assess the role of I/Q imbalances on the link performance in typical multi-antenna system without lengthy system simulations, and therefore give a valuable tool for the system and transceiver designers. In general, based on the analysis results, the resulting link-level SIR values are *considerably lower* than the corresponding qualities of the individual radios. This thus basically shows that traditional imbalance analysis using the image attenuations of the individual radios alone is *not* sufficient anymore. The proposed link-level analysis is thus proven to be necessary in this context for fully understanding and appreciating the impact of I/Q imbalance on multi-antenna transmission systems. Altogether I/Q imbalances can lead to a severe reduction in the overall link noise margin, especially with higher-order spectrally efficient modulation methods, such as 64QAM.

Next, stemming from the derived overall link signal models, two types of digital compensation methods were proposed for jointly mitigating the I/Q imbalance effects due to imperfections of the individual radio front-ends on the receiver side. The first method is based on a pilot-based estimator-compensator structure and is applicable in both single-carrier and multi-carrier multi-antenna transmission systems with minor modifications. The second one builds on blind signal separation principles combined with proper I/Q decomposition of the received signal, and is mainly targeted for the single-carrier transmission case. Both methods were shown to be robust to many practical aspects and to provide compensation performance close to or practically at the perfectly matched reference system bound under rather realistic signaling assumptions.

In addition to joint link compensation, we also considered mitigation and calibration of I/Q imbalances within individual radio transceiver. More specifically, pilot-based compensators for calibrating the transmitter and receiver I/Q imbalances within single transceiver were proposed. On the transmitter side, feedback from RF back to the transmitter digital parts was deployed, combined with proper pilot data, to estimate and calibrate I/Q imbalances. On the receiver side, in turn, the estimation and compensation of effective I/Q imbalances was based on a properly designed pilot data structure together with the algebraic properties of the derived received signal

models. In a multi-antenna multi-radio terminal, a sequential approach was then also proposed to calibrate the overall transceiver.

In general, both of the above compensation approaches can be efficiently applied for I/Q imbalance mitigation. The first one, the joint compensation approach, is conceptually simple and has low implementation complexity in the sense that the joint impact of all the radios is combated as a whole. Yet it needs precise coordination between both sides of the link in terms of time and frequency synchronization. On the other hand, the latter compensation approach of individual transceiver compensation is simple and practical in the sense that only transceiver-internal signal processing is needed. Yet the needed feedback loop may increase the overall implementation complexity, which is especially critical on the terminal side.

In general, with different system setups, implementation resources and practical considerations, it is likely that there is no perfect universal solution for arbitrary multi-antenna multi-radio impairment mitigation. Thus, regarding the I/Q imbalance compensation issue in the multi-antenna transmission context, in addition to proposing different solutions, it is of the same importance to devise proper compensation strategies conforming with the given system specifications and available signal processing resources. In addition, if other imperfections, e.g., CFO, phase noise and nonlinearities, are also considerably affecting the transmitted and/or received signal quality, possibly combined with mobility effects, even more sophisticated signal processing techniques are most likely needed.

Chapter 9

Summary of Publications and Author's Contributions

Here we shortly summarize the contents of the original publications [P1]–[P8] and also review the contributions of the thesis author to individual publication contents.

9.1 Summary of Publications

The fundamental idea of viewing the effects of I/Q imbalances on multi-antenna transmission systems, taking both transmitter and receiver into accounts, is originally introduced in [P4]. The system level signal model for the receiver output in the 2×1 STC single-carrier systems is then addressed, together with the performance analysis on the resulting SIR assuming frequency-independent I/Q imbalances. In [P1], this analysis is extended to a more general case where 2 transmitters and N_R receivers are implemented. As shown by the analysis, the traditional imbalance analysis using the image attenuations of the individual radios alone is not sufficient any more. The proposed system level SIR analysis does provide much insight in evaluating the role of I/Q imbalance problem in multi-antenna systems. Two types of digital compensation methods, pilot-based and BSS-based, are then proposed for combating the I/Q imbalance effects on the receiver side. In addition to single-carrier systems, the performance of STC transmission system under I/Q imbalances is also studied with OFDM waveforms in [P2] and [P5]. The corresponding spatial multiplexing MIMO-OFDM case is, in turn, addressed in [P8]. While [P1], [P4] and [P5] mainly concentrate on the frequency-independent signal models, the effects of frequency-selective mismatches on wideband multi-antenna transmission are thoroughly addressed in [P2] and [P8]. Based on the closed-form frequency-domain link performance analysis in [P2] and [P8], with bandwidths in the order of several MHz, the values of SIR are shown to vary as a function of frequency. The

derived SIR values are subcarrier specific and give an upper bound on the achievable overall SINR in the system prior to the data detection. Furthermore, the impact of I/Q imbalances on the channel estimation in the STC-OFDM transmission context is also analyzed in [P2]. Stemming from the derived signal models, practical pilot-based I/Q imbalance compensation schemes are also proposed in [P2], being able to jointly compensate the effects of frequency-selective I/Q imbalances as well as channel estimation errors. In [P6], this algorithm is further modified with the pilot interpolation idea. The performance of this compensator is shown to be able to virtually reach the perfectly matched reference system performance with rather low pilot overhead. In general, the paper [P2] can be clearly regarded as the core of this thesis. In [P8], similar signal modeling and performance studies are carried out in the SM-MIMO-OFDM context. A closed-form solution for the effective SINR at the input of the receiver detection stage due to frequency-selective transmitter and receiver I/Q imbalances is derived. Again, the derived SINR can be directly mapped to the achievable detection error rate at high SNR regime, yielding a valuable analytical tool for radio transceiver designers to analyze the imbalance effects at link-level without any actual system simulations.

After addressing the analysis and compensation of transmitter and receiver I/Q imbalances jointly on the receiver side, the task of estimating and calibrating the I/Q imbalances of single OFDM radios is studied in [P7] and [P3]. More specifically, in [P7], a feedback loop from RF to baseband is deployed, which together with a properly-designed pilot signal structure, enables efficient estimation of transmitter I/Q imbalance properties in a subcarrier-wise manner. Then based on the obtained I/Q imbalance knowledge, the imbalance effects on the actual transmit waveform are mitigated by baseband predistortion acting on the mirror-subcarrier signals. For receiver calibration, the proposed algorithm in [P3] extracts the I/Q imbalance properties using a differential pilot method and then co-compensates the received data at mirror-subcarrier pairs.

9.2 Author's Contributions to the Publications

The research work for this thesis was carried out at the Department of Communications Engineering (DCE), Tampere University of Technology (TUT), Finland. Originally, the research topic was proposed by the author. The idea of building an overall link-level signal model, taking both transmitter and receiver I/Q imbalances into account, was also originally introduced by the author. Then this idea was formalized and extended to the link-level SIR analysis by the supervisor, Prof. Valkama, resulting in publication [P4] where the author served as the second author. After the initial studies, all the rest I/Q signal processing research

reported in this thesis was done mainly by the author, naturally supervised and guided by the thesis supervisor Prof. Valkama. Thus, the author is the primary author in all the original papers [P1], [P2], [P5]–[P8]. It goes without saying that the numerous informal discussions between the author and the supervisor have contributed to the reported results, to the publication writing as well as to the general research directions considerably.

In general, the credit for writing the bulk of script for [P1], initially viewing the I/Q imbalance problem in the OFDM context in frequency-dependent manner and using interpolation techniques to reduce pilot overhead in compensation stage belongs to the thesis supervisor Prof. Valkama. As the main contributor to the original papers [P1], [P2], [P5]–[P8], the author has developed all the signal models, carried out all the performance analyses, and performed the computer simulations reported in the publications. In addition, the author also wrote the scripts of [P2], [P5]–[P8]. Naturally, the supervisor Prof. Valkama contributed to the final appearance of all the papers.

The publication [P3] is basically a co-publication stemming from the international cooperation between TUT, Finland, and DICE, Austria. Dr. Hueber, from DICE, was the first author and organizer of this paper. Other contributors from DICE are Dr. Dufrene and Dr. Stuhlberger. The author of this thesis contributed all the content and script writing regarding the I/Q imbalance issues in [P3] (Section V).

Appendix

RF-IC I/Q Imbalance Laboratory Measurements

In this Appendix, a laboratory measurement setup and procedures for characterizing the mirror-frequency attenuation (IRR) of a complete RF-IC are briefly described. The basic measurement system is shown in Figure A-1 below. Special RF measurement equipment and software, namely Rohde&Schwarz SMIQ and WinIQSim, are used for generating the RF signals with the possibility of feeding the modulating baseband or IF signals through a lab PC. Then the generated RF signal is fed into the RF-IC which includes tunable RF low-noise amplifier (LNA), I/Q demodulator, BB filters and BB amplifiers, converting the incoming RF signal into low-frequency I and Q components. Then, following the I and Q outputs of the RF-IC, two samplers and ADCs are deployed for transforming the analog I and Q signals into digital domain. These digitized I and Q signals are then stored into memory with a link to lab PC for further digital processing. The final data processing and mirror-frequency attenuation evaluations are then carried out in a laboratory computer.

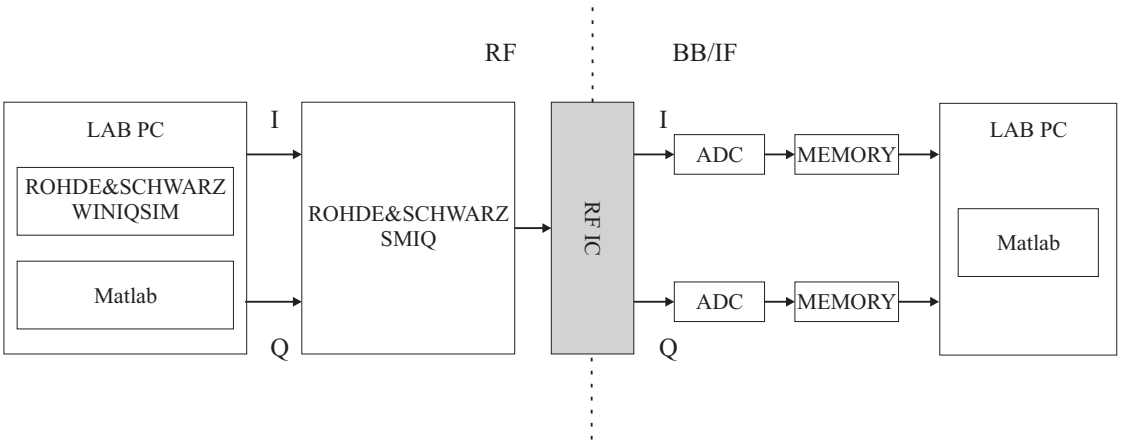

Figure A-1: *Principal block-diagram of the laboratory measurement system.*

Using the measurement system setup shown in Figure A-1 and above-mentioned test procedures, the IRR characteristics of the RF-IC shown is then analyzed by using multi-tone RF test signals. More specifically, altogether 10 sinusoidal RF carriers are fed into the receiver either below or above 2 GHz which is the assumed operating frequency of the used RF-IC. The RF input power and gain settings of the amplification stages are set such that reasonable dynamics is observed at the ADC inputs. Then the sampled signals are stored into memory, loaded into PC and processed and analyzed using Matlab. As a result, the measured IRR curve as a function of frequency depicted in Figure 3-3 is finally obtained.

Bibliography

[1] 3GPP Technical Specification Group Radio Access Network, "LTE physical layer – General description," TR 36.201, Nov. 2007.

[2] 3GPP Technical Specification Group Radio Access Network, "Overall description of E-UTRA/E-UTRAN; Stage 2," TR 36.300, V8.3.0, Dec. 2007.

[3] 3GPP Technical Specification Group Radio Access Network, "High speed downlink packet access (HSDPA); Overall description; Stage 2," technical specification TS 25.308, V8.1.0, Mar. 2008.

[4] 3GPP Technical Specification Group Radio Access Network, "User equipment (UE) radio transmission and reception (FDD)," technical specification TS 25.101, V8.2.0, Mar. 2008.

[5] A. A. Abidi, "Direct conversion radio transceivers for digital communications," *IEEE J. Solid-State Circuits*, vol. 30, pp. 1399–1410, Dec. 1995.

[6] A. A. Abidi, "Low-power radio-frequency ICs for portable communications," in L. E. Larson, Ed., *RF and Microwave Circuit Design for Wireless Communications*. Norwood, MA: Artech House, 1996, pp. 43–98.

[7] A. A. Abidi, "CMOS wireless transceiver: The new wave," *IEEE Commun. Mag.*, vol. 37, pp. 119–124, Aug. 1999.

[8] A. A. Abidi, "RF CMOS comes of age," *IEEE J. Solid-State Circuits*, vol. 39, no. 4, pp. 549–561, 2004.

[9] S. M. Alamouti, "A simple transmit diversity technique for wireless communications," *IEEE J. Sel. Areas Commun.*, vol. 16, pp. 1451–1458, Oct. 1998.

[10] L. Anttila, M. Valkama, and M. Renfors, "Frequency-selective I/Q mismatch calibration of wideband direct-conversion transmitters," *IEEE Trans. Circuits Syst. II, Exp. Briefs*, vol. 55, pp. 359–363, Apr. 2008.

[11] L. Anttila, M. Valkama and M. Renfors, "Circularity-based I/Q imbalance compensation in wideband direct-conversion receivers," *IEEE Trans. Veh. Technol.*, vol. 57, pp. 2099–2113, July 2008.

[12] L. Anttila, M. Valkama and M. Renfors, ” Efficient mitigation of frequency-selective I/Q imbalance in OFDM receivers”, in *Proc. IEEE Veh. Technol. Conf.,* Calgary, Canada, Sep. 2008.

[13] S. Baro, G. Bauch, and A. Hansmann, “Improved codes for space-time trellis-coded modulation,” *IEEE Commun. Lett.*, vol. 4, pp. 20–22, Jan. 2000.

[14] J. B. Barry, D. G. Messerschmitt and E. A. Lee, *Digital Communications*. New York: Springer, 2003.

[15] M. G. Di Benedetto and P. Mandarini, “Analysis of the effect of the I/Q base-band filter mismatch in an OFDM modem,” *Wireless Personal Communications*, vol. 12, pp. 175–186, 2000.

[16] P. A. Bello, "Characterization of randomly time-variant channels," *IEEE Trans. Commun.*, vol. 11, no. 4, pp. 360–393, 1963.

[17] H. Boelcskei, D. Gesbert, and A. J. Paulraj, “On the capacity of OFDM based spatial multiplexing systems,” *IEEE Trans. Commun.*, vol. 50, no. 2, pp. 225–234, Feb. 2002.

[18] D. Brennan, “Linear diversity combining techniques,” *Proc. IRE*, vol. 47, pp. 1075–1102, June 1959.

[19] M. Cao and Hongya Ge, “I/Q imbalance in MIMO STBC communication systems: Impact and solution,” in *Proc. IEEE Military Commun. Conf.*, San Diego, CA, Nov. 2008.

[20] M. Cao and H. Ge, “GLCP OFDM systems with I/Q imbalance,” *IEEE Commun. Lett.*, vol. 13, pp. 230–232, Apr. 2009.

[21] J. F. Cardoso and B. H. Laheld, “Equivariant adaptive source separation,” *IEEE Trans. Signal Process.*, vol. 44, pp. 3017–3030, Dec. 1996.

[22] J. F. Cardoso, “Blind signal separation: Statistical principles,” *Proc. IEEE*, vol. 86, pp. 2009–2025, Oct. 1998.

[23] H. H. Chen, M. Guizani, and J. F. Huber, Eds., “Multiple access technologies for B3G wireless communications,” *IEEE Commun. Mag.*, vol. 43, pp. 65–67, Feb. 2005.

[24] C. Chien, *Digital Radio Systems on a Chip*. Norwell, MA: Kluwer, 2001.

[25] R. Clarke, "A statistical theory of mobile-radio reception," *Bell Syst. Technol. J.*, No. 7, pp. 957–1000, 1968.

[26] J. Crols and M. S. J. Steyaert, *CMOS Wireless Transceiver Design*. Dordrecht, the Netherlands: Kluwer, 1997.

[27] S. Diggavi, N. Al-Dhahir, A. Stamoulis, and A. Calderbank, "Great expectations: The value of spatial diversity in wireless networks," *Proc. IEEE*, vol. 92, no. 2, pp. 219–270, Feb. 2004.

[28] R. Eickhoff, R. Kraemer, I. Santamaria, and L. Gonzalez, "Developing energy-efficient MIMO radios," *IEEE Veh. Technol. Mag.*, vol. 4, no. 1, pp. 34–41, Mar. 2009.

[29] G. Fettweis *et al.*, "Dirty RF," in *Proc. Wireless World Research Forum (WWRF) Meeting 11*, Oslo, Norway, June 2004.

[30] G. J. Foschini, "Layered space-time architecture for wireless communication in a fading environment when using multiple antennas", *Bell Lab. Technol. J.*, vol. 1, no. 2, pp. 41–59, 1996.

[31] G. J. Foschini, "On limits of wireless communications in a fading environment when using multiple antennas," *Wireless Personal Commun.*, vol. 6, pp. 311–335, 1998.

[32] M. E. Frerking, *Digital Signal Processing in Communication Systems*. New York: Chapman & Hall, 1994.

[33] J. Gao, X. Zhu, Hai Lin and A. Nandi, "Blind I/Q imbalance compensation using independent component analysis in MIMO OFDM systems", in *Proc. IEEE Wireless Commun. Netw. Conf.*, Budapest, Hungary, Apr. 2009.

[34] D. Gesbert *et al.*, "From theory to practice: An overview of MIMO space-time coded wireless systems," *IEEE J. Sel. Areas Commun.*, vol. 21, pp. 281–302, Apr. 2003.

[35] H. Geun Park, C. Park, H. Oh, and M. Geon Kyeong, "RF gain/phase and I/Q imbalance error correction technique for multi-channel array antenna systems," in *Proc. IEEE Veh. Technol. Conf.*, Rhodes, Greece, May 2001, pp. 175–179.

[36] G. T. Gil, Y. D. Kim, and Y. H. Lee, "Non-data-aided approach to I/Q mismatch compensation in low-IF receivers" *IEEE Trans. Signal Process.*, vol. 55, pp. 3360–3365, Jul. 2007.

[37] Q. Z. Gu, *RF System Design of Transceivers for Wireless Communications*. New York: Springer, 2005.

[38] H. F. Harmuth, "Fundamental limits for radio signals with large bandwidth," *IEEE Trans. Electromagn. Compat.*, vol. EMC23, pp. 37– 43, Feb. 1981.

[39] S. Haykin, *Adaptive Filter Theory*, 3rd ed. Upper Saddle River, NJ: Prentice-Hall, 1996.

[40] S. Haykin, Ed., *Unsupervised Adaptive Filtering, vol. I: Blind Source Separation*. New York: John Wiley & Sons, 2000.

[41] L. He, T. Thaiupathump, and S. A. Kassam, "Blind separation of complex I/Q independent sources with phase recovery," *IEEE Signal Process. Lett.*, vol. 12, pp. 419–422, May 2005.

[42] A. A. Hutter, J.S. Hammerschmidt, E. de Carvalho, and J.M. Cioffi, "Receive diversity for mobile OFDM systems", in *Proc. IEEE Wireless Commun. and Netw. Conf.,* vol. 2, pp. 707–712, Sep. 2002.

[43] T. Kaiser, A. Bourdoux, H. Boche, J.R. Fonollosa, J.B. Andersen, and W. Utschick, *Smart Antennas: State of the Art*. Hindawi Publication Corporation, 2005.

[44] H. Kamata, K. Sakaguchi, and K. Araki, "An effective IQ imbalance compensation scheme for MIMO-OFDM communication system," in *Proc. IEEE Int. Symp. Pers., Indoor, Mobile Radio Commun.*, Berlin, Germany, Sept. 2005.

[45] P. Kenington, *RF and Baseband Techniques for Software Defined Radio*. Norwood, MA: Artech House, 2005.

[46] D. R. Kincaid and E. W. Cheney, *Numerical Analysis: Mathematics of Scientific Computing*. Brooks Cole, 2001.

[47] P. Kiss and V. Prodanov, "One-tap wideband I/Q compensation for zero-IF filters," *IEEE Trans. Circuits Syst. I, Reg. Papers*, vol. 51, pp. 1062–1074, June 2004.

[48] M. Krondorf and G. Fettweis, "Numerical performance evaluation of Alamouti space time coded OFDM under receiver impairments," *IEEE Trans. Wireless Commun.*, vol. 8, pp. 1446–1455, Mar. 2009.

[49] S. Krone and G. Fettweis, "Capacity analysis for OFDM systems with transceiver I/Q imbalance", in *Proc. Global Telecommun. Conf.*, New Orleans, CA, Nov. –Dec. 2008, 1317–1321.

[50] E. A. Lee and D. G. Messerschmitt, *Digital Communication*, 2nd ed. Norwell, MA: Kluwer, 1994.

[51] K. Lee and D. Williams, "A space-time coded transmitter diversity technique for frequency selective fading channels," in *Proc. IEEE Sensor Array Multichannel Signal Process.Workshop*, Cambridge, MA, Mar. 2000, pp. 149–152.

[52] L. Li, F. Lin, and H. Chuang, "Complete RF-system analysis of direct conversion receiver (DCR) for 802.11a WLAN OFDM system," *IEEE Trans. Veh. Technol.*, vol. 56, pp. 1696–1703, Part 1, July 2007.

[53] X. Li and M. Ismail, *Multi-Standard CMOS Wireless Receivers*. Norwell, MA: Kluwer, 2002.

[54] H. Lin, T. Adachi, and K. Yamashita, “Carrier frequency offset and I/Q imbalances compensation in OFDM systems”, in *Proc. Global Telecommun. Conf.*, Washington DC, USA, Nov. 2008, pp. 2883–2888.

[55] H. Lin and K. Yamashita, “Subcarrier allocation based compensation for carrier frequency offset and I/Q imbalances in OFDM systems,” *IEEE Trans. Wireless Commun.*, vol. 8, pp. 18–23, Jan. 2009.

[56] J. Liu *et al.*, “Impact of front-end effects on the performance of downlink OFDM-MIMO transmission”, in *Proc. IEEE Radio Wireless Conf.*, Atlanta, GA, Sept. 2004, pp. 159–162.

[57] S. Mirabbasi and K. Martin, “Classical and modern receiver architectures,” *IEEE Commun. Mag.*, vol. 38, pp. 132–139, Nov. 2000.

[58] A. F. Molisch, ed., *Wireless Communications.* Chichester: Wiley, 2005.

[59] B. Narasimhan, D. Wang, N. Al-Dhahir, and H. Minn, "Digital baseband compensation for mobile SFBC-OFDM systems with receiver I/Q imbalance," in *Proc. Global Telecommun. Conf.*, New Orleans, CA, Nov. –Dec. 2008.

[60] B. Narasimhan, S. Lu, N. Al-Dhahir, and H. Minn, "Digital baseband compensation of I/Q imbalance in mobile OFDM," in *Proc. IEEE Wireless Commun. & Network Conf.*, Las Vegas, NV, 2008, pp. 1183–1187.

[61] B. Narasimhan, S. Narayanan, N. AlDhahir, and H. Minn,”Digital compensation of joint Tx/Rx frequency-dependent I/Q imbalance in mobile MIMO-OFDM transceivers,” in *Proc. Conf. Inf. Science and Systems*, Baltimore, MD, Mar. 2009, pp. 545–550.

[62] B. Narasimhan, D. Wang, S. Narayanan, H. Minn, and N. AlDhahir, ”Digital compensation of frequency-dependent joint Tx/Rx I/Q imbalance in OFDM systems under high mobility,” *IEEE J. Sel. Topics Signal Process.*, vol. 3, pp. 405–417, Jun. 2009.

[63] R. van Nee and R. Prasad, *OFDM Wireless Multimedia Communications*. Norwood, MA: Artech House, 2000.

[64] R. van Nee, A. van Zelst, and G. Awater, “Maximum likelihood decoding in a space division multiplexing system", in *Proc. IEEE Veh. Technol. Conf.*, Tokyo, Japan, May 2000, vol. 1, pp. 6–10.

[65] M. N. Neto, R. D. Souza, A. N. Barreto and A.M. Cavalcante, “Exploiting I/Q imbalance in direct conversion transceivers for improving the performance of a V-BLAST OFDM system”, in *Proc. IEEE Veh. Technol. Conf.*, Barcelona, Spain, Apr. 2009.

[66] Radio aspects for the terrestrial component of IMT-2000 and system beyond IMT-2000. Rec. ITU-RM.2074, 2005.

[67] A. Papoulis, *Probability and Statistics*. Upper Saddle River, NJ: Prentice-Hall, 1990.

[68] A. Paulraj, R. Nabar, and D. Gore, *Introduction to Space-Time Wireless Communications*. Cambridge, UK: Cambridge University Press, 2003.

[69] A. Paulraj, D. Gore, R. Nabar, and H. Bolcskei, "An overview of MIMO communications: A key to gigabit wireless," *Proc. IEEE*, vol. 92, no. 2, pp. 198–218, Feb. 2004.

[70] J. G. Proakis, *Digital Communications*, 4th ed. New York, NY: McGraw-Hill, 2001.

[71] G. G. Raleigh and J. M. Cioffi, "Spatio-temporal coding for wireless communication," *IEEE Trans. Commun.*, vol. 46, pp. 357–366, Mar. 1998.

[72] R. M. Rao and B. Daneshrad, "I/Q mismatch cancellation for MIMO-OFDM systems," in *Proc. IEEE Int. Symp. Pers., Indoor, Mobile Radio Commun.*, Barcelona, Spain, Sept. 2004, pp. 2710–2714.

[73] R. M. Rao and B. Daneshrad, "Analog impairments in MIMO-OFDM systems," *IEEE Trans. Wireless Commun.*, vol. 5, pp. 3382–3387, Dec. 2006.

[74] B. Razavi, "Design considerations for direct-conversion receivers," *IEEE Trans. Circuits Syst. II, Analog Digit. Signal Process.,* vol. 44, pp. 428–435, June 1997.

[75] B. Razavi, *RF Microelectronics*. Upper Saddle River, NJ: Prentice-Hall, 1998.

[76] S. de Rore *et al.*, "Joint estimation of carrier frequency offset and IQ imbalance for 4G mobile wireless systems," in *Proc. IEEE Int. Conf. Commun.*, Istanbul, Turkey, June 2006, pp. 2066–2071.

[77] P. Rykaczewski, D. Pienkowski, R. Circa, and B. Steinke, "Signal path optimization in software defined radio systems," *IEEE Trans. Microw. Theory Tech.*, vol. 53, pp. 1056–1064, Mar. 2005.

[78] P. Rykaczewski, M. Valkama and M. Renfors, "Analytical approach to I/Q imbalance in OFDM, CDMA and MC-CDMA based systems", in *Proc. IEEE Radio and Wireless Symp.*, San Diego, CA, Jan. 2006, pp. 555–558.

[79] H. Sampath, S. Talwar, J. Tellado, V. Erceg, and A. Paulraj, "A fourth-generation MIMO-OFDM broadband wireless system: Design, performance, and field trial results," *IEEE Commun. Mag.*, vol. 40, no. 9, pp. 143–149, Sept. 2002.

[80] T. C. W. Schenk, P. F. M. Smulders, and E. R. Fledderus, "Estimation and compensation of TX and RX IQ imbalance in OFDM-based MIMO systems," in *Proc. IEEE Radio Wireless Conf.*, San Diego, CA, Jan. 2006, pp. 215–218.

[81] T. C. W. Schenk, P. F. M. Smulders, and E. R. Fledderus, "Estimation and compensation of frequency selective TX/RX IQ imbalance in MIMO-OFDM systems," in *Proc. IEEE Int. Conf. Commun.*, Istanbul, Turkey, June 2006, pp. 251–256.

[82] T. C. W. Schenk, "RF impairment in multiple antenna OFDM: Influence and mitigation," Ph.D. dissertation, Eindhoven University of Technology, Eindhoven, the Netherland, Nov. 2006.

[83] T. C. W. Schenk, E. R. Fledderus, and P. F. M. Smulders, "Joint performance analysis of zero-IF MIMO OFDM transceivers with IQ imbalance," *Journal of Commun.*, vol. 2, no. 7, pp. 9–19, Dec. 2007.

[84] P. J. Schreier and L. L. Scharf, "Second-order analysis of improper complex random vectors and processes," *IEEE Trans. Signal Process.*, vol. 51, pp. 714–725, Mar. 2003.

[85] A. Schuchert, R. Hasholzner, and P. Antoine, "A novel IQ imbalance compensation scheme for the reception of OFDM signals," *IEEE Trans. on Consum. Electron.*, vol. 47, pp. 313–318, Aug. 2001.

[86] M. Schwartz, W. R. Bennett, and S. Stein, *Communication Systems and Techniques*. McGrawHill, 1966.

[87] I. H. Sohn, E. R. Jeong, and Y. H. Lee, "Data-aided approach to I/Q mismatch and DC-offset compensation in communication receivers," *IEEE Commun. Lett.*, vol. 6, pp. 547–549, Dec. 2002.

[88] T. B. Sorensen, P. E. Mogensen, and F. Frederiksen, "Extension of the ITU channel models for wideband (OFDM) systems," in *Proc. IEEE Veh. Technol. Conf.*, Dallas, TX, Sep. 2005, pp. 392–396.

[89] K.Y. Sung and C. Chao, "Estimation and compensation of I/Q imbalance in OFDM direct-conversion receivers," *IEEE J. Sel. Topics Signal Process.*, vol. 3, pp. 438–453, Jun. 2009.

[90] R. Tafazolli, Ed., *Technologies for the Wireless Future: Wireless World Research Forum (WWRF)*. Chichester, U.K.: Wiley, 2004.

[91] Y. Tanabe *et al.*, "Suitable MIMO-OFDM decoders to compensate IQ imbalance," in *Proc. IEEE Wireless Commun., Netw. Conf.*, Hong Kong, Mar. 2007, pp. 863–868.

[92] D. Tandur and M. Moonen, "Compensation of RF impairments in MIMO OFDM systems", in *Proc. IEEE Int. Symp. Commun., Control and Signal Process.*, Las Vegas, NV, Mar.–Apr., pp. 3097–3100.

[93] D. Tandur and M. Moonen, "STBC MIMO OFDM systems with implementation impairments", in *Proc. IEEE Veh.r Technol. Conf.,* Calgary, Canada, Sep. 2008.

[94] A. Tarighat and A. H. Sayed, "Space-time coding in MISO-OFDM systems with implementation impairments," in *Proc. IEEE Sensor Array and Multichannel Signal Process.*, Barcelona, Spain, July 2004, pp. 259–263.

[95] A. Tarighat, R. Bagheri, and A. H. Sayed, "Compensation schemes and performance analysis of IQ imbalances in OFDM receivers," *IEEE Trans. Signal Proces*s., vol. 53, pp. 3257–3268, Aug. 2005.

[96] A. Tarighat and A. H. Sayed, "MIMO OFDM receivers for systems with IQ imbalances," *IEEE Trans. Signal Process.*, vol. 53, pp. 3583–3596, Sept. 2005.

[97] A. Tarighat and A. H. Sayed, "Joint compensation of transmitter and receiver impairments in OFDM systems," *IEEE Trans. Wireless Commun.*, vol. 6, pp. 240–247, Jan. 2007.

[98] V. Tarokh, N.Seshadri, and R.A. Calderbank, "Space-time codes for high data rate wireless communication: Performance criterion and code construction," *IEEE Trans. Inf. Theory*, vol. 44, pp. 744–765, Mar. 1998.

[99] V. Tarokh, H. Jafarkhani, and A. R. Calderbank, "Space-time block codes from orthogonal designs," *IEEE Trans. Inf. Theory*, vol. 45, no. 5, pp. 1456–1467, Oct. 1999.

[100] E. Telatar, "Capacity of multi-antenna gaussian channels," *Internal Technol. Memo*, Bell Laboratories, Murray Hill: NJ, pp. 1–28, Jun. 1995.

[101] E. Telatar, "Capacity of multi-antenna Gaussian channels," *European Trans. Telecommun.*, vol. 10, no. 6, pp. 585–595, Nov.–Dec. 1999.

[102] D. Tse and P.Viswananth, *Fundamentals of Wireless Communication*, Cambridge University Press, 2005.

[103] W. Tuttlebee, Ed., *Software Defined Radio: Enabling Technologies.* Chichester, U.K.: Wiley, 2002.

[104] J. Tubbax et al., "Compensation of IQ imbalance and phase noise in OFDM systems," *IEEE Trans. Wireless Commun.*, vol. 4, pp. 872–877, May 2005.

[105] S. Traverso, M. Ariaudo, I. Fijalkow, J.L. Gautier, and C. Lereau, "Decision-directed channel estimation and high I/Q imbalance compensation in OFDM receivers," *IEEE Trans. Commun.*, vol. 57, pp. 1246–1249, May 2009.

[106] M. Valkama, "Advanced I/Q signal processing for wideband receivers: Models and algorithms," Ph.D. dissertation, Tampere University of Technology, Tampere, Finland, Nov. 2001.

[107] M. Valkama and M. Renfors, "Digital I/Q imbalance compensation in direct-conversion receivers," in *Proc. 2002 Workshop on Software Radios*, Karlsruhe, Germany, Mar. 2002, pp. 51–55.

[108] M. Valkama, J. Pirskanen, and M. Renfors, "Signal processing challenges for applying software radio principles in future wireless terminals: An overview," *Int. J. Commun. Syst.*, vol. 15, pp. 741–769, Oct. 2002.

[109] M. Valkama, M. Renfors, and V. Koivunen, "Blind I/Q signal separation -based solutions for receiver signal processing," *EURASIP J. Applied Signal Process.*, vol. 2005, no. 16, pp. 2708–2718, Sept. 2005.

[110] M. Valkama, M. Renfors, and V. Koivunen, "Blind signal estimation in conjugate signal models with application to I/Q imbalance compensation," *IEEE Signal Process. Lett.*, vol. 12, pp. 733–736, Nov. 2005.

[111] B. Widrow, P. E. Mantey, L. J. Griffiths, and B. B. Goode, "Adaptive antenna systems," *Proc. IEEE*, vol. 55, pp. 2143–2159, Dec. 1967.

[112] M. Windisch and G. Fettweis, "Adaptive I/Q imbalance compensation in low-IF transmitter architectures," in *Proc. IEEE Veh. Technol. Conf.*, Los Angeles, CA, Sept. 2004, pp. 2096–2100.

[113] G. Xing, M. Shen, and H. Liu, "Frequency offset and I/Q imbalance compensation for direct-conversion receivers," *IEEE Trans. Wireless Commun.,* vol. 4, pp. 673–680, Mar. 2005.

[114] A. van Zelst, "Space division multiplexing algorithms," in *Proc. Mediterranean Electrotech. Conf.*, vol. 3, pp. 1218–1221, 2000.

Publications